"CONTRIBUTION TO LIQUID LENS TECHNOLOGY"

Thesis submitted in partial fulfillment of the requirement for the PhD Degree issued by the Universitat Politècnica de Catalunya, in its Electronic Engineering Program

Nom del doctorand

Maziar Ahmadi Zeidabadi

Directors:

Prof. Dr. Luis Castañer
Prof. Dra. Sandra Bermejo

data de lectura de la tesi
Mayo 2016

Contents

Figures and Tables

To my Parents, my Sister and Gina...

Abstract

The interest on microfluidic systems based on electrowetting-on-dielectric (EWOD) and the miniaturization of such integrated devices, has increased significantly mainly due to the advent of mass market applications such as lab-on-chip, liquid lenses and reflective displays. The main objective of this work focuses on the scientific and technological challenges that the fabrication and optimization of liquid lens faces. Those are mainly related to the materials used and their associated fabrication techniques, in order to have stable devices with high performance for long term functionality. The work reported here contributes the research to reduce the actuation voltage and to increase stability and reliability of electrowetting devices such as liquid lenses at laboratory scale.

We address various aspects related to liquid lenses: (a), improvement of the hydrophobic layer deposition process leading contact angle recovery enhancement, (b) investigation of the dielectric materials and deposition techniques to reduce the required applied voltage (c) specific design of electrodes for 2D movement of the liquid lens, and (d) investigation of nonaqueous liquids to improve the dynamic behavior and long term cycling functionality. (e) An attempt is made to develop behavioral models that can explain EWOD phenomena with electronic circuit software.

RESUMEN

El interés en los sistemas microfluídicos basados en electrohumectación sobre un dieléctrico (electrowetting-on-dielectric, EWOD) y la miniaturización de dichos dispositivos integrados, ha aumentado significativamente, principalmente debido a la llegada de aplicaciones del mercado de masas, como lab-on-chip, lentes líquidas y pantallas reflectantes. El objetivo principal de este trabajo se centra en los retos científicos y tecnológicos de la fabricación y la optimización de una lente líquida. Principalmente, los que están relacionadas con los materiales utilizados y sus técnicas de fabricación asociadas, con el fin de tener dispositivos estables con un alto rendimiento para la funcionalidad a largo plazo. Este trabajo describe la investigación llevada a cabo para reducir la tensión de accionamiento y para aumentar la estabilidad y la fiabilidad de los dispositivos EWOD, tales como lentes líquidas, a escala de laboratorio.

Los principales aspectos relacionados con lentes líquidas trabajados en esta tesis son los siguientes: (a) la mejora del proceso de depósito de la capa hidrofóbica que determina el ángulo de contacto y mejora su recuperación, (b) la investigación de los materiales dieléctricos y técnicas de depósito para reducir la tensión aplicada, (c) el diseño específico de electrodos para el movimiento en 2D de la lente líquida, y (d) la investigación de los líquidos no acuosos para mejorar el comportamiento dinámico y la funcionalidad en frecuencia a largo plazo. (e) También se ha iniciado el desarrollo de modelos de comportamiento que puedan explicar fenómenos EWOD con un software de circuitos electrónicos.

RESUM

L'interès en els sistemes microfluídics basats en electrohumectació sobre un dielèctric (electrowetting-on-dielectric, EWOD) i la miniaturització d'aquests dispositius integrats, ha augmentat significativament, principalment a causa de l'arribada de les aplicacions del mercat de masses, com poden ser el lab-on-chip, les lents líquides i les pantalles reflectants. L'objectiu principal d'aquest treball se centra en els reptes científics i tecnològics de la fabricació i l'optimització d'una lent líquida. Principalment, els que tenen a veure amb els materials utilitzats i les seves tècniques de fabricació associades, amb la finalitat de tenir dispositius estables amb un alt rendiment per a la funcionalitat a llarg plaç. Aquest treball descriu la investigació duta a terme per a reduir la tensió d'accionament i per a augmentar l'estabilitat i la fiabilitat dels dispositius EWOD, tals com les lents líquides, a una escala de laboratori.

Els principals aspectes relacionats amb les lents líquides treballats en aquesta tesi són els següents: (a) la millora del procés de dipòsit de la capa hidrofòbica que determina l'angle de contacte i millora la seva recuperació, (b) la investigació dels materials dielèctrics i les tècniques de dipòsit per a reduir la tensió aplicada, (c) el disseny específic d'elèctrodes pel moviment en 2D de la lent líquida, i (d) la investigació dels líquids no aquosos per a millorar el comportament dinàmic i la funcionalitat en freqüència a llarg termini. (e) També s'ha iniciat el desenvolupament de models de comportament que puguin explicar fenòmens EWOD amb un programari de circuits electrònics.

Chapter 1:

Summary

1.1 Introduction
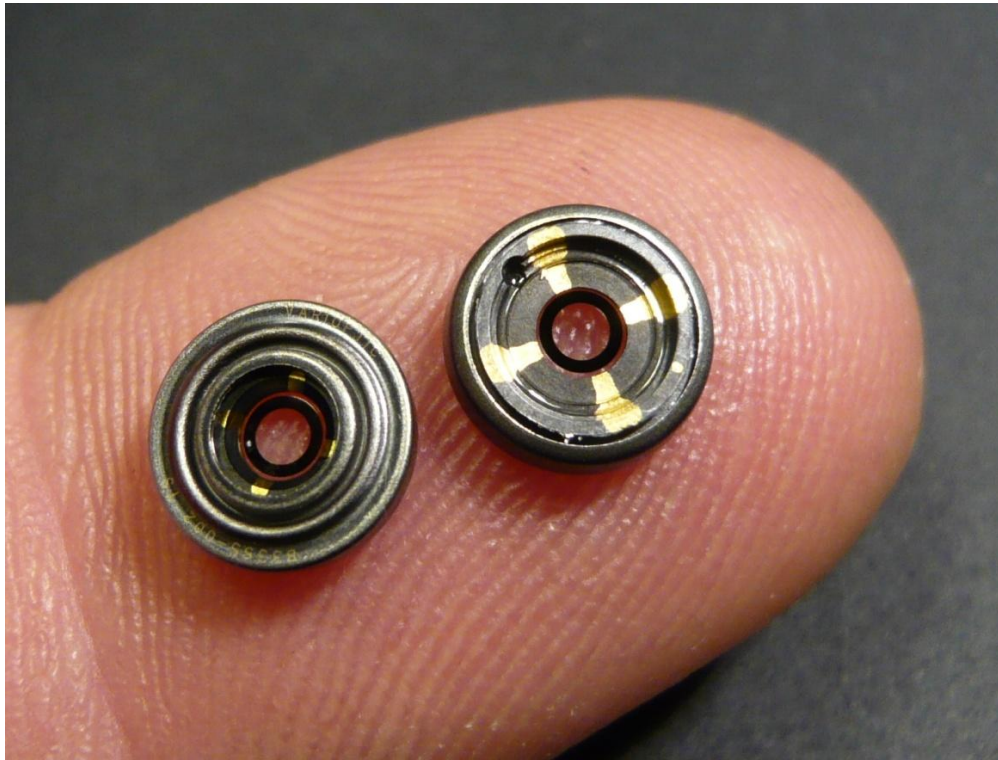
Figure 1 Varioptic lens

Micro-optic technology is becoming increasingly important for a wide range of Micro-Opto-Electro-Mechanical systems (MOEMs) applications [1–8], especially the movement of liquids based on electrowetting on dielectric phenomena (EWOD), applied to miniaturized devices such as tiny lens [9–14]with high variation of focal length and ultra-fast focusing in comparison to conventional convex lenses. The electrowetting driven liquid lenses offers several key features that are unmatched by other ways to achieve a large range of optical variation.

In fact, the smoothness of a liquid surface is not achievable by conventional lens carving procedures and the displacement of the liquid interface by electric means allows large shape modifications   and high focus variations. Liquid lenses can work for over 100 million cycles without any performance degradation compared to mechanical systems such as piezomotors and coil motors which are typically limited to a few hundred thousand cycles [15]. Under shock resist test, the liquid lens behaves much better than mechanical solutions[16]. Liquid response can be as fast as tens of milliseconds. These time scales are well adapted to human interfaces, video, photo capture etc. Additionally, an advantage of liquid lenses is the ultra-low energy consumption compared to other mechanical or electromechanical driver.

In fact, compared to mechanical systems, liquid lenses have no hysteresis, thereby the position of the lens surface is completely controllable by an applied voltage and there is no

need for image processing of additional tools for controlling the focus. The liquid lens performance can be easily calibrated, enabling both fast closed loop mode and ultra-fast open loop mode (see for example Varioptic lens with focusing time less then 20ms)[4,15].

The control of the movement and shape of the liquid in two dimensions (2D), although already used in lab-on-chip applications to liquid transport , particle sorting , liquid mixing and droplet splitting , has not been sufficiently exploited in liquid lenses . This technology has many of applications in the medical and pharmaceutical industry [6,17]such as medical analysis [7] and drug delivery [18] etc.

In electrowetting device basically consists on a thin electrode layer, a dielectric and a hydrophobic layer on top of each other. If the liquid is electrically conductive, movement of the triple line (TPL) between substrate, liquid and surrounding medium is originated when an electric potential is applied between a needle, or other kind of upper electrode in contact with the drop, and a bottom electrode. In fact the energy stored in the capacitor formed between the liquid and the bottom electrode unbalances the surface tension equilibrium. As predicted by the Lippmann–Young law [19] the contact angle decreases when the applied voltage increases, at least for a range of values of the voltage and before a saturation regime is reached. If the applied voltage is switched to zero, the contact angle usually does not fully recover the initial value [20–22][9].

Most of the experimental work in electrowetting has been performed using droplets of distilled water (DW) because water has a high surface tension value and high contact angle on hydrophobic surfaces. Among the results that are available in the literature it is seen that the use of DW creates several problems such as corrosion of the electrodes, electrolysis, bubbling and tendency to permeate through polymers[23]. This is enhanced by the use of high values of the actuation voltage that are commonly required. In this work attention is being paid to the changes in structural design of the electrowetting devices to be able to reduce the actuation voltage value.

Besides the alternative to use different liquids has attracted the attention of researchers, particularly conductive high surface tension liquids as listed in reference [23], some of them able to sustain low temperatures for use in some outdoor electrowetting applications. In this work we have contributed to the research of such liquids

1.2 Thesis challenges and outlines

The main objectives of the thesis are the investigation of critical issues on the optimization of the fabrication process of liquid lenses based on electrowetting-on-dielectric. After summarizing the theory of EWOD in **chapter 2**, the thesis concentrates on low voltage, highly reversible, long life cycle, low working temperature liquid lenses and 2D drive. The state of art and literature will be investigated, in **chapter 3** we address one critical problem concerning the Teflon layer integrity that is compromised when voltage is applied on a distilled water drop the wettability of the surface will increase and it will cause the hydrolysis of distilled water that will damage the electrode. The electrowetting performance depends on the one hand on the hydrophobic material, thickness and deposition technique   and on the liquid used.

Distilled water is commonly used as liquid for microfluidic systems based on EWOD because of its high surface tension and ease of use, but there are several problems such as corrosion of electrodes, hydrolysis of liquid, freezing in low working temperature, short life time for long cycling. In **chapter 4** we investigate the use of non-aqueous liquids instead of distilled water which shows high static contact angle with high reversibility in comparison to water and stable life time during long cycling.

We have investigated superhydrophobic materials in particular one of the most commonly used superhydrophobic materials [FDTS (1H,1H,2H,2H-perfluorodecyltrichlorosilane)] in collaboration with The National Institute of Advanced Industrial Science and Technology (AIST) in Japan. We have deposited superhydrophobic FDTS material on top of a substrate and we have discovered that in the contact mode EWOD FDTS layer shows poor stability which causes degradation of the layer and hydrolysis of water or creating bubbles in non-aqueous liquid, As interest on contactless EWOD is increasing for different applications, in the **chapter 5** we have studied contactless EWOD with superhydrophobic layer of FDTS.

In **chapter 6**, an attempt is made to develop PSpice models to allow microfluidic application to be incorporated into electronic circuit simulation environment.

Finally **in chapter 7**, the problem of 2D movement of liquid lens is investigated using different designs. Both electrodes are placed on the bottom of the device and one of the electrodes is split to provide several positions for the control and hence allowing 2D control of the droplet shape. The approach is based on capacitive − coupled electrowetting is described. It is shown that reversible control is feasible with applied voltage depending on the thicknesses of the dielectric and the hydrophobic layer.

Chapter 2:

Liquid lens

(Fundamentals and theory)

2.1 Liquid lens devices overview

The study of variable focus micro lenses has been an area of research activity for many years. Several recent publications [24–34] have recognized the potential of variable micro lens to impact significantly on the field of optical applications. Variable focal length lenses can be made by changing the shape of the lens or by changing the refraction index. In most of optical systems, tuning of focal length is obtained by displacement of lenses and by variation of the distance between lenses using electromechanical motors. Scaling of such systems to millimeter/micron size is complicated because of the fabrication process itself and due to the large number of micro-size components required to assemble a micro-lens. Additionally, the use of electromechanical drivers requires large electric power consumption. The necessity for highly reliable lens with high variation of focal length, large number of cycles and low consumption is clear [9]. It is of great interest to be able to fabricate miniaturized lens that can change their parameters without any mechanical movement. Different solutions have been presented for the fabrication of electrically variable lenses such as: liquid lenses [27] , elastomeric-deformable lenses [35], or liquid crystal (LC) lenses [36]. In recent years, liquid lenses have attracted a widespread attention because of the advantages and simplicity of the structure, low cost , high speed and more than 100000 cycle life. The focal length can be easily tuned by changing the meniscus between two immiscible liquids. The working principle of a liquid lens is the change of the curvature and shape of a liquid meniscus by the change of the surface tension (or of the chemical modification of surface) to increase or reduce wettability. Several methods for energy surface modification of liquid lens has been used such as: electrical mechanical actuation[8,37–42], acoustic radiation forces [43], electromagnetic control [44,45], ferrofluidic actuator[46,47] , dielectric force (dielectrophoretic) [48–52] and electrostatic force (electrowetting) [16,53–55]. Among them, Electrowetting-on-dielectric (EWOD) and Dielectrophoretic liquid lenses are promising due to low voltage actuation and variation of focal length. In both cases, in order to obtain lens curvature , two immiscible medium (liquid-liquid , vapor-liquid) are used. For the EWOD technique, the liquid should be electrically conductive in order to generate an electrostatic force by applying a voltage. This voltage deforms the shape of the drop and hence changes the focal length. The same effect happens for dielectric lenses but here, the two medium should be insulators but with different dielectric constants.

2.2 Basic principles of capillarity and wetting

Physics and chemistry principles govern the shape of a drop of liquid on top of a substrate. In the micro scale, a molecule of liquid located inside the drop is equally attracted in all directions by the molecules surrounding it and, as a consequence, the total force exerted on it is zero. However, a molecule located close to the drop surface is attracted mainly by its inner neighbors and, therefore is subject to a resultant force in the direction of the other molecules (Figure 2)[56]. This effective attraction and net force of a molecule on the surface of liquid creates the surface tension.

The surface tension is a physical quantity measured in units of force per unit length, (or equivalently in units of energy per unit area), and it expresses the amount of energy necessary to enlarge the surface by one surface unit. Since the sphere has the lowest surface area per given volume, it is easy to understand that this is also the state with the lowest surface energy, which generates the spherical shape of the drops (Figure 2). In different fluids, intermolecular forces show different characters and intensities.
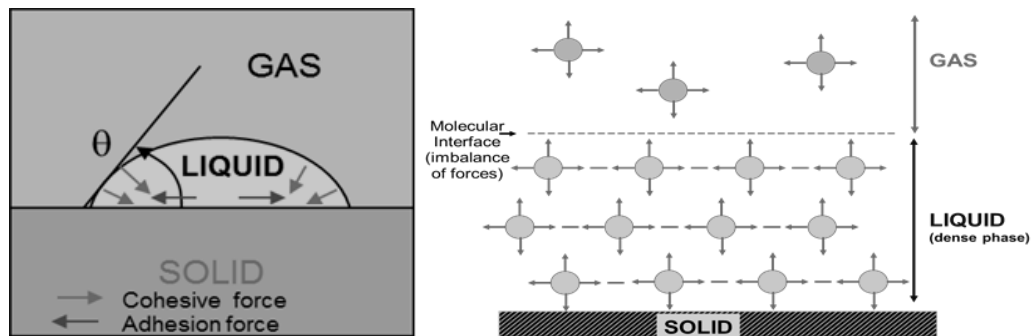
Figure 2 (a) Cohesive forces vs. adhesion forces (b) Boundary tension

Wetting is the ability of a liquid to maintain contact with a solid surface, resulting from intermolecular interactions when the two are brought together. The degree of wetting (wettability) is determined by a force balance between adhesive and cohesive forces.
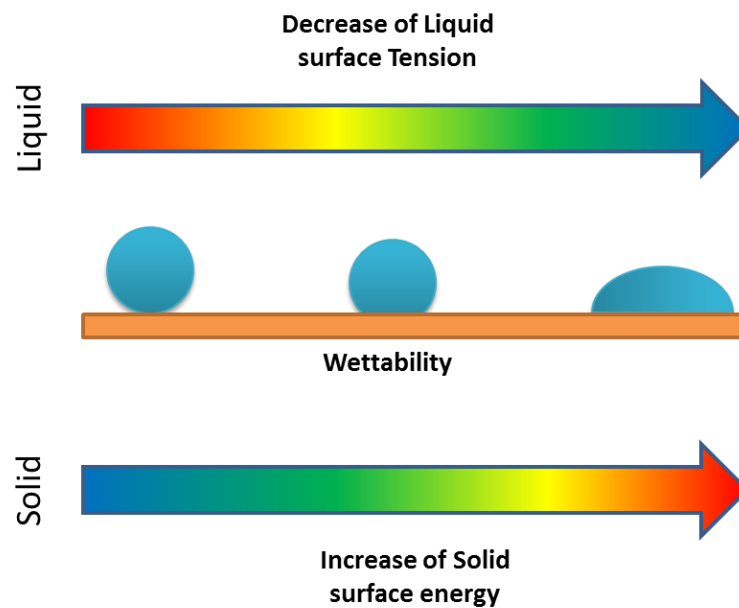
Figure 3 Wettability versus surface tension

The wetting phenomena is playing an important role in technology processes according to their applications. For example, it is necessary to have hydrophobic surface (low wettability) to repel the water and hydrophilic to attract the water. Wettability is a measure of the preferential tendency of the fluids to wet (spread or adhere to) to the surfaces of the solid. The wettability of a drop on a solid surface is dependent on the three interfacial tensions between solid, gas, and liquid phases. The tangential force balance between these interfacial tensions on the three-phase contact line leads to the following well-known Young's equation (Equation 1). In 1805 the British physician Thomas Young of Cambridge University found the relationship between the contact angle of a liquid surface with a solid [19] (the angle between the surface of the drop and the solid surface on which it was laid upon) Figure 4. In absence of external electric fields, the shape of the droplets is determined by surface tension alone. The free energy F of a droplet is a functional of the droplet shape. Its value is given by the sum of the areas A_i of the interfaces between three phases, the solid substrate (s), the liquid droplet (l), and the ambient phase, which we will denote as vapor (v), Therefore there are surface tension between the drop and the solid surface (γ_{sl}), surface tension between the solid surface and vapor (γ_{sv}) and the surface tension between the drop and the air (γ_{lv}).
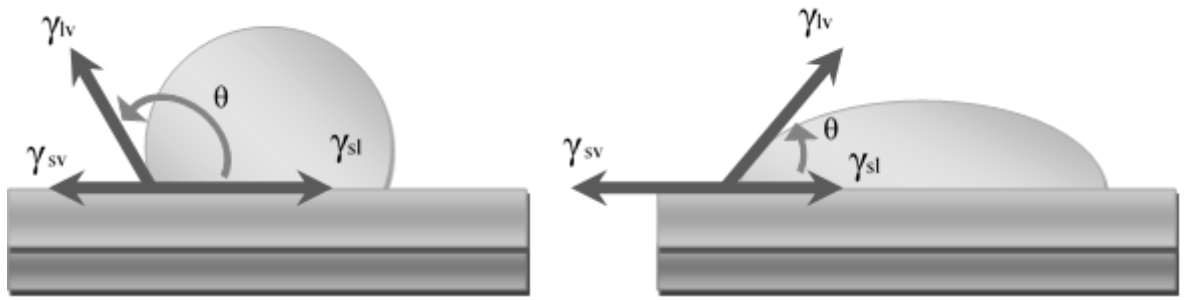
Figure 4 the contact angle θ related to the surface tension

The Young's equation that describes the relationship of surface tensions among the three phases is:

$$\gamma_{lv} \cos\theta = \gamma_{sv} - \gamma_{sl} \qquad [1]$$

Young derived the above equation by considering the balance of surface forces acting on the triple line where the solid, liquid, and vapor phases meet. Hereby wetting is quantitatively defined by the value of contact angle and if the contact angle is equal to zero, the phenomenon is called complete wetting. If the contact angle is not zero, it is called partial wetting.

2.3 Hydrophobic surfaces

Hydrophobicity was originally observed in nature (e.g., on lotus leaves), and today is a relevant property of use in a wide range of scientific and technological applications, including development of coatings with self-cleaning properties[57–60], As it illustrated in the SEM image of Lotus leaves[61], The roughness of lotus leaf surface is combination of micro scale roughness and nano scale roughness with low surface energy, creates a water repellant surface, which is common among all natural hydrophobic surfaces.[62–68]]. There are different definitions for superhydrophobicity but mainly a surface is said to be so, when the contact angle of water drop on top of it is larger than 120º. There are two main ways the liquid can sit on rough surfaces described by: the Wenzel mode[69,70]l and the Cassie-Baxter model[71], as illustrated in Figure 5
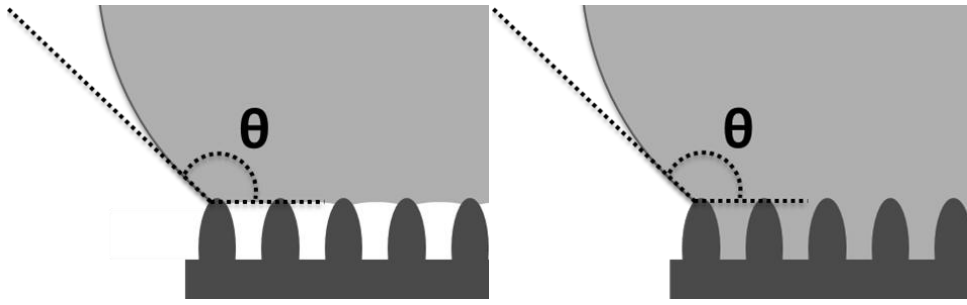
Figure 5: Wenzel model (left), Cassie-Baxter model (right)

In the Cassie-Baxter model air is trapped between the drop surface and the rough solid surface. In Wenzel model however, the liquid follows the roughness of the solid surface.

2.3.1 Wenzel model

Liquid drop in the Wenzel state has high contact angle but low mobility and high hysteresis. The Wenzel model was originally disclosed in 1936 by Robert N. Wenzel [69]. He showed that an increase in solid surface roughness will reduce the surface energy leading to an increase of contact angle. The roughness is usually defined as the ratio of the actual surface and the geometrical surface. The roughness has direct effect on wettability of surface that is strongly related to natural surface tension of surface.

$$\cos \theta = r . \cos \theta_0 \qquad\qquad [2]$$

θ_0 is the initial contact angle base on Lippmann-Young equation, θ is the contact angle of liquid on solid influenced by the roughness r. According to Equation 2 the Wenzel model wettability is based on the natural surface tension and roughness of solid surface, For example, if a hydrophobic surface with contact angle $\theta_0 > 90°$, the roughness will be increased, magnifying the hydrophobicity of the surface, but if $\theta_0 < 90°$ the results will be highly hydrophobic even when the roughness is high. Thus as conclusion the effect of roughness magnifies the natural wettability of surface.

2.3.2 Cassie-Baxter model

Cassie and Baxter [71] presented a model for hydrophobicity of liquid on the surface with two different materials and surface energy, according to Young's relation the apparent contact angle is given by:

$$\cos\theta = f_1\cos\theta_1 + f_2\cos\theta_2 \qquad [3]$$

The contact angles θ_1 and θ_2 are the natural contact angles of the two materials and f_1 and f_2 are the fraction of surface for each material so that ($f_1 + f_2 = 1$). If one of the two materials is air then the liquid is in touch with both solid and air. In this case the fractions f1 and f2 would be f_s and (1-f_s) and the respective contact angles θ_s and 180° for air. As a result the apparent contact angle of a rough hydrophobic surface will be

$$\cos\theta = -1 + f_s(\cos\theta_s + 1) \qquad [4]$$

According to cassie equation P. van der wal [72] presented increase of hydrophobicity of Teflon (natural contact angle ≈ 104°) to 171° by introducing roughness into a surface, as well in the chapter 4 we will demonstrate effect of roughness onto water-repellent surface.

2.4 Electrical Control of the surface wettability

The modification of surface wettability and the transition from hydrophobic to hydrophilic is a fundamental requirement in microfluidic devices. The control of wettability requires the manipulation of interfacial energies (surface tensions) that can be done by two main methods: faradaic electrochemical [73] and non-faradaic electrochemical or electrowetting [74].

2.4.1 Chemical modification of surface by faradaic electrochemistry

Electrochemical ferrocene surfactants were used for modification and control of the interfaces in the reduced and oxidized states [73,75,76]; The use of this technique was demonstrated by Gallardo et al. [73] If along a microfluidic channel a solution with concentration of 0.1mM redox-active surfactants in water, an oxidation potential is applied to an electrode liquid droplets can be moved an driven when the oxidation of the surface occurs

and the surface energy is increased to a maximum value of 22mN/m. In the other electrode reduction occurred .
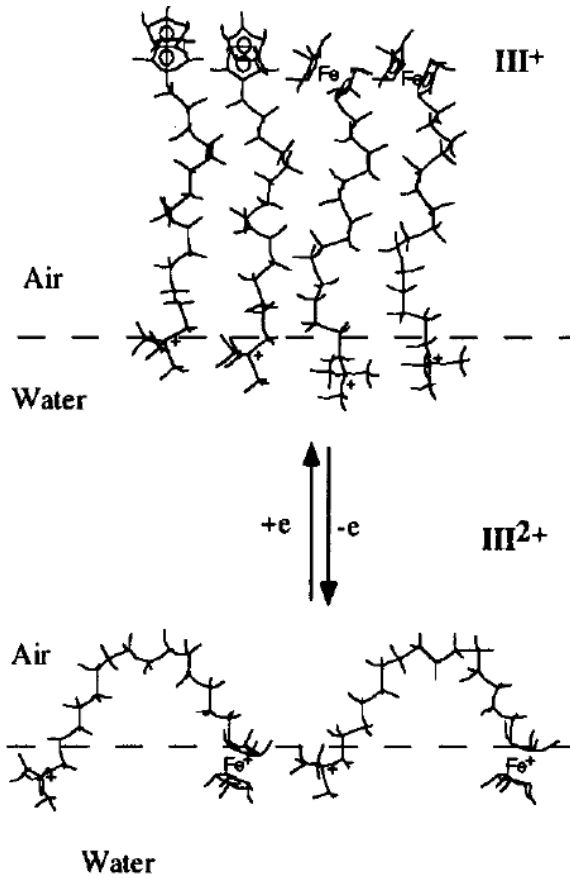
Figure 6 Schematic example of possible conformations of ferrocenyl surfactants at the surface of aqueous solutions: reduced (top row) and oxidized (bottom row) states[76]

Even though faradaic electrochemical process works at low voltage (<1V) the controlled modification of surface tension is limited to non-aqueous liquids and, because of the chemical reaction, an electrochemical gradient must be established along the full length of the channel. Due to this limitation, few practical applications of this technique are found in the literature compared to electrowetting which we discuss in the next part.

2.4.2 Electrowetting on dielectric (EWOD)

Electrowetting is defined as a modification of the surface wettability by applying a voltage that causes changes in the free energy due to the stored charge in the solid-liquid interface capacitor leading to a modification of the interfacial surface energies. This ends up with a change in the contact angle. This is also known as non-faradaic electrochemical process for active control of physicochemical properties of interfaces [77]. In 1990 B. Berge demonstrated how the use of a thin dielectric layer deposited between the solid and the liquid

could avoid electrolysis of an aqueous solution thereby opening the door for practical applications. The general experiment scheme for electrowetting on dielectric (EWOD) is shown in Figure 7.
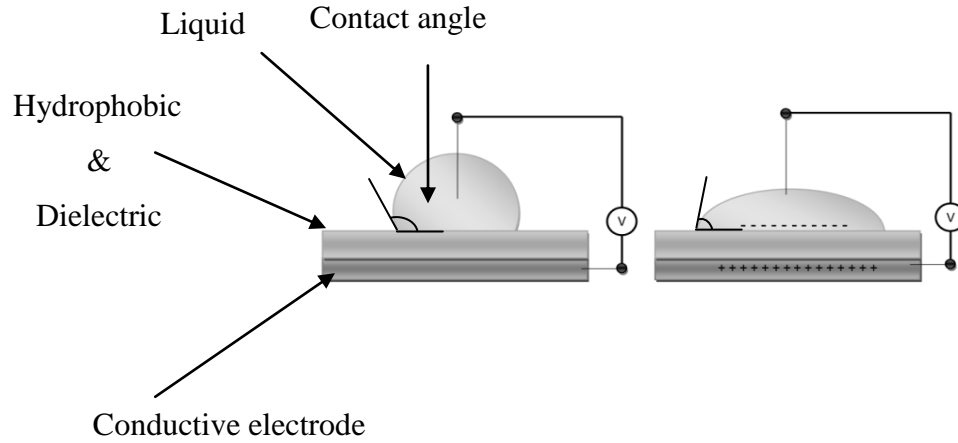
Figure 7 Schematic view Electrowetting on dielectric surface

A potential is applied between a conducting liquid on an insulating layer and a counter electrode positioned below the insulating layer. Charge accumulates on the solid-liquid interface, leading to a change of the contact angle, the main equation governing electrowetting is the well known Lippmann-Young equation[19]

.

$$\gamma_{sl} = \gamma_{^\circ sl} - F$$

$$\gamma_{sl} = \gamma_{sv} - \gamma_{lv} \cos \theta$$

$$\theta = \cos^{-1} \left(\frac{\gamma_{sv} - \gamma_{^\circ sl} - F}{\gamma_{lv}} \right) \qquad [5]$$

Or

$$\cos \theta = \cos \theta_0 + \eta \qquad [6]$$

Where $\gamma_{^\circ sl}$ is the surface tension between the drop and the solid surface at zero electric field, γ_{sv}, γ_{sl}, and γ_{lv} are the surface tensions of the solid–vapor, solid– liquid, and liquid–vapor surfaces, respectively θ_0 is initial static contact angle and θ is the contact angle between the drop and the dielectric after applying voltage. F is electrostatic force created by applied voltage:

$$F = \frac{CV^2}{2} = \frac{\varepsilon_0 \varepsilon_r V^2}{2d} \cdot L \qquad [7]$$

Where C is the capacitance of the interface, ε_0 the permittivity of vacuum, ε_r the relative permittivity of dielectric, d is dielectric thickness; V is applied voltage which can be negative or positive and L is the electrode length. η is defined as the electrowetting number represented by:

$$\eta = \frac{F}{\gamma_{lv}} = \frac{\varepsilon_0 \varepsilon_r V^2}{2d\gamma_{lv}} \qquad [8]$$

In reality the variation of contact angle does not completely follow the Lippmann-Young equation. For the movement of drop base on EWOD at zero state all forces are balance on TPL contact point. In the real surfaces when a force applied to the drop (ex. gravity force when the surface is tilted), the drop does not immediately slip on the hydrophobic surface, instead it's form like Figure 8. The contact angle hysteresis is defined as the difference between two receding (minimum) and advancing (maximum) contact angles [78–82]. The contact angle hysteresis is mostly related to the roughness and non-homogeneity of solid surface but still origin of the phenomena has not been completely explored. The required force to move the drop on the surface is defined by [83,84]:

$$F = \gamma_{lv} w (\cos \theta_r - \cos \theta_a) \qquad [9]$$

Where θ_r and θ_a are respectably receding contact angle and advancing contact angle, w is width of the drop bottom perpendicular to the direction of sliding force:

$$w = 2R \sin \left(\frac{\theta_r + \theta_a}{2} \right) \qquad [10]$$

Where the R is radius of drop that ideally deepens on static contact angle and volume of drop[85]:

$$R = \left(\frac{3vol}{\pi} \right)^{\frac{1}{3}} \frac{\sin \theta}{(2 - 3\cos \theta + \cos^3 \theta)^{\frac{1}{3}}} \qquad [11]$$

According to Equation 9 in order to minimize effect of sliding force there are two ways: The minimization of contact angle hysteresis that could be obtained by reducing the roughness of surface or, increasing the hydrophobicity to have superhydrophobic surface (Cassie state by increasing roughness) that lead to have negligible hysteresis.
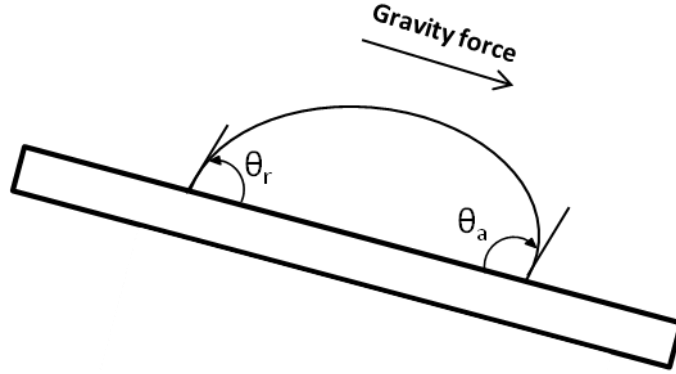
Figure 8 Contact angle hysteresis

The contact angle hysteresis is an important factor for the drop motion; here as we don't have movement of drop the contact angle hysteresis did not consider. So the minimum voltage can be represented as:

$$V = \sqrt{\frac{2d\gamma_{lv}(\cos\theta - \cos\theta_0)}{\varepsilon_0\varepsilon_r}} \qquad [12]$$

This equation describes the correlation between applied voltage and variation of contact angle. Unfortunately the Lippmann-Young equation is not valid for all applied voltages. Theoretically it is possible to obtain a complete wetting (zero contact angle) by increasing sufficiently the applied voltage. However, complete wetting has never been observed experimentally. The experimental results show the increasing of applied voltage does not lead to an increase in contact angle. The parabolic relation between the observed contact angle and the applied voltage described by Equation 12 was only applicable below a given value of voltage. Above a certain voltage the electrowetting contact angle starts to deviate from the equation and saturates. The exact mechanism of the contact angle saturation has not yet been elucidated and it is the object of numerous debates[86]. The contact saturation is attributed in some theories to the charge build up in the dielectric [87,88], to insulating fluid charge to instabilities, to micro-droplet ejection and to gas ionization[89–91].
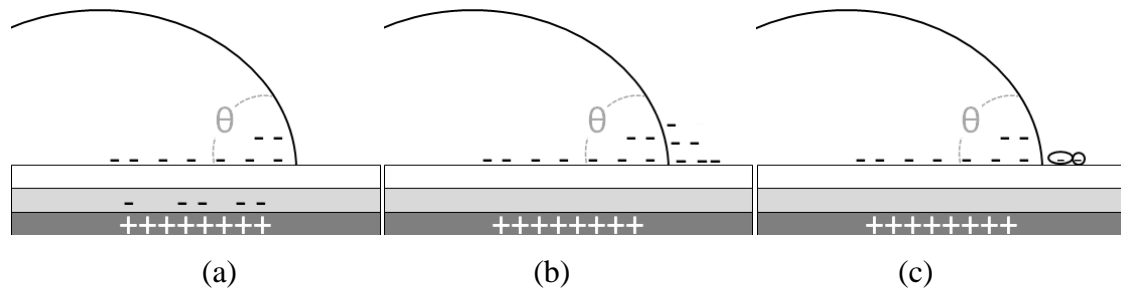
Figure 9 Different hypothesis of contact angle saturation Dielectric Charging (left), Insulating Fluid Charging (middle), Instabilities, Micro-droplet Ejection and Gas Ionization (right)

Previous studies on the contact angle saturation clearly show that several parameters are involved when the contact angle saturation is occurring, but mainly it is a time-dependent phenomenon, with different physical mechanisms dominating the saturation behavior over different time scales. Independence of the contact angle saturation reduction of applied voltage will be systematically investigated and an alternative polar liquid mixture for distilled water will be presented.

Chapter 3:

Low voltage EWOD

3.1 Introduction

Liquid lenses based on electrowetting on dielectric (EWOD) are an emerging field of investigation due to its versatility and potential in many applications. EWOD is the most efficient and feasible technique for integrated microfluidic devices in lab-on-a-chip applications, the integration of liquid lens or EWOD microfluidic device revealed limitations on performance, such as high driving voltage [92–95], electrolysis [21,96–99], degradation of hydrophobic layer[100,101], reversibility [102,103] and etc. Mainly in most common EWOD devices, in order to obtain high variation of contact angle, it is necessary to apply a high voltage due to materials properties and fabrication process. High applied voltage limits implementation of liquid lens in micro-devices, as well may cause degradation of the hydrophobic layer, electrolysis, dielectric breakdown [94]. On other hand, reproducibility of EWOD performance is an important factor to have highly stable with long life cycle liquid lens. For integration of an EWOD device is necessary to have low driving voltage, recently several works has been done to achieve low-voltage EWOD but still it is insufficient [104–109]. As a liquid lenses mainly consists of a transparent conductive layer, a hydrophobic layer, a dielectric layer and a transparent conductive liquid drop, this chapter main focus is on the fabrication process and material selection for liquid lens in order to fulfill two main issues. First, to reduce the applied voltage and obtain low voltage EWOD liquid lens and Second, to increase stability and cyclability of the liquid lens by optimizing the hydrophobic layer. In this chapter we will select the best parameters for the deposition process of conductive transparent layers of ITO for obtaining high conductive and high transparent layer. Then different dielectric layers and the effect of their thickness and dielectric permittivity on the required voltage will be compared. By selecting an adequate dielectric layer (to achieve low voltage and highly stable with long life cycle) the last layer (hydrophobic layer) will be optimized.

3.2 Experimental results

3.2.1 Optimization of conductive transparent layer with low resistance and high transparency

Since first discovery of transparent conductive films such as Indium Tin Oxide (ITO) [110,111] and due to its high conductivity and transparency in the visible light, it has become an attractive material used in several fields such as electro-optic devices, liquid crystal displays, and photovoltaics among many others[112–114]. Depending on the application, ITO can be deposited by different methods such as thermal evaporation, spray pyrolysis, pulsed laser deposition, screen printing techniques, and the most common method, and the preferred in the industry, sputtering[111,114–128]. Transparency and conductivity of the resulting ITO layer depends on the type and on the conditions of the deposition process. In the case of a liquid lens the transmittance should be >80% in the visible light with high conductivity of <100 $\Omega/\square$ [129], thus it is necessary to characterize an ITO film deposition process. One of the objectives of this work is to optimize the ITO film deposition and to fabricate the planar electrodes for liquid lens. To do this, the electrical conductivity and optical transmittance were characterized and analyzed. There are several parameters of the sputtering process that affect the properties of the ITO layer such as the power distribution on the target, the gas (argon or oxygen), the gap distance between the anode and cathode, the chamber pressure, the annealing temperature, the annealing time and the deposition time. In order to optimize the process, the gas flow and the chamber pressure were considered as fixed parameters. The effect of annealing at less than 150ºC on conductivity and transmittance is negligible thus for optimization purposes we did not investigate this part. The gap distance between the anode and the cathode was studied at a power of 50W, pressure of 1.3×10^{-5}mBar and gas flow of 7sccm during 45min; the results are shown in Figure 11. The optimized distance of shutter in order to achieve higher conductivity is 13cm. As it is illustrated, the gap distance has negligible effect on the deposition rate but it is strongly related to power (Figure 11), we can conclude that on slower deposition rate allow creating better bonding that lead to achieve low resistivity.
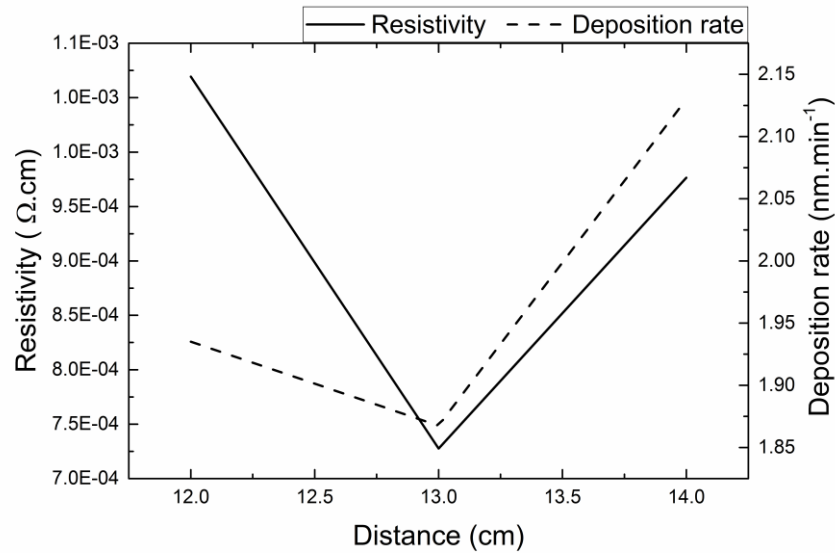
Figure 10 effect of gap distance on resistivity and deposition rate
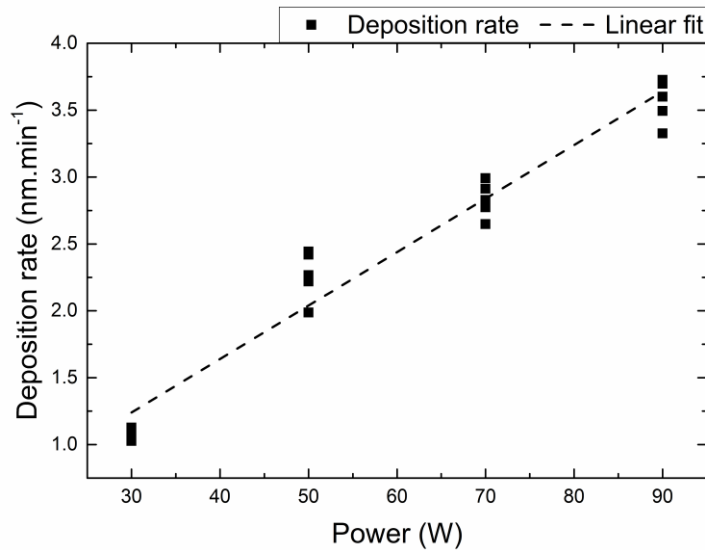
Figure 11 Deposition rate versus applied power for deposition of ITO with sputtering technique

By considering a constant gap distance of 13cm, the detailed studies of the properties of deposited indium tin oxide (ITO) are shown in Table 1. The results show that deposition with power of 30W and 50W for 45min give high transparent conductive layer (transmittance >80%) with low resistivity of <100 $\Omega/\square$, as the transmittance of 80% is acceptable; the ITO layer with higher conductivity was selected. For the fabrication processes devices in this work the ITO layer deposition conditions were selected: power 50W, 45min, gap distance of 13mm, pressure of 1.3×10^{-5}mBar and gas flow 7sccm.

Material	Power (w)	Time (min)	Thickness (nm)	Transmittance at 555nm (%)	Resistance (Ω/□)	Deposition rate (nm/min)
ITO	30	45	49.09886	89.5353	55.6	1.091086
ITO	50	45	102.0294	79.5854	27.2	2.26732
ITO	70	45	127.395	77.2482	27	2.831
ITO	70	45	160.5771429	70.3678	15.2	3.568381

Table 1 Properties of deposited ITO with sputtering technique under different conditions

3.2.2 Comparison of different dielectric materials and effect on the required voltage:
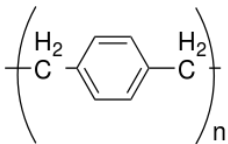
In order to achieve low voltage operation of EWOD device, the dielectric layer needs to be optimized. According to Lippmann–Young equation, the applied voltage has a direct relation with the thickness and with the dielectric permittivity of the dielectric film. For larger dielectric permittivity and lower thickness of the dielectric layer, the capacitance of the insulating layer increases and that will lead to obtain higher variation of contact angle at lower applied voltage. The dependence of the applied voltage on dielectric thickness is given by the simple EWOD Equation 13. In the Table 2 several dielectric materials that have been used within EWOD device are presented [94,130–132]:

Table 2 Dielectric materials use in EWOD device

Dielectric material	Formula	Dielectric Strength (kV/mm)	εr	Deposition technique
Silicon dioxide	SiO_2	600-1,100	4 – 5	Thermal xidation
Silicon nitride	Si_3N_4	500	7.5	Chemical vapor deposition
Aluminium oxide	Al_2O_3	500-800	8 - 9	Atomic layer deposition
Tantalum pentoxide	Ta_2O_5	150-300	23 - 25	Tantalum sputtering followed by anodization
Barium strontium titanate	$(Ba, Sr)TiO_3$	18-54	180 – 265	Metalorganic chemical vapor Deposition
SU8		1120	3.2-4.1	Spin coating
PDMS	$(C_2H_6OSi)_n$	12-16	2.3-2.8	Spin coating

Among different common dielectric materials used on microfluidic devices, in this work PDMS (polydimethylsiloxane), SU8 (negative photoresist) and Alumina (Aluminum oxide Al_2O_2) have been selected because of their ease of fabrication process and popularity within microfluidic devices. The hydrophobicity is a key factor. PDMS, due to its surface chemistry, is hydrophobic so there is no need for another hydrophobic layer. SU8 and alumina are hydrophilic and it is required an additional hydrophobic layer. For the microfluidic systems different materials presented in Table 3[94].

Table 3 Hydrophobic materials use in EWOD device

Hydrophobic material	Formula	EBD (kV/mm)	εr	Applied voltage (V)	Deposition technique
Cytop	Not available (NA)	110	2.1	120	Spin or dip coating
Teflon AF 1600	Random copolymer of 4,5-difluoro-2,2-bis(trifluoromethyl)-1,3 dioxole and tetrafluoroethylene	21	1.9	-	Spin or dip coating
Parylene C	$\left(-\overset{H_2}{C}-C_6H_4-\overset{H_2}{C}-\right)_n$	260	3.15	±240	Chemical vapor Deposition
Teflon (PTFE)		60	2.1	<300	Commercial
Polyimide		22	3.4	<400	Spin coating

For this purpose, amorphous fluoropolymer Teflon AF1600 (Dupont) with thickness of 550nm was used in Equation 13 and experimental results.

$$\cos\theta = \cos\theta_0 + \frac{C.V^2}{2\gamma_{LV}} \qquad [13]$$

θ_0 is the initial contact angle value before applying voltage and γ_{LV} is the liquid-vapor surface tension. The specific capacitance of a dielectric layer is given by Equation 14. If there is one layer hydrophobic dielectric, C depends on the dielectric constant and the thickness of the layer but if there are several stacked dielectric materials, then C depends on an equivalent ε_r that relates to dielectric permittivity and thickness of each layer as follows (Figure 12).
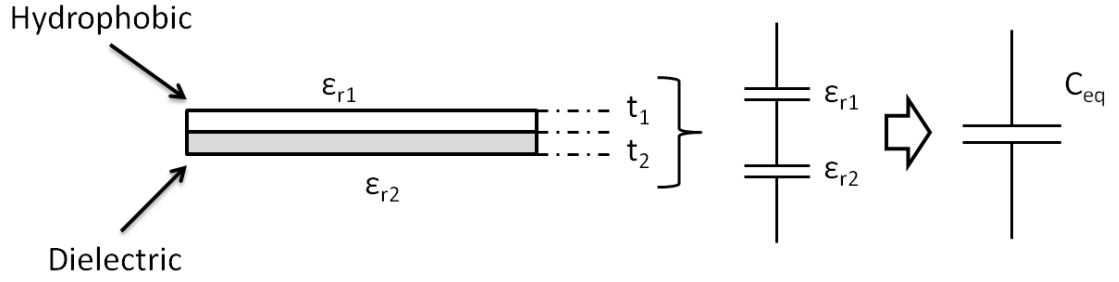
Figure 12 Equivalent capacitor of dielectric and hydrophobic layer use EWOD device

$$C = \frac{\varepsilon_0.\varepsilon_r}{t} \qquad [14]$$

$$C_{eq} = \varepsilon_0.\frac{\varepsilon_{r1}.\varepsilon_{r1}}{\varepsilon_{r1}.t_2 + \varepsilon_2.t_1} \qquad [15]$$

Where ε_0 is vacuum permittivity, ε_{r1} is the dielectric constant of dielectric and ε_{r2} is the dielectric constant of the hydrophobic layer, and t_1 and t_2 are the thicknesses of the two layers. For a single hydrophobic dielectric layer, the required voltage to achieve the specific variation of contact angle depends on the square root of the thickness of the dielectric layer with a fixed dielectric constant. For combination of a dielectric and a hydrophobic layer, the thickness of hydrophobic layer was assumed to be fixed at 550nm. The Lippmann–Young equation was used to calculate the dielectric thickness required to achieve $\Delta\theta = 3^\circ$, $\Delta\theta = 10^\circ$, $\Delta\theta = 20^\circ$ and $\Delta\theta = 30^\circ$ with an initial contact angle of 110° as described below. In order to confirm the dielectric thickness effect on the required voltage, the specific thickness of each dielectric layer was selected and fabricated following a deposition process. The samples were placed onto a specific lens holder and goniometric device (CAM200) to measure the contact angle, see Figure 13 , 10µl drops of the conductive liquids were placed using a vertical syringe on top of the samples surface. Side-view images of the drops were obtained using a high speed digital camera with zoom lens. A voltage difference was applied across the bottom electrode and a platinum needle in contact with the liquid (Power supply Agilent 4156C). According to the literature , higher variation of contact angle was obtained for negative voltage [96]. A high speed camera (BASLER A602F), with resolution of 640x480 pixels with capturing speed rate of 400 f/s, was used. Real time image processing commercial software has been used to analyze the drop shape. Performing edge detection to extract the drop profile close to the contact line, the contact angle (θ) is obtained by evaluating the slope of a third order polynomial fit.
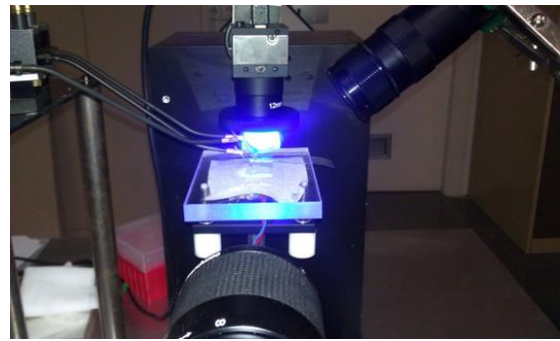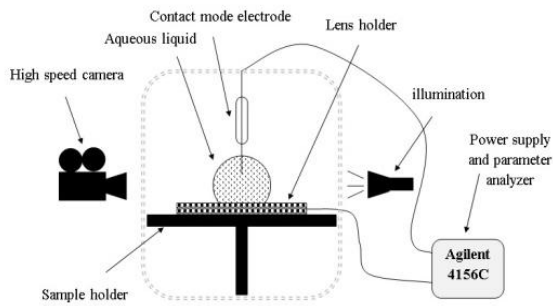
Figure 13 (a) Schematic of contact mode measurement setup (b) Picture of the experimental set-up (CAM200)

3.2.2.1 Polydimethylsiloxane (PDMS) hydrophobic dielectric layer

PDMS with dielectric constant of $\varepsilon_r = 2.5$ is a well-known hydrophobic material used in microfluidic devices based on EWOD [130,131,133] but the deposition process of PDMS layer has limitation of minimum thickness [134] the minimum achievable thickness of PDMS is 5-10 µm depending on the fabrication process and on the velocity of the spin coater, thus in order to validate the experimental results , the thickness of 10µm is selected for this work. Lippmann–Young equation shows the required applied voltage for different thickness of PDMS to obtain 4 different values of $\Delta\theta$. It is shown that with 10µm thick PDMS a high voltage (> 50V) is required to have 3º variation of contact angle or higher voltage (>100V) for $\Delta\theta$=10º. (See Figure 14)
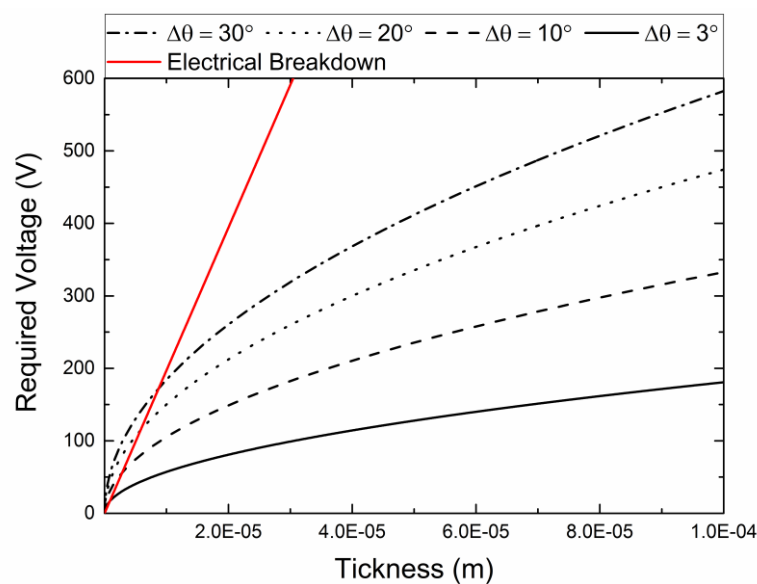
Figure 14 Lippmann–Young calculation for PDMS (Voltage vs. thickness)

For coating PDMS thin film, Sylgard 184 elastomer (Dow-Corning Corporation, USA) is mixed with its curing agent with rate 10:1 (wt/wt). After mixing, trapped air in the mixture is removed in vacuum for about 15min. The thickness of PDMS depends on the velocity of spin coater[134]. The thin layer of PDMS (10 μm) deposited on ITO layer was achieved by ramp acceleration of 1000rpm for 10s and 6000 rpm during 60 s, After that it is heated for polymerization at 155ºC for 7mins.
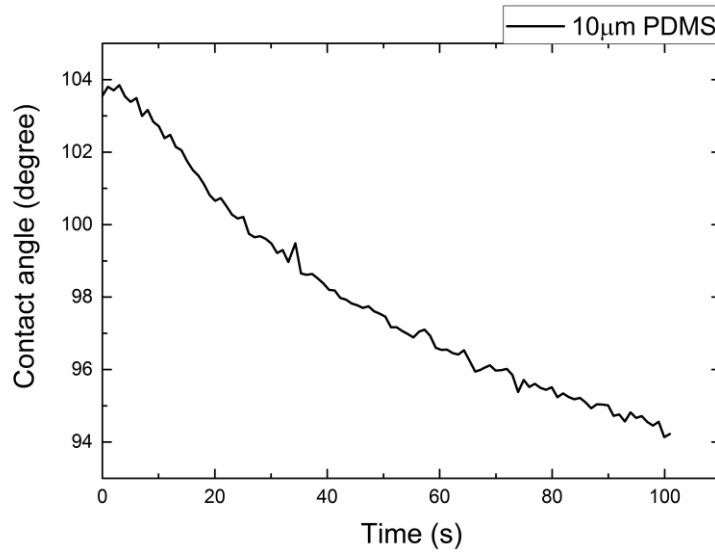
Figure 15 Experimental results of EWOD with PDMS as hydrophobic insulator for applied 100V

For validation of EWOD calculation the characterization of PDMS layer within EWOD phenomena was done with 10μL water placed on top of PDMS, variation of contact angle were captured by CAM200 , The results are shown in Figure 15, Applying -100V on a drop of water Δθ=10º was achieved. The experimental results validate the calculation done with Lippmann–Young equation.

3.2.2.2 SU8 negative photoresist used as dielectric layer

SU8 is commonly used as a negative photoresist for fabrication of microfluidic devices [132,135–138]. Lately, SU8-2 with dielectric constant of $\varepsilon_r \approx 4$ has been used in order to achieve thin dielectric layers. As the SU8 is hydrophilic, it is required to deposit an additional hydrophobic layer on top such as Teflon AF1600 (with dielectric constant of $\varepsilon_r \approx 1.93$). For Lippmann–Young calculation thickness of the hydrophobic layer is considered with 550nm.
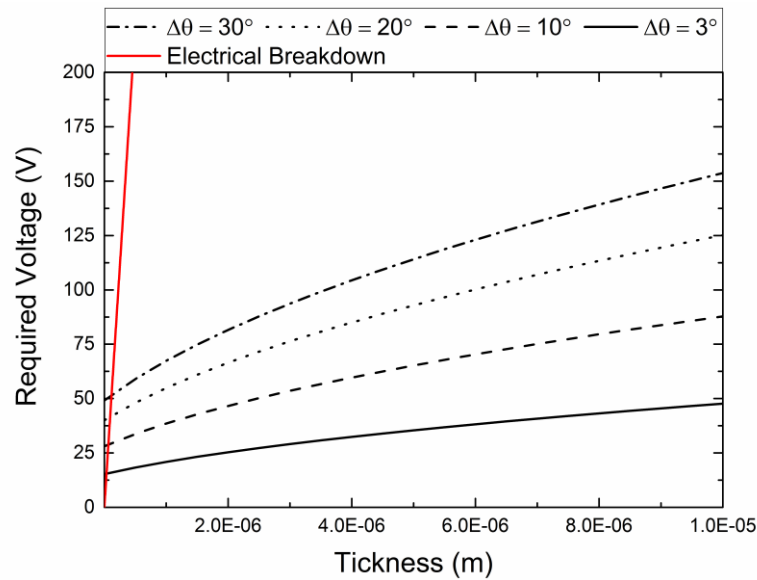
Figure 16 Lippmann–Young calculation for SU8 1.5μm and Teflon AF1600 550nm (Voltage vs. thickness)

Figure 16 shows that with a thickness of the hydrophobic layer of 550nm, in order to achieve a variation of contact angle of Δθ =3º a voltage of ≈15V is required. SU8 deposition is also limited by the velocity of spin coater and viscosity, the minimum achievable thickness of SU8 is ≈1.5μm. For a thickness of 1.5μm, in order to obtain a variation of contact angle, for example of Δθ= 20º, a voltage of V=55 V is required. In this work a dielectric layer of negative photoresist SU-8 2 from Micro ChemicalsTM, was spin-coated over the substrate with a ramp to a velocity of 500 rpm at 100 rpm/sec (5sec), then to 3000rpm at 1000rpm/sec for 60s. The layer is then pre-backed for 15min at 95ºC, then exposed to UV for 30s and post-backed on a hotplate for 30min at 95ºC resulting in 1.5μm robust SU8 layer. As it mentioned before SU8 is hydrophobic, it is required to deposit an additional hydrophobic layer upon SU8 layer. A 10% Teflon AF solution (DuPont) was spin-coated over a dielectric layer at 3000 rpm for 60s, giving 550 nm thick Teflon film with relative permittivity value of $\varepsilon_r \approx 1.93$. The film thickness was controlled by varying the concentration of the Teflon solution by diluting with Fluorinert FC-40 (DuPont). The Teflon deposited on substrate is heated for 6 minutes at 112 °C in air, then 5 minutes at 165 °C, in order to remove any residual solvent and improve the adhesion of the Teflon layer to the substrate. Finally it is baked for 15 min at 328 °C.
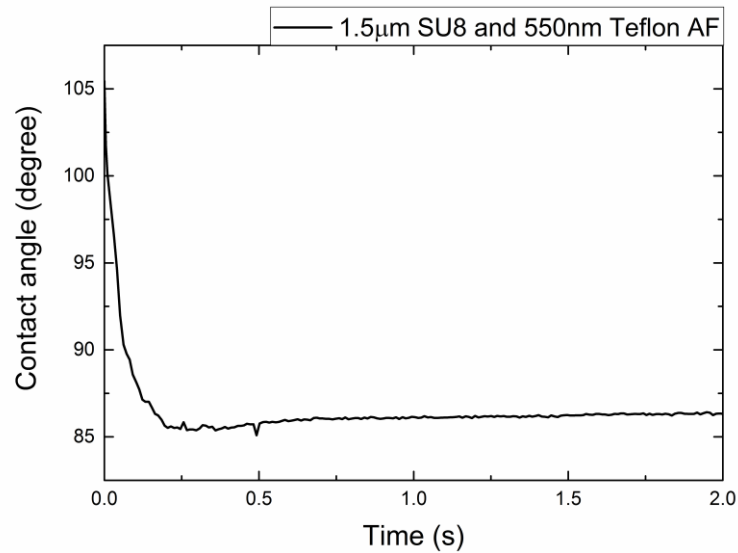
Figure 17 Experimental results of EWOD with SU8 as dielectric and Teflon AF1600 as hydrophobic layer

The experimental results of EWOD are shown in the Figure 17, where the time evaluation of the contact angle of 10µl water drop placed on top of a lens holder when a 55V voltage is applied. We were able to achieve a high variation of contact angle ($\Delta\theta = 20^\circ$) as was predicted. Still 55V is very high voltage for smart integration of liquid lens.

3.2.2.3 Highly robust dielectric layer of Alumina with high dielectric constant

The reduction of the applied voltage is a big challenge in the fabrication of micro-fluidic devices and liquid lenses. As it mentioned before, in order to reduce the applied voltage required it is necessary to have a very thin layer of dielectric plus a hydrophobic layer. According to our previous results , even with a very thin layer of SU8, high voltage is required to obtain $\Delta\theta=20^\circ$ hence, in order to have low voltage EWOD we need to reduce the thickness of the dielectric layer to nano-metric scale with higher dielectric permittivity. Alumina (Al_2O_3) is a good candidate as it is a transparent dielectric with high relative permittivity value ($\varepsilon_r \approx 9.8$). One of the reasons to select alumina as dielectric layer is that it is highly robust , preventing hydrolysis of water. Alumina was deposited by atomic layer deposition (ALD) technique. Atomic layer deposition (ALD) is a chemical vapor deposition technique based on sequential self-terminating gas–solid reactions. For about four decades it has been applied to deposit conformal layers of inorganic material with thicknesses down to the nanometer range. Figure 18 show the chemical vapor deposition process of Alumina.

$$Al(CH_3)_3(g) + 1.5\ H_2O(g) \rightarrow 0.5\ Al_2O_3(s) + 3\ CH_4(g)$$
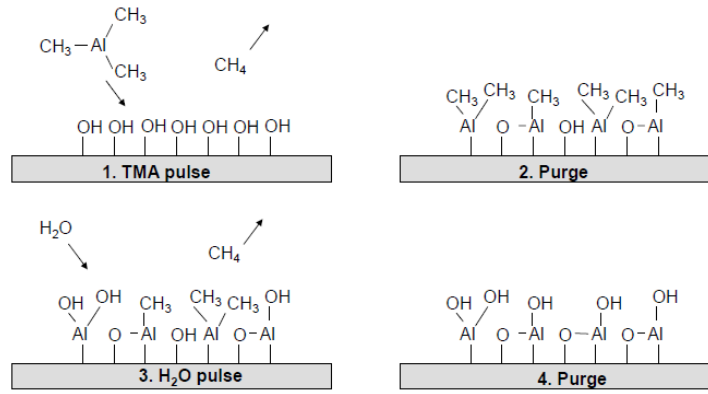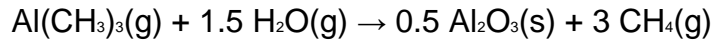
Figure 18 ALD Growth of Alumina

Alumina is also hydrophilic and thus is it necessary, like with SU8, to deposit a hydrophobic layer on top. The same thickness of Teflon (550nm) was considered. As illustrated in Figure 19 the minimum applied voltage is same as SU8 due to thickness and dielectric constant of the Teflon layer. For thickness less than 100nm of Alumina it is observed that the required voltage depends on the thickness of Teflon and the effect of the thickness of alumina on the applied voltage is negligible. Here alumina is working as robust protection barrier to avoid hydrolysis of water which in the next sections it is shown that the Alumina film will allow having a thinner layer of Teflon. According to Lippmann–Young equation in order to obtain $\Delta\theta=20^{\circ}$ a voltage of 40V is required, so lower voltage compared to SU8 and PDMS.
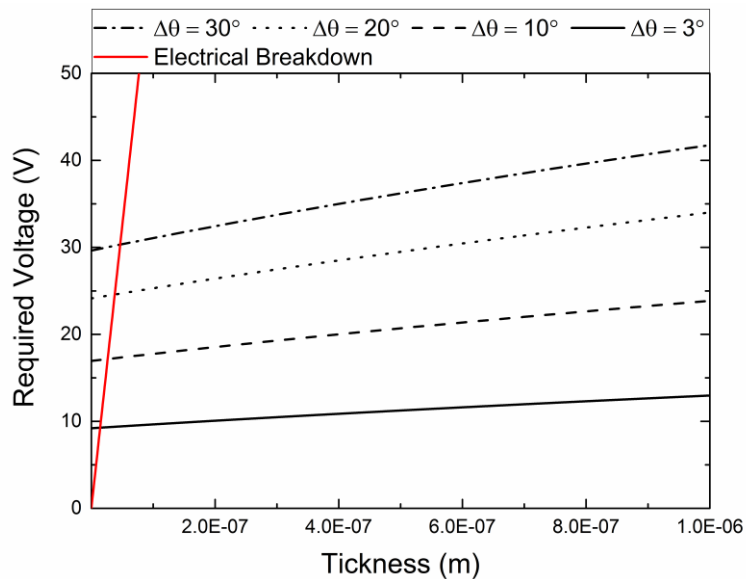
Figure 19 Lippmann–Young calculation for Alumina and Teflon AF1600 550nm (Voltage vs. thickness)

Following our calculation in order to validate the results, a 24nm thick Alumina was deposited on top of ITO, Then 550nm thick Teflon AF1600 was deposited as hydrophobic layer on top of alumina by spin coating process explained in the previous section. As illustrated in the SEM image (Figure 20) we were able to fabricate quite thin and uniform alumina layer.
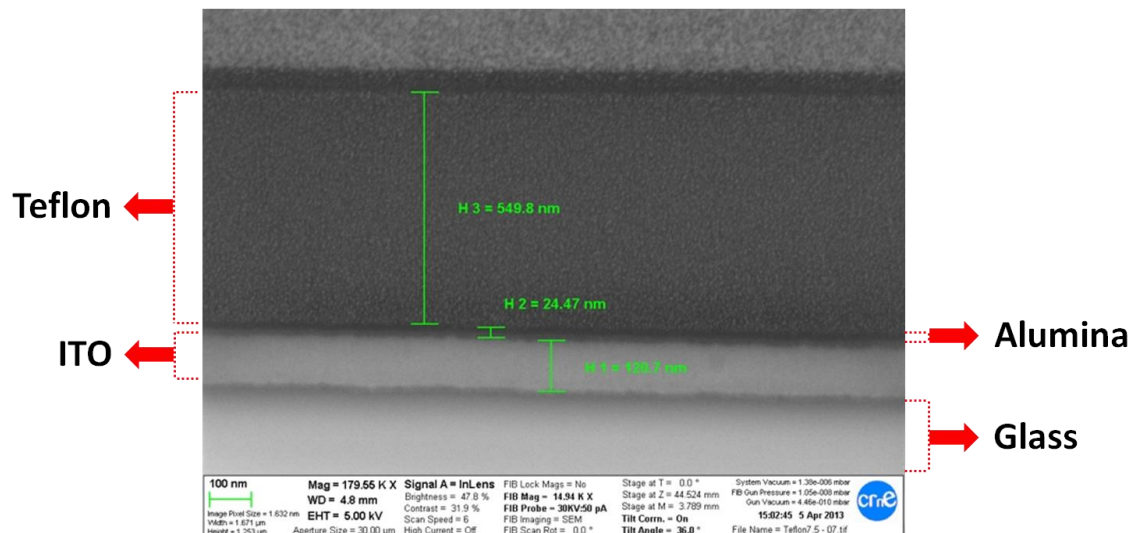
Figure 20 Cross view SEM image of liquid lens setup

By placing the holder on the goniometric device (CAM200) the change of contact angle of 10µl drop of water was captured by applying 25V and 40V as it is shown in Figure 21. High variation of contact angle ($\Delta\theta=20°$) was obtained with 40V and $\Delta\theta\approx10°$ was obtained with 25V. It was not possible to obtain visible change for lower voltage because of the thickness of Teflon layer. Thus next the hydrophobic layer of Teflon will be optimized in order to obtain lower voltage and highly reversible EWOD phenomena by using Alumina as dielectric layer.
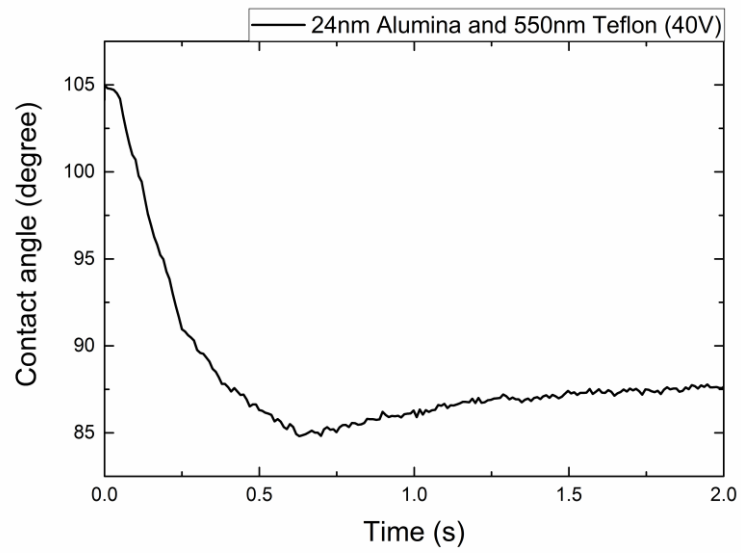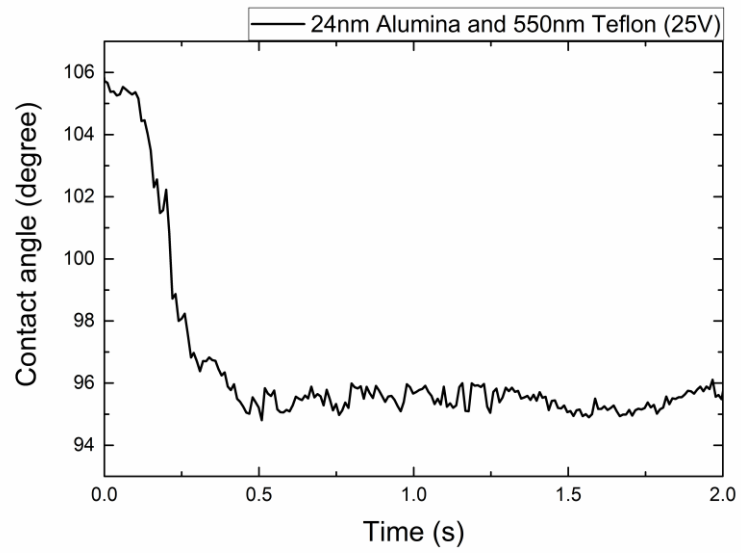
Figure 21 Experimental results of EWOD with Alumina as dielectric and Teflon AF1600 as hydrophobic layer

3.2.3   Improvement of Hydrophobic layer to obtain low voltage EWOD

As it described previously described using dielectric materials with high dielectric permittivity could also enable reduced voltage. However, it was found that this option is not practically viable, because the thickness of the hydrophobic layer plays an important role on the minimization of the required voltage. Using Alumina as dielectric layer we were able to reduce the applied voltage. In order to obtain even lower voltage for high variation of contact angle Δθ, it is required to also reduce the thickness of the hydrophobic layer. Using 24nm Alumina later the results are shown in Figure 22:
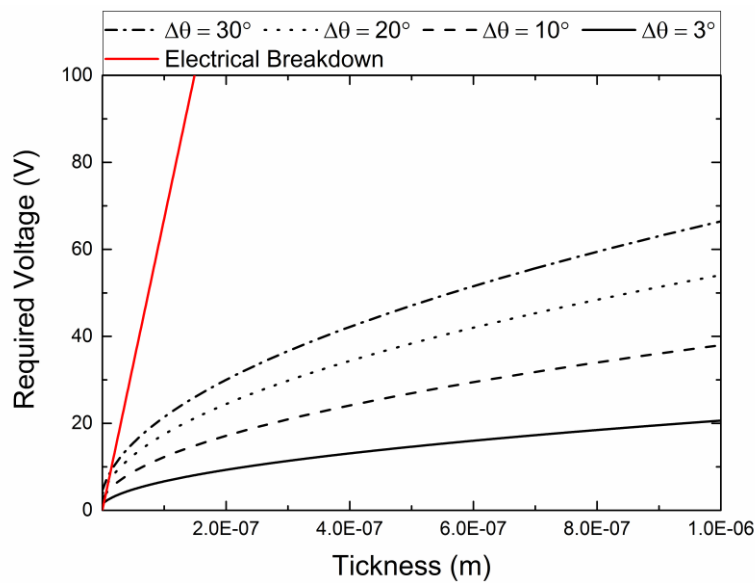
Figure 22 Lippmann–Young calculation for sample with 24nm Alumina and 200nm Teflon

As can be seen Δθ=30 degrees can be achieved at 25V with a 24nm thick alumina layer and 200nm Teflon layer. After several experiments we realized that even though low voltage EWOD is achievable the contact angle after removing voltage did not recover to the initial value because of degradation of the Teflon layer. By analyzing the surface morphology of Teflon, we observed that one of the critical problems is that the Teflon layer integrity is compromised when applying voltage on a distilled water drop, hence the wettability of surface will increase and it will also cause the hydrolysis of distilled water that will damage the hydrophobic layer and electrode. The results are shown in (Figure 23) where magnified pictures of the surface of Teflon before and after applying a 10V to a DI water droplet are shown. As it is illustrated by applying voltage the liquid starts to hydrolyze and create

bubbles inside liquid drop as can be seen the application of voltage has produced a surface degradation jeopardizing the reproducibility of the measurements.
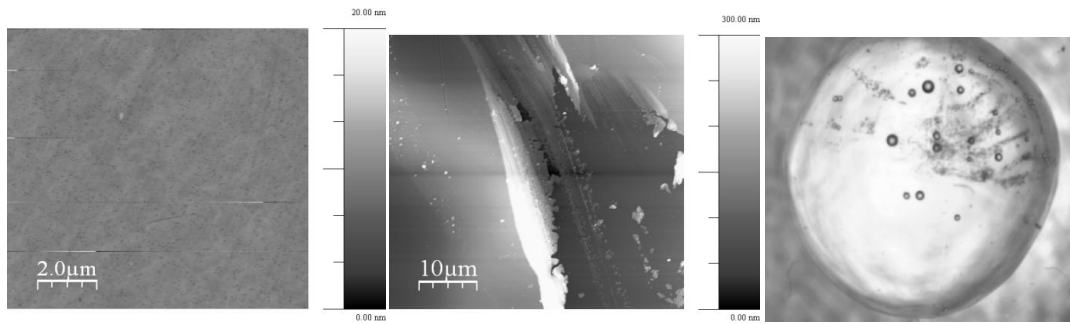
Figure 23 a) AFM image of Teflon 10% layer before applying 10V b) AFM image of Teflon 10% layer after applying 10V

Hence in order to have highly robust and low voltage EWOD with high reversibility further optimization of hydrophobic layer is mandatory in order to obtain low voltage EWOD. We have undertaken research on the deposition of HMDS thin film [139]. HMDS is a hydrophobic material widely used in microelectronics processing to improve adhesion of photoresist layers. HMDS was deposited by spin coating with a speed of 7000rpm, acceleration of 1000rpm/s for 60s in order to achieve very thin layer (the thickness of HMDS were considered negligible compared to the thickness of Alumina and Teflon). The HMDS layer helps to improve of the hydrophobicity of the Teflon layer by increasing the stability of the hydrophobic layer allowing us to deposit much thinner and robust Teflon layer (200nm). The effect of the adhesion promoter HMDS treatment on the hydrophobicity of Teflon layer is shown in Figure 24 where the values of the initial contact angle of water drop upon the surface was measured. As it is illustrated in Figure 24, the initial contact angle is improved by more than a 20%.
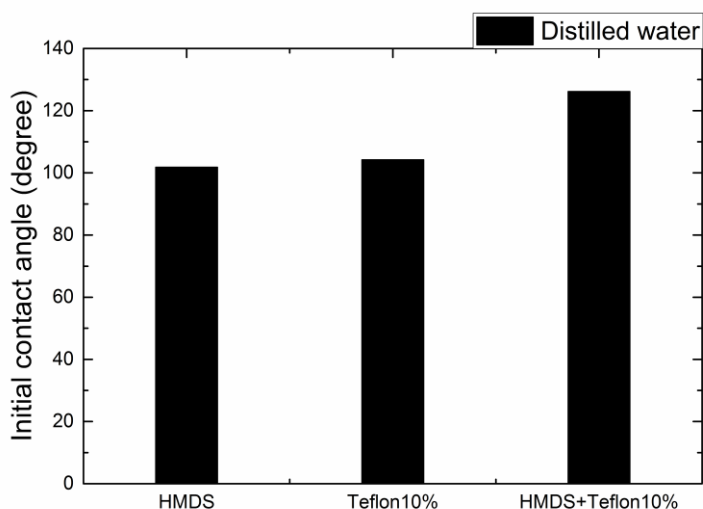
Figure 24 Initial contact angle of distilled water on different hydrophobic layers (only HMDS, only Teflon 10% and HMDS+Teflon 10%)

We have checked the reversibility of the contact angle change after applying voltage between 5 and 50V as shown in Figure 25 and Figure 26the contact angle variation 0.25º< Δθ < 37º and high recovery rate of more than 87% was obtained. In view of these results, we established as our baseline a substrate, a 100nm conductive transparent ITO, 24nm of Alumina layer, HMDS treatment and Teflon 10% for the rest of the experiments.
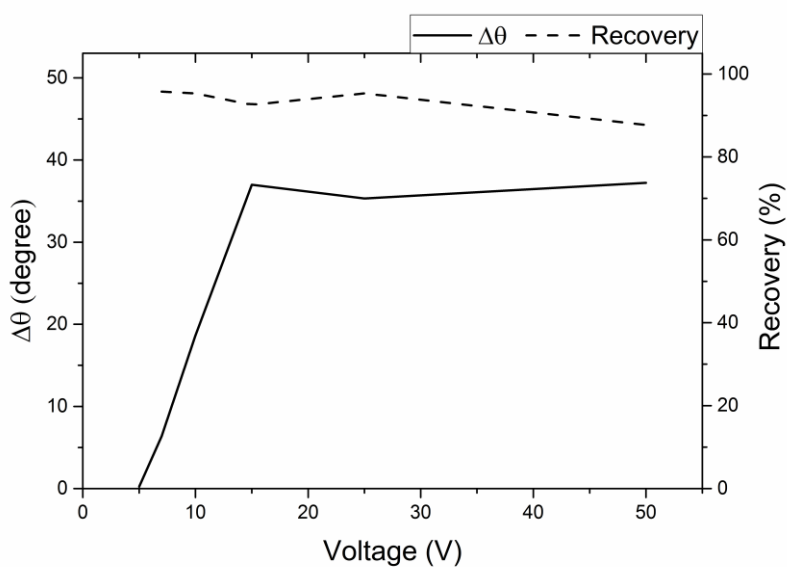
Figure 25 Variation of contact angle and recovery percentage depend on applied voltage
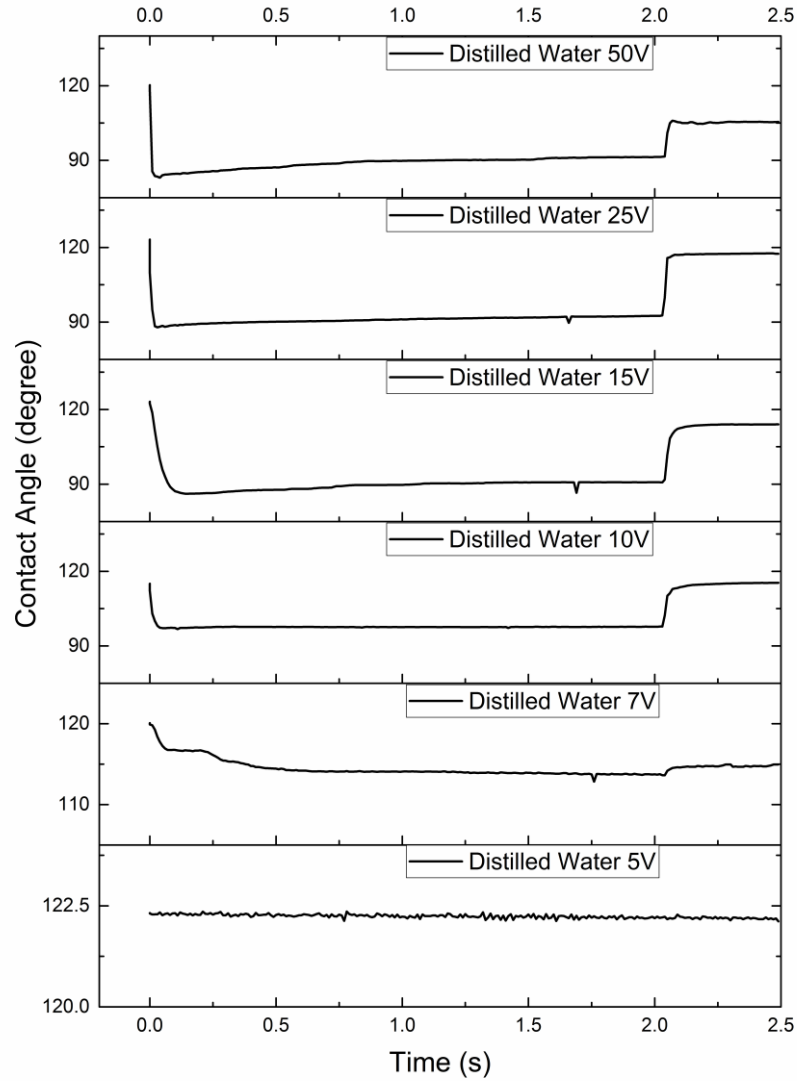
Figure 26 Variation of contact angle of water on protected hydrophobic by different applied voltage

3.3 Conclusion ad discussion

According to the Lippmann–Young equation, the thickness and the dielectric permittivity of the dielectric layer are the main parameters that can reduce the required voltage for EWOD (Table 4). As predicted, using materials with high dielectric constant and with thicknesses in nanometric range the required voltage to achieve high variation of contact angle ($\Delta\theta>20°$) is significantly reduced. Experimental results demonstrate quantifiably these effects. Even though we were able to reduce the voltage using alumina, we were not able to decrease the thickness of the Teflon layer because of breakdown voltage was reduced and physical defects appeared. HMDS has proved to improve the value of the initial contact angle

and the stability of the film allowing us to decrease the Teflon layer thickness and achieve lower voltage for EWOD. Quantitatively a high variation of contact angle ($\Delta\theta > 20°$) was obtained at 10V for a 100nm conductive transparent ITO, 24nm of Alumina layer, HMDS treatment and Teflon 10% of 200nm thickness.

Table 4 Working voltage for combination of different dielectric and hydrophobic layers

Reference	Dielectric layer	Hydrophobic layer	Required voltage(V)
[140]	Parlyene	Teflon	30-100
[3]	PECVD Oxide	Teflon	100
[141]	SiO2	Cytop	100
[142]	Parlyene	Teflon	85 Vac
[143]	Parlyene	Teflon	80
[144]	SiO2	Teflon	110 Vrms
[145]	SiO2	Teflon	45
[146]	Parlyene	Teflon	80-150
[147]	SiO2	Teflon	50-200
[132]	SU8	-	70
[148,149]	Alumina	Teflon	<15
[150]	Parlyene	Cytop	7.2-11.4
This work	Alumina	HMDS+Teflon	5-50

Chapter 4:

EWOD using nonaqueous liquids: dynamic response

4.1.1 Introduction

Following our study on optimization of bottom layer by improving the stability and hydrophobicity of Teflon layer and reducing the required voltage value by using thin and high dielectric constant material such as alumina, now we address in this Chapter an investigation on the conductive liquid to build EWOD liquid lenses. Water or water solutions (aqueous electrolyte) are commonly used in microfluific devices based on EWOD because of their simplicity, low cost, high electrical conductance, high surface tension and high contact angle on hydrophobic surfaces. However, the idea of EWOD liquid lens is to have high variation of focal length by applying as low voltage as possible. The use of water limits the implementation of liquid lenses because as several problems have been observed when they operate under applied voltage, such as corrosion of electrodes, electrolysis, bubbling, tendency to permeate through or swell numerous polymers, and ability to degrade some materials. Besides, water has a freezing temperature preventing its use in some outdoor electrowetting applications such as aerospace cameras or outdoors cameras. Moreover, as predicted by the Lippmann–Young equation, the contact angle gets smaller when the applied voltage increases until a certain saturation value is reached and when, the voltage is reversed to zero, the contact angle for water does not fully recover to the initial value. According to our measurements we observed that water loses its performance in long term cycling of liquid lenses (dynamic EWOD). All those problems have motivated the systematic research on non-aqueous liquids suitable for electrowetting applications. In the literature , several studies have been done on conductive liquids such as DMSO, Ehtylene Glycol, Formamide, γ-butyrolactone, N-metil formamide, etc[23]. and also, more recently, on room-temperature ionic liquids (RTILs) as electrolytes [151,152]. Among the aqueous/non-aqueous liquids proposed in the literature, we have concentrated on mixtures of two organic liquids: ethylene glycol, which was studied by Heikenfeld [23], and a liquid which is widely used in microfluidics and in printed electronic applications: glycerol. Ethylene glycol has a freezing point of -13°C and a dielectric permittivity of 37, by mixing with Glycerol with a dielectric permittivity of 42.5, the freezing point will reduce to -36.4°C and both have better conductivity than water. Ethylene-glycol and glycerol are known as polar liquids, both suffer from 2 issues: ethylene glycol is low in surface tension and glycerol has a too high viscosity. A mixture of those two components allows obtaining a workable electrowetting solution where surface tension is not too low and viscosity not too high. The mixtures of Ethylene glycol and Glycerol (Polar liquid mixture, PLM) are investigated as an alternative liquid for water because of their high surface tension and wide operating temperature as well we have
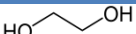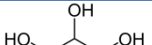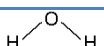
measured the initial contact angle, the dynamic change of the contact angle value after a given voltage is applied, the time response, the contact angle reversibility after the voltage is removed and the response of the liquid drop to a series of pulses of different frequencies.

4.1.2   Experimental results

4.1.2.1   Physical properties of polar liquid mixture

The liquids we have used in our experiments, are five different homogeneous mixtures of polar liquids (PLM): ethylene glycol and glycerol (Table 5) using 10mL solvent (Ethylene Glycol) and several amounts of glycerol (7.5mL, 5.824, 5mL ,4.146mL ,3.333mL , 2.5mL , and 1.25mL), resulting in glycerol percentage of 42.86%, 36.84%, 33.33%, 29.25%, 25%, 20%, 11.11% respectively.

Table 5 Polar liquids and their properties

Name	Structure	Surface tension (mN.m⁻¹)	Conductivity (µS/cm)	Reflective index (n)	Miscibility with Water
Ethylene Glycol	HO⌒⌒OH	47.7	1.07e-6	1.43824	Yes
Glycerol	HO⌒⌒OH (OH)	64	0.064	1.4722	Yes
Water	H⌒O⌒H	75.64	0.01	1.333	Yes

As the liquid used for EWOD liquid lens need to be conductive and transparent, the conductivity of different mixtures has been measured using a conductometer. As it is illustrated in Table 5 the conductivity of polar liquids are much higher than that of water. Moreover the transparency of the liquid in the visible range is an important factor for liquid lenses. In Figure 27 the refractive index of the PLM mixture and conductivity are plotted as a function of the percentage of the mixture. The value of the refractive index is similar to water but it has higher electrical conductivity.
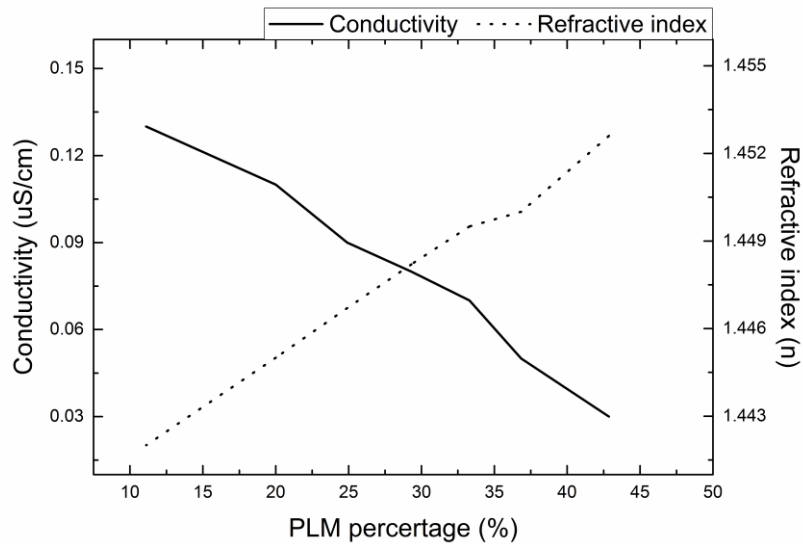
Figure 27 Refractive index and conductivity of different mixture of PLM

The experimental studies reported in this chapter were carried out using samples that were fabricated following the process described in chapter 2. First a 96.7 nm thick indium-tin oxide (ITO) layer was sputtered on a glass substrate as the bottom electrode. After that, a 25 nm thick alumina (Al_2O_3) was deposited by an Atomic Layer Deposition (ALD) system. Before depositing a Teflon layer, we deposited an HMDS layer by spin-coating at 3000 rpm and then we typically completed the surface treatment by another spin-coating at 3000 rpm for 60s of a 10% Teflon AF solution (DuPont), resulting in a 200 nm thick film. The enhancement of the hydrophobicity and stability of the Teflon layer, the initial contact angle of drops of PLM mixture were also improved. This can be seen in Figure 28 where the initial contact angle of PLM 33.3% was compared to that of water before and after optimization of the hydrophobic layer.
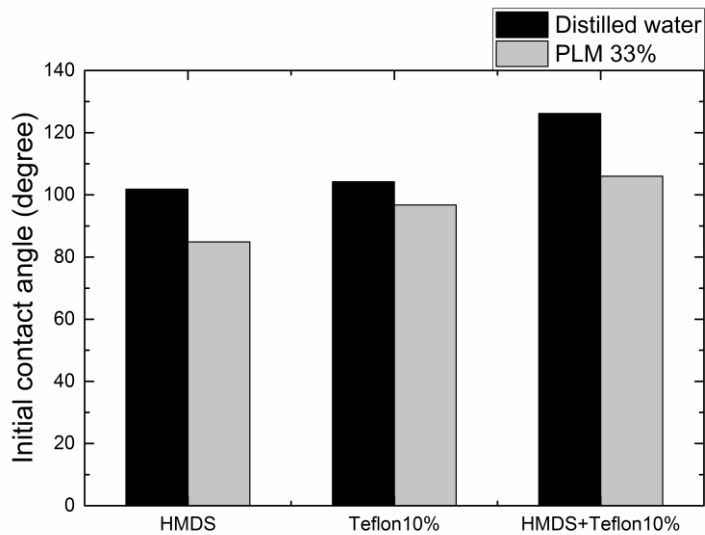
Figure 28 Initial contact angle of selected PLM33.3% and water before and after optimization of hydrophobic layer

The initial contact angle of PLM mixture measured by CAM200 equipment is shown in Figure 29. The values are in the range between 101.7º and 106º slightly increasing with the glycol concentration. The contact angle of water was between 115º and 123º. These results show that by improving hydrophobicity of the surface, a high contact angle of 105.998º has been achieved for the largest glycerol concentration used in our experiments (PLM 33.3%). That is comparable to 104º for water on Teflon according to the datasheet.
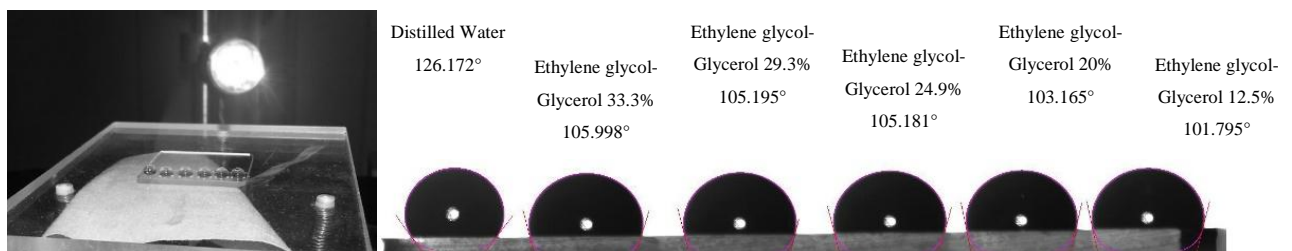
Figure 29 Side pictures of liquid droplets. Number (1) shows the water Initial contact angle, which is 126.17º. The values for the PLM mixtures (2-6) are detailed in Table 6.

4.1.2.2 Electrowetting characterization of polar liquid mixture

Experimentally parameters such as initial contact angle, variation of contact angle, recovery percentage, and fall time for different mixtures of PLM have been investigated. The summary of all experimental results are shown in Table 6. All electrowetting tests were done by applying -15V on 10μl droplets. With the PLM mixture we obtained a high variation of contact angle $\Delta\theta > 28°$ which is significant even for this moderate value of voltage. As it is observed, the initial contact angle increases as the glycol contents is increased and similar behavior is observed for the variation of contact angle $\Delta\theta$, the recovery percentage and fall time. The recovery percentage was calculated as the ratio of the final stable recovered contact angle divided by the initial contact. As well we estimated the fall time as the time lapse between the 10% and 90% of the total angle change. The definition of delay time, response time, falling time and variation of contact angle is shown in Figure 30. Our measurements were performed using a time step of 10ms and in the lower contents of glycol the fall time was smaller than the time resolution of the equipment.
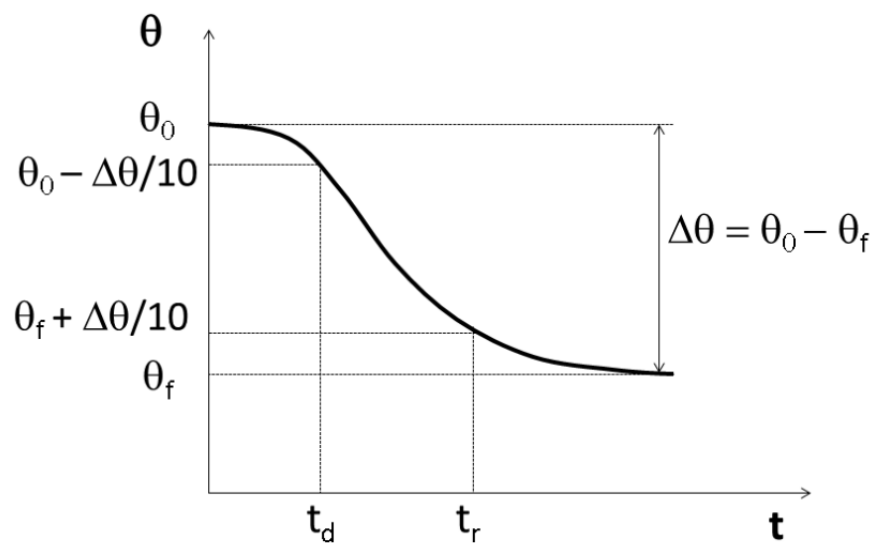
Figure 30 Definitions of the delay time t_d, the time to respond, t_r, and the difference between t_d and t_r called falling time

Table 6 Conductivity and electrowetting measurements for several mixtures of Ethylene glycol and Glycerol for 15 V of applied voltage.

Liquid Material	Viscosity (cP)	Initial contact angle (deg.)	Contact angle change (deg.)	Fall time*(s)	Contact angle recovery (%)
PLM 11.11%	37.3	101.7945	15.131	0.01	92
PLM 20%	60.2	103.1655	9.65	0.08	93
PLM 25%	65.4	105.181	12.841	0.095	95
PLM 29.25%	73.7	105.1955	12.2105	0.08	95
PLM 33.3%	92.8	105.9975	20.4195	0.06	97
PLM 36.84%	94.2	103.808	7.033	0.048	95
PLM 42.86%	120.6	96.879	6.869	0.06	91

* Estimated as time step of measurement was 0.01s

By a preliminary test on different mixtures of PLM we observed that PLM-33.3% gives better performance than the other mixtures, Even though the fall time is longer, it has a significant variation of contact angle with the low voltage of 15V and high recovery of 96.13% . This makes this mixture a suitable alternative instead of water for EWOD micro-devices. In Figure 31 full EWOD characterization for a 10µl PLM-33.3% droplet is shown by applying different voltage values namely 5V, 7V, 10V, 15V, 25V and 50V and compared to a full transient measurement of the contact angle of 10µl water. The transients shown are a sequence of applied voltage on the OFF_ON switch mode followed by an ON_OFF switch after 2 seconds.
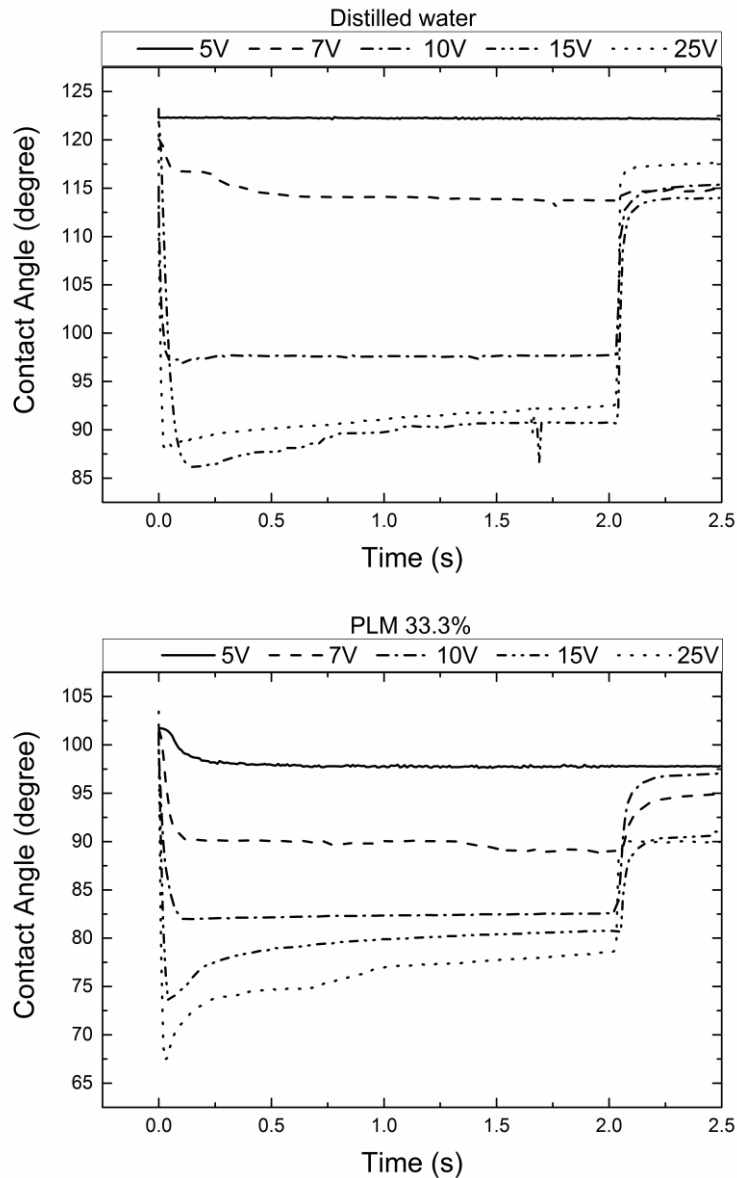
Figure 31 Transient contact angle by applying a step voltage of OFF-ON-OFF for 2s with 5V, 7V, 10V, 15V, 25V to water 10μl and PLM 33.3%.

Once the voltage is applied, we observe that the transient exhibits a sharp drop of the contact angle value. In the case of higher voltages, an overshoot is observed followed by a stabilization phase towards a steady state value. Also the variation of contact angle when 5V are applied for water is negligible whereas PLM-33% shows a variation of $\Delta\theta\approx4^{\circ}$. Full electrowetting characterization of PLM- 33.3% and water by different applied voltage is shown in Table 7. We summarize our results for the contact angle change, fall time and contact angle recovery percentage for both water and PLM-33.3%. We observed that by applying low voltage V<15V, with PLM as liquid we obtained higher variation of the change of contact angle (ex. For 10V , $\Delta\theta\approx20^{\circ}$) compared to water, thus in terms of the variation of

the contact angle, the PLM at voltages less than 25 V gives better performance than water. The fall time decreases as the voltage is increased, although this has to be taken cautiously, as in the larger voltages the transient has an overshoot and then the relevant figure should be the settling time (time required to reach the steady state value) instead of the fall time. Taking into account the different values of the initial contact angle, Table 7 also shows the percentage recovery. As can be seen a recovery greater than 85% is observed in all cases and the PLM recovers quite similarly to water.

Table 7 Summary of electrowetting measurements for distilled water and 33% mixture of ethylene glycol and glycerol for several values of applied voltage.

Liquid Droplet	Voltage (V)	Contact angle change (deg.)	Fall time*(s)	Contact angle recovery (%)
Distilled Water	5	0.24	-	-
	7	6.35	0.17	95.74
	10	18.63	0.11	100
	15	36.99	0.15	92.57
	25	35.33	0.04	95.32
	50	37.23	0.03	87.71
Ethylene glycol-Glycerol 33%	5	3.83	0.43	96.12
	7	11.66	0.33	93.40
	10	19.48	0.12	95.71
	15	27.21	0.03	95.51
	25	35.95	0.03	86.97
	50	37.78	0.01	86.82

According to the Lippmann–Young equation the plot of the ($\cos\theta$-$\cos\theta_0$) value is shown in Figure 32, where θ is the contact angle at the steady state (taken at a time t= 2s just before the voltage is removed), and θ_0 is the initial contact angle value. The values are plotted as a function of the applied voltage V. The logarithm of the Lippmann-Young equation can be written as:

$$log\ (cos\ \theta - cos\ \theta_0) = log\ \frac{\varepsilon_0 \varepsilon_r}{d\gamma_{lv}} + 2\ log\ V \qquad [16]$$
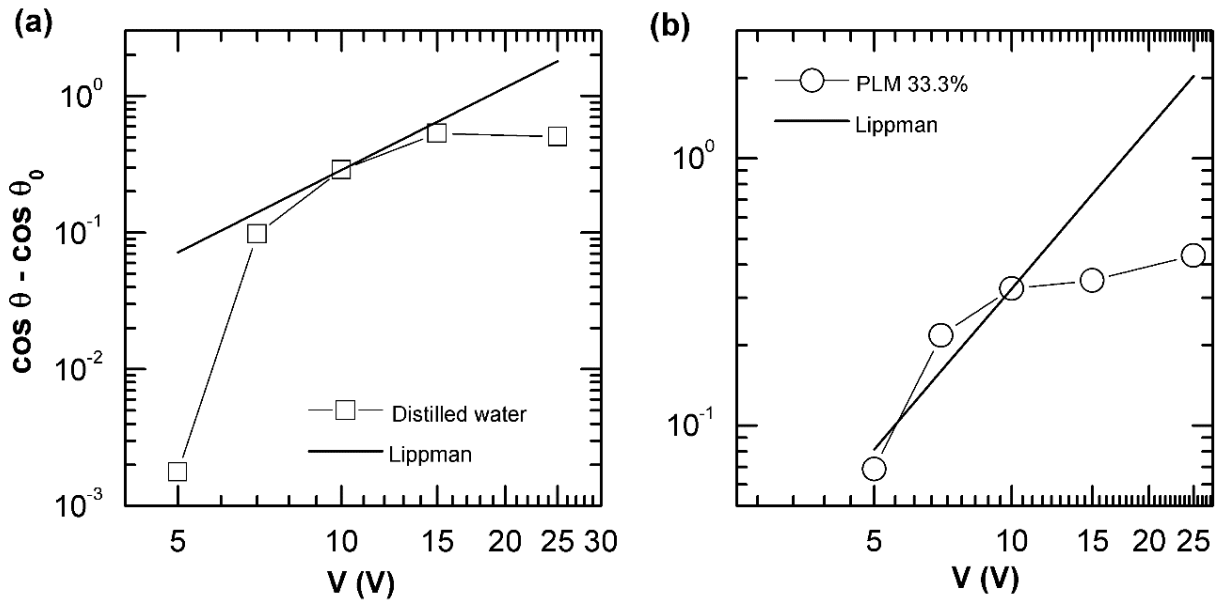
Figure 32 Plot of the value of the difference (cos θ-cosθ0) as a function of the applied voltage for: (a) water, and (b) ethylene glycol-glycerol 33.3%.

Where d is the thickness of the dielectric, γ_{lv} is the surface tension, ε_0 is the vacuum permittivity ε_r is the relative permittivity of the dielectric layer and V is the applied voltage between the droplet and the substrate. It is clear from Equation 16 that the value of the slope of the plot of log (cos θ - cosθ$_0$) as a function of log V should have a value of 2. Our best fit of the Lippmann -Young equation in Figure 32 in the range where it holds in the experiments, gives us a value of the electrowetting number is equal to 3.25e-3 for the PLM33.3% and 5.23e-3 for water. We also see that the contact angle saturation is reached for voltages between 10V and 15V in all cases.

4.1.2.3 Cycling EWOD properties of PLM droplets

The reliability is the ability of a the device to keep its performance and maintain its initial physical properties, such as initial contact angle and variation of contact angle after a set of tests and even long term testing. For a liquid lens, the reliability may be evaluated by the measurements of the stability of the response after switching the applied voltage on and off several thousands or millions of times. The cycling EWOD experiments were performed using a square signal of a given amplitude and frequency. We have registered the contact angle when a 10V amplitude, 2 Hz (Figure 33a) and 5 Hz (Figure 33b) frequency were applied. We can observe that for frequency of 2Hz the PLM-33.3% shows an initial contact angle degradation in the first few cycles but after that it reaches a regime of almost constant amplitude and stability. On the other hand, water for the first few cycles shows high

performance and high variation of contact angle with high recovery but after a few cycles significantly degrades. By increasing frequency to 5Hz, in both cases it is observed that we are above the higher cut-off frequency and the liquid does not reach the maximum variation of contact angle. The PLM-33.3% mixture shows periodic behavior. This would mean that the cut-off frequency of the system explored in this work is in the range of 2 to 5 Hz for 10μl droplets.
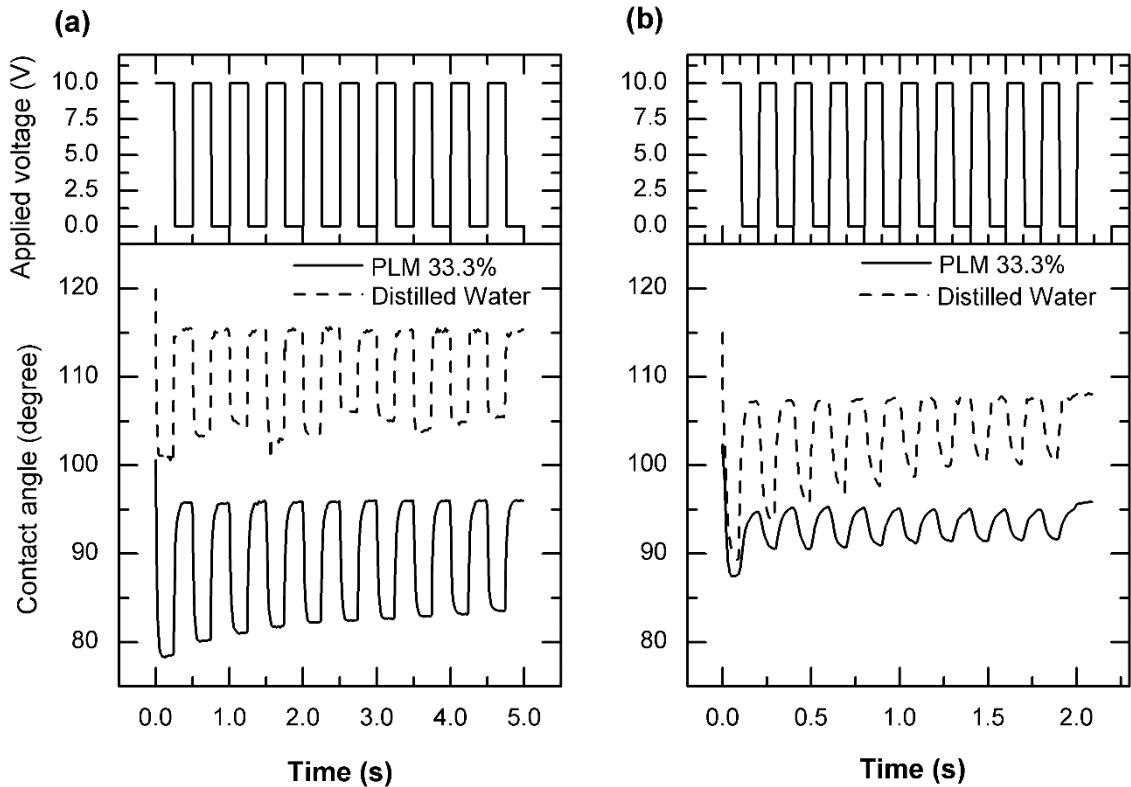
Figure 33 Dynamic EWOD measurements on water and ethylene glycol-glycerol 33% for: (a) 2Hz and (b) 5Hz 10V amplitude signal

In order to verify the reliability of the transients during long cycling experiments of the applied voltage, we have registered up to 1000 cycles of 10 V amplitude frequency of 2Hz signal for both distilled water and PLM -33.3% droplets. This is illustrated in Figure 34 .As can be seen for water a significant drop in performance is seen and after some 100 cycles and after that the variation of contact angle drops to almost zero. On other hand PLM-33.3% droplet, although a performance loss is observed after the first 30 cycles it reaches a steady regime with an stable approximate variation of contact angle of 10 degree.
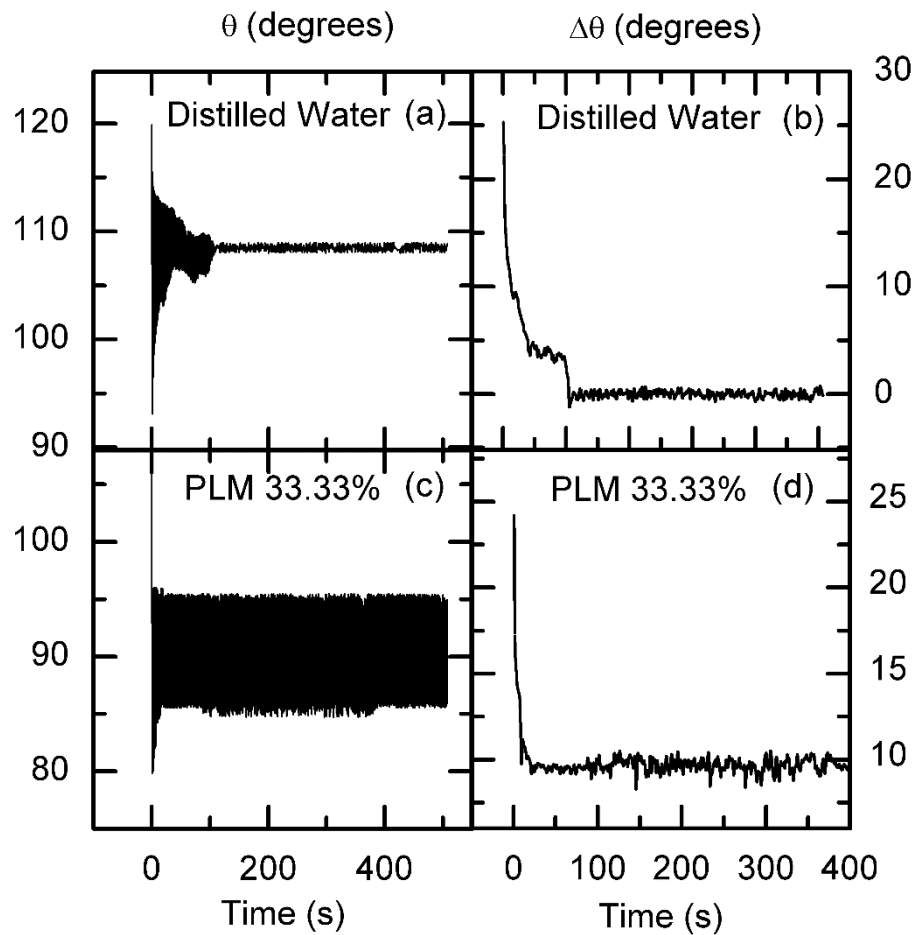
Figure 34 Applying 1000 cycles of 10 V amplitude signal to both distilled water and PLM 33.3% samples

The periodic behavior of PLM-33.3% droplet compared to the non-periodic behavior of water was verified as well by applying a staircase up and down voltage ramp. With this technique we were able to characterize liquid behavior more precisely. The ramp voltage was applied from 0V to 50V with 2V steps every 50ms. The measured change of contact angle in the up-staircase regime shows that both water and PLM-33.3% droplet follow closely the change of the applied voltage but in the down- staircase regime, the water droplet shows a time delay on the recovery response that could be explained as a sort of memory effect On the contrary the PLM-33.33% droplet fully recovers without significant delay. The memory effect could be explain by effect of the leak resistance and the charge build up in the dielectric [87,88], to insulating fluid charge to instabilities, to micro-droplet ejection and to gas ionization[89–91].
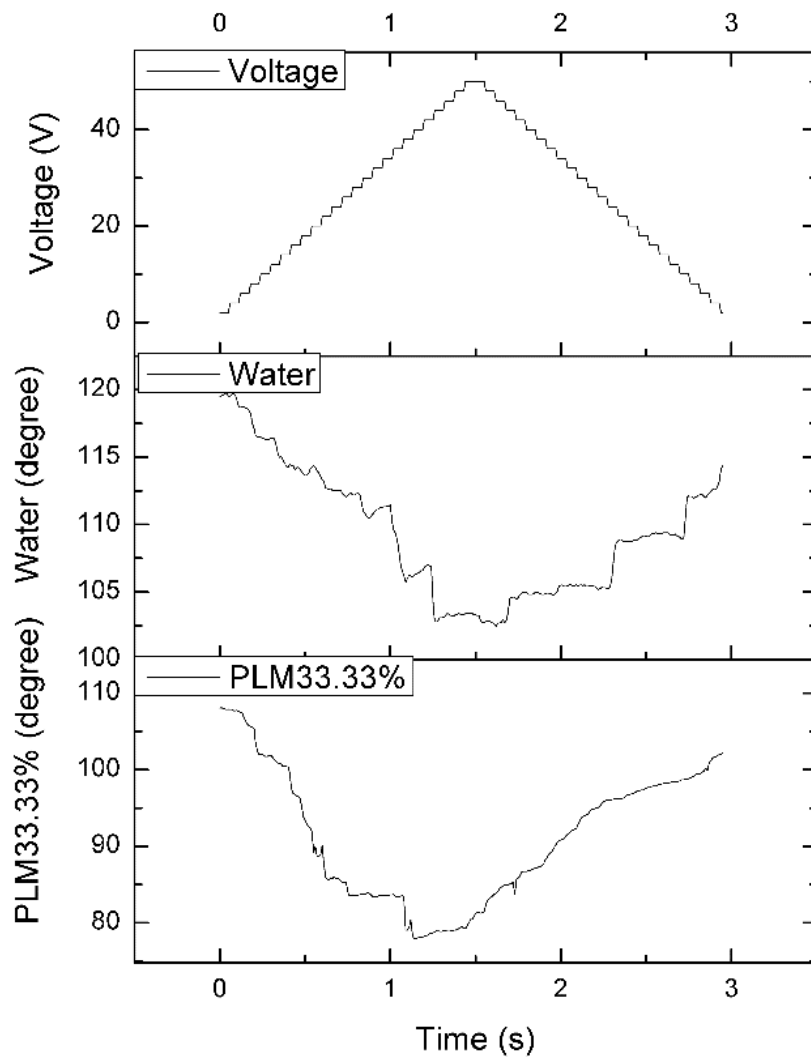
Figure 35 Staircase up and down voltage ramp and dynamic recovery of the DIW and of the PLM33.3%

By the simultaneous measurement of the applied voltage and of the electrical current during the applied staircase up and down voltage ramp, the PLM-33.3% droplet shows a typical capacitive behavior contrary to the water droplet. This can be the reason for th different staircase behavior.
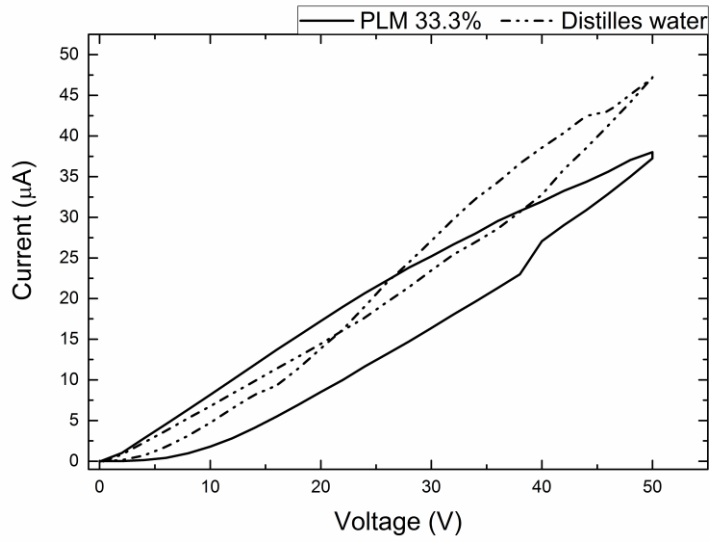
Figure 36 Electrochemical characterization of Water and PLM33.3%, applied voltage versus measured current

Theoretically ideal capacitor can be defined as Equation 17, here v is equal to $\frac{dV}{dt}$:

$$Q = C.V \quad \blacktriangleright \quad I = C.\frac{dV}{dt} \qquad [17]$$
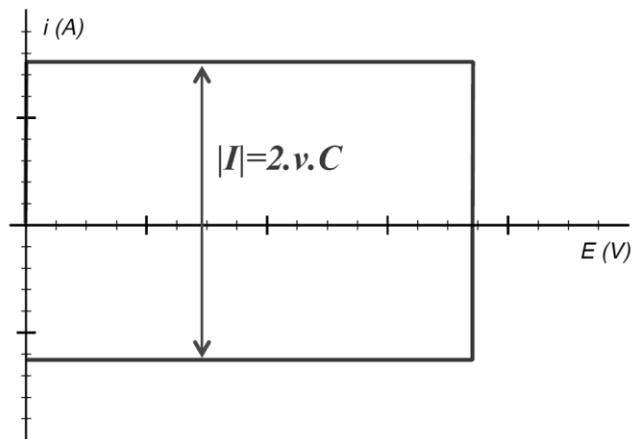
Figure 37 ideal capacitor

Capacitors with leak resistance are defined as:

$$I = C.\frac{dV}{dt} + \frac{(V_0 + \frac{dV}{dt}.t)}{R_f}, \tan a = \frac{1}{R_f} \qquad [18]$$
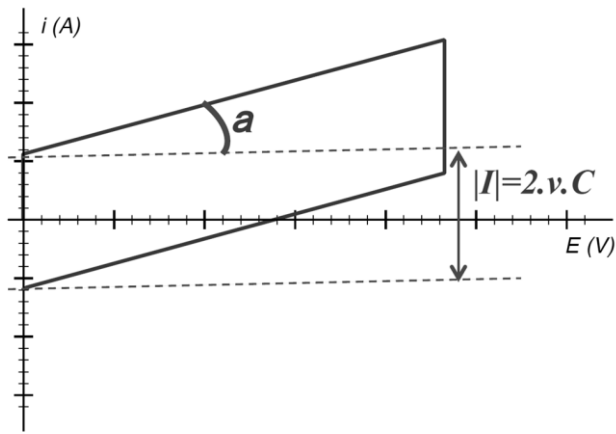
Figure 38 Capacitor with leak resistance

And real capacitor is defined as:

$$I = C.\frac{dV}{dt}.\left(1 - e^{\left(\frac{-t}{R_{s}.C}\right)}\right) + \frac{\left(V_0 + \frac{dV}{dt}.t\right)}{R_f} \qquad [19]$$
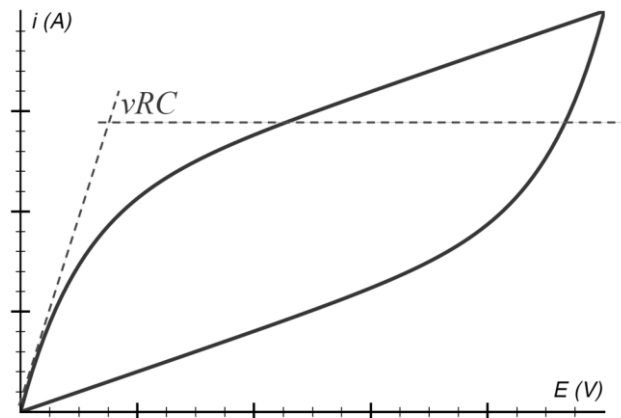
Figure 39 real capacitor

As the results the leak resistance for PLM drop is equal to 1.313Ω and the equivalent capacitor measured by applying staircase voltage is equal to 226.4nF.

4.1.3   Conclusions and discussion

In this chapter we report on the characterization of the polar liquid mixtures as liquids for elctrowetting lenses and compare the results with that of distilled water. We have used an alternative optimized polar liquid mixture (PLM) (Ethylene glycol and Glycerol) and we have characterized the physical properties of PLM mixture such as the elctrical conductivity, the refraction index. We have done experimental electrowetting characterization of the initial contact angle, and os the contact angle after different voltages were applied. Our best results were obtained using a PLM of 33% having a high initial contact angle value of $\approx 106°$. With the optimized electrode material layers we find significant electrowetting for low voltage for example a high change of contact angle value of $19.48°$ when $10V$ were applied in comparison to $\Delta\theta = 18.63°$ for water. We have shown that the PLM-33.3% mixture can be an alternative to water in terms of contact angle change, time response and recovery. Additionally it shows stability after 1000 cycle of switching voltage with periodic variation of contact angle and capacitive behavior.

Chapter 5:

Potential of superhydrophobic FDTS for EWOD

5.1.1 Introduction

In previous chapters we have described our work on low voltage electrowetting. Recently the interest on using superhydrophobic layers in a variety of industrial applications, such as anticorrosive protective coatings, microfluidics (microchannels and reactors, lab-on-a-chip devices and biomedical devices) [153–155] , self-assembly of particles [156,157] and self-cleaning surfaces, such as window glasses [158], paints, and fabrics, green engineering [159], marine fouling [160], anti-icing surface [161,162], drag reducing surfaces [163], increased significantly. Among the superhydrophobic materials, 1H,1H,2H,2H-perfluorodecyltrichlorosilane (FDTS) is widely used in MEMs applications and microfluidic devices[164,165]. By reducing significantly the thickness of the hydrophobic layer combined with the use of ultrathin dielectric later with high dielectric permittivity, should lead to an increase of the initial contact angle value and to achieve a large change of the contact angle even at modest voltages. FDTS has a long chain and forms nanometer scale clouds leading to ultrathin (nanometer scale) superhydrophobic layers which have great potential to be used as alternative to Teflon [157]. In this chapter we describe experiments aimed to (a) assess the superhydrophobicity of FDTS layers in structures suitable for EWOD, that is to say on top of ITO transparent electrodes covered by a thin dielectric layer (alumina in this Chapter following the experience gained in previous chapters), (b) to check the recovery of the contact angle after electrowetting and (c) to examine the integrity of the FDTS layer in EWOD operating conditions for electrowetting applications. Furthermore we have discovered conventional contact mode EWOD cause degradation of FDTS layer which lead to hydrolysis of liquid hence here for the first time we have presented contactless EWOD on superhydrophobic layer of FDTS.

5.1.2 Experimental results

5.1.2.1 Fabrication

Based on Chapter 2 the fabrication process started by the sputter deposition of a conductive transparent layer of ITO with a gap distance between substrate and target of 13cm a power of 50W for 45min. Typically 100nm thick layers of ITO were obtained. The fabrication process is shown in Figure 40 In order to have contact with the ITO layer a first photolithography step to pattern the ITO has been carried out by spin coating of a photoresist on top of ITO, thermal curing , UV exposed and etch as shown in Figure 40-2. A 24nm thick

alumina layer is then deposited by ALD and then the FDTS monolayer is deposited. The final step is to open window for the ground electrode using a lift-off step.
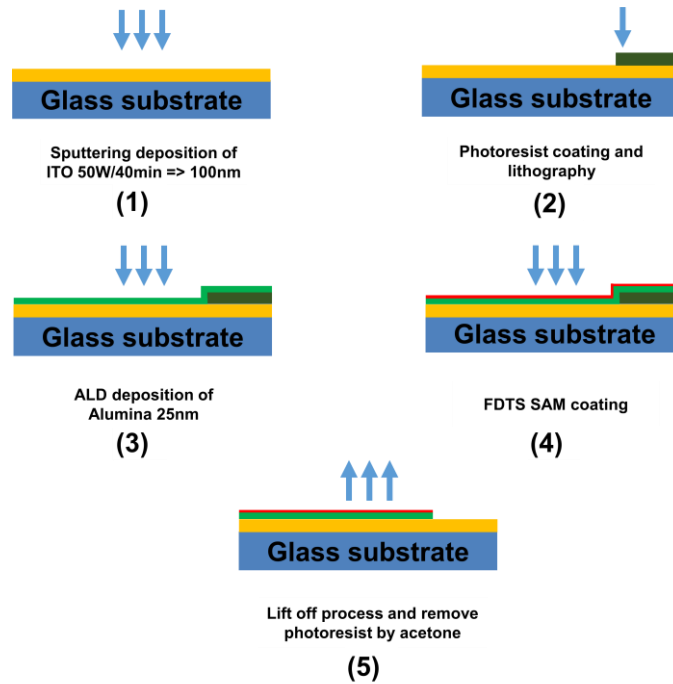
Figure 40 fabrication steps of liquid holder for appying EWOD

The deposition step of the FDTS layer is illustrated in the Figure 41 First a reaction of perfluorodecyltrichlorosilane with water is performed to form hydroxyl groups and HCl as by product followed by the deposition of the self-assembled hydroxyl chain on the substrate. In order to achieve superhydrophobic layer it is required to the liquid source in the first step to be heated at 100ºC otherwise it will form FOTS. At the end of the procedure 4nm thick FDTS layer was obtained (This deposition was performed at the Laboratory of National Institute of Advanced Industrial Science and Technology (AIST) Japan.
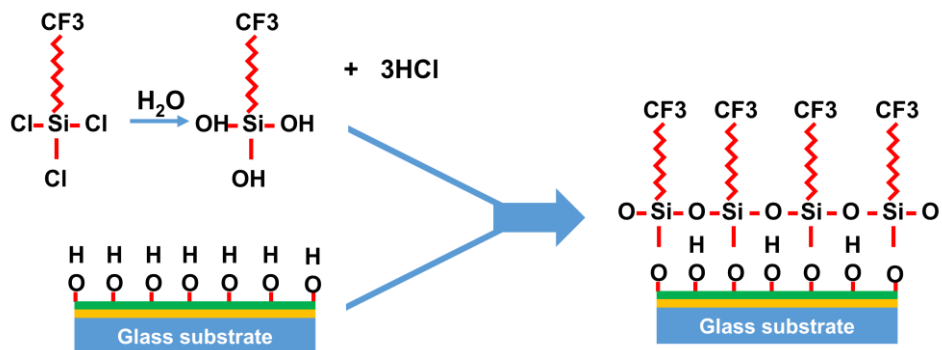
Figure 41 FDTS deposition steps

Perfluorodecyltrichlorosilane (FDTS), usually form densely packed monolayers by horizontal polymerization. The desired hydrophobic properties are obtained typically by coating a substrate with SAMs of trifunctional silanes to form by horizontal polymerization densely packed monolayers with low energy. The concentration of water inside the chamber plays an important role. If the concentration of water is low the rate of reaction is low causing formation of hydroxyl whereas if the concentration of water is high it causes non-homogeneous deposition and high aggregation rate of FTDS.

5.1.2.2 Hydrophobicity and effect of roughness

As illustrated in Figure 42 the surface of the FDTS layer is a combination of micro and nano scale roughness. An increase of roughness has direct relation with wettability of surface, if the surface has low surface tension, increasing the roughness will increase the hydrophobicity of the solid layer. The hydrophobicity and contact angle of a 10µl drop of liquid were measured by a goniometric device (CAM200). Two types of liquid were compared: water and a mixture PLM-33.3% (see chapter 3), the liquid were placed by a vertical syringe on top of FDTS surface.
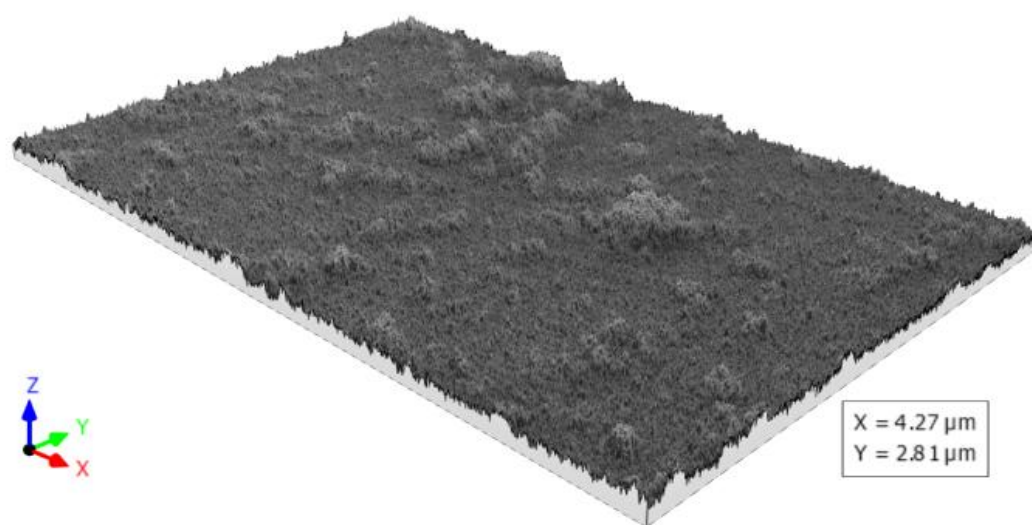
Figure 42 3D image of FDTS layer

In Figure 43 the initial contact angle for both water and PLM-33.3% were measured giving a high initial contact angle value of 165.68º for water and 148.26º for PLM-33.3%.
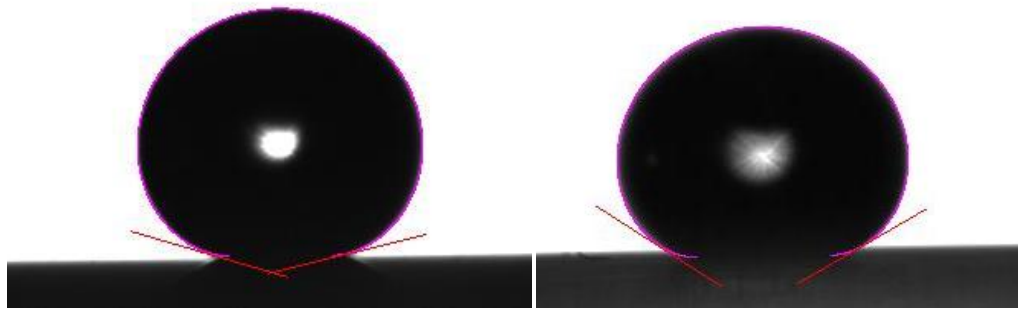
Figure 43 Initial contact angle of water 165.68º , PLM33.3% 148.26º

In the SEM image shown in Figure 44 we observed that the deposition process of the FDTS layer with SAM technique creates a cloud of nanoparticles in the surface increasing the roughness and reducing the wettability of the surface [166–170]. The cleaning of the surface from nanoparticles, was performed by soaking the sample inside acetone and applying ultrasonic bath for 1min, washing with distilled water and drying in the oven with nitrogen flow of 2sccm. A significant percentage of the nanoparticles cloud were washed out (Figure 45), so the cleaning process reduced the roughness of the surface thus , considering Wenzel-Cassie theory, the wettability of surface should be increased and the contact angle reduced.
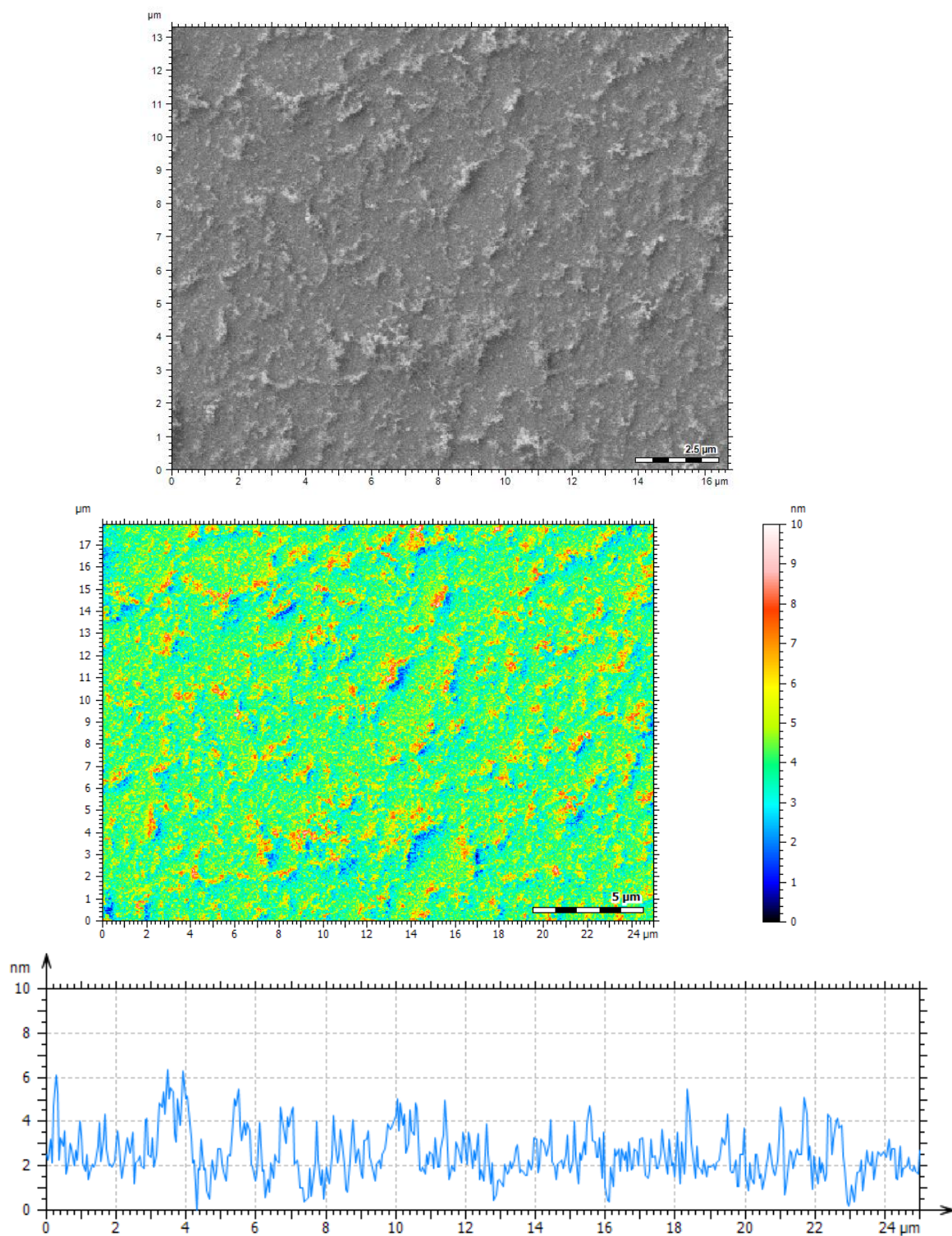
Figure 44 Surface characterization of FDTS before cleaning process
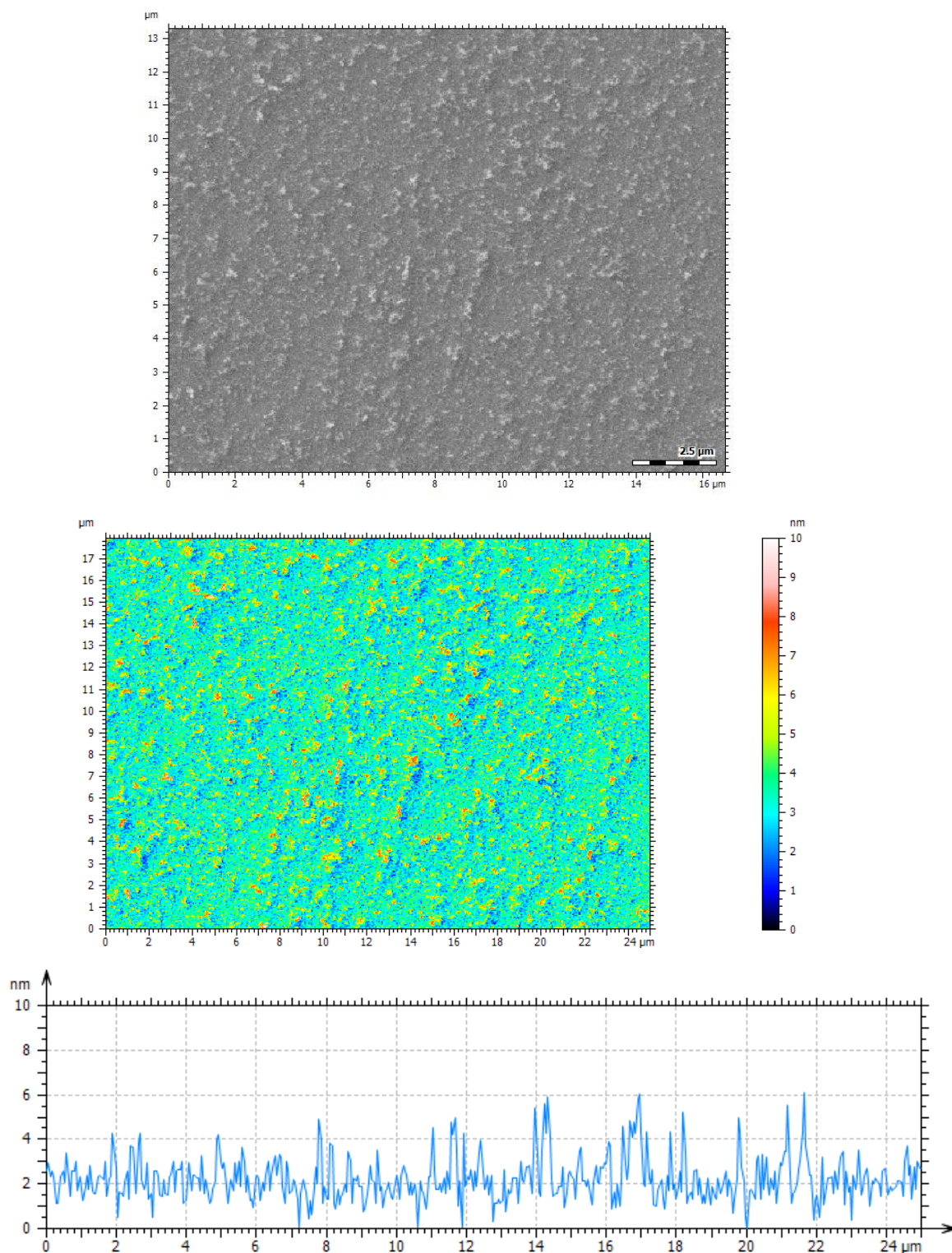
Figure 45 Surface characterization of FDTS after cleaning process

This modification makes an important difference in terms of hydrophobicity as the rougher surface shows a contact angle in the range of 165.68º whereas the washed surface exhibits ~108.15º, much lower Figure 46.
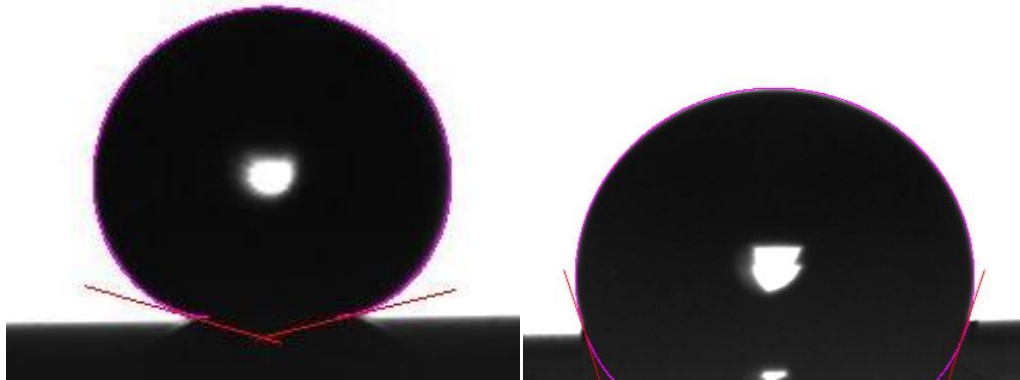
Figure 46 before washing surface (Left), after washing surface (Right)

5.1.2.3   Contact mode EWOD

10μl drops of conductive liquids (water and polar liquid mixture) were placed using a vertical syringe on top of the surface of the samples. Real time image processing system with high speed camera (BASLER A602F), with resolution of 640x480 pixels was used to capture the dynamic change of contact angle with recording velocity of 400f/s. To apply voltage to the liquid, a 0.1mm platinum wire was used in order to avoid any oxidation or reaction with liquid.
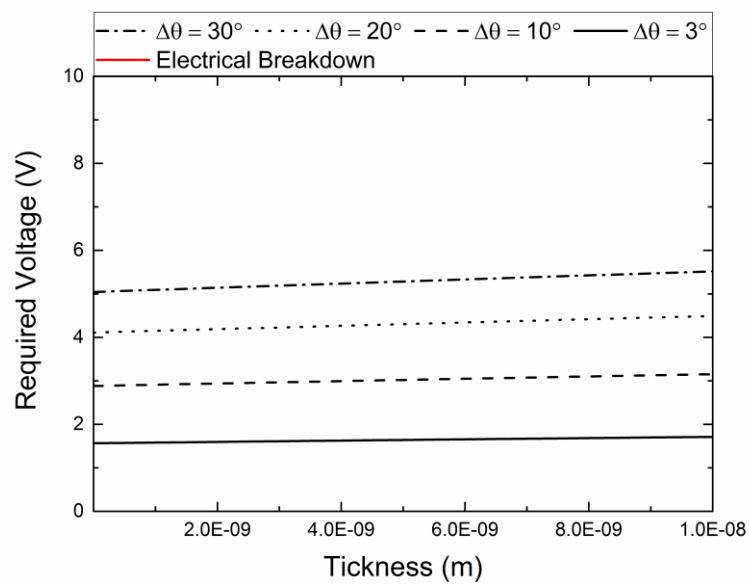
Figure 47 Lippmann–Young calculation for 24nm Alumina and FDTS layer as hydrophobic

According to the Lippmann–Young equation and using a dielectric constant value of εr = 17 for the FDTS later, calculations show that with 4nm thickness of FDTS applying less of 5V we achieve a large change of the contact angle value. At 2V the contact angle change was very small (negligible) as it was expected. After drying the surface on a hot plate we observed that the FTDS layer begun to degrade in the contact area between the drop and the substrate (Figure 48), the characterization of EWOD on FDTS layer were repeated with 5V and 10V as well, it is illustrated in the below figures applying higher voltage just increased the degradation of FDTS layer.
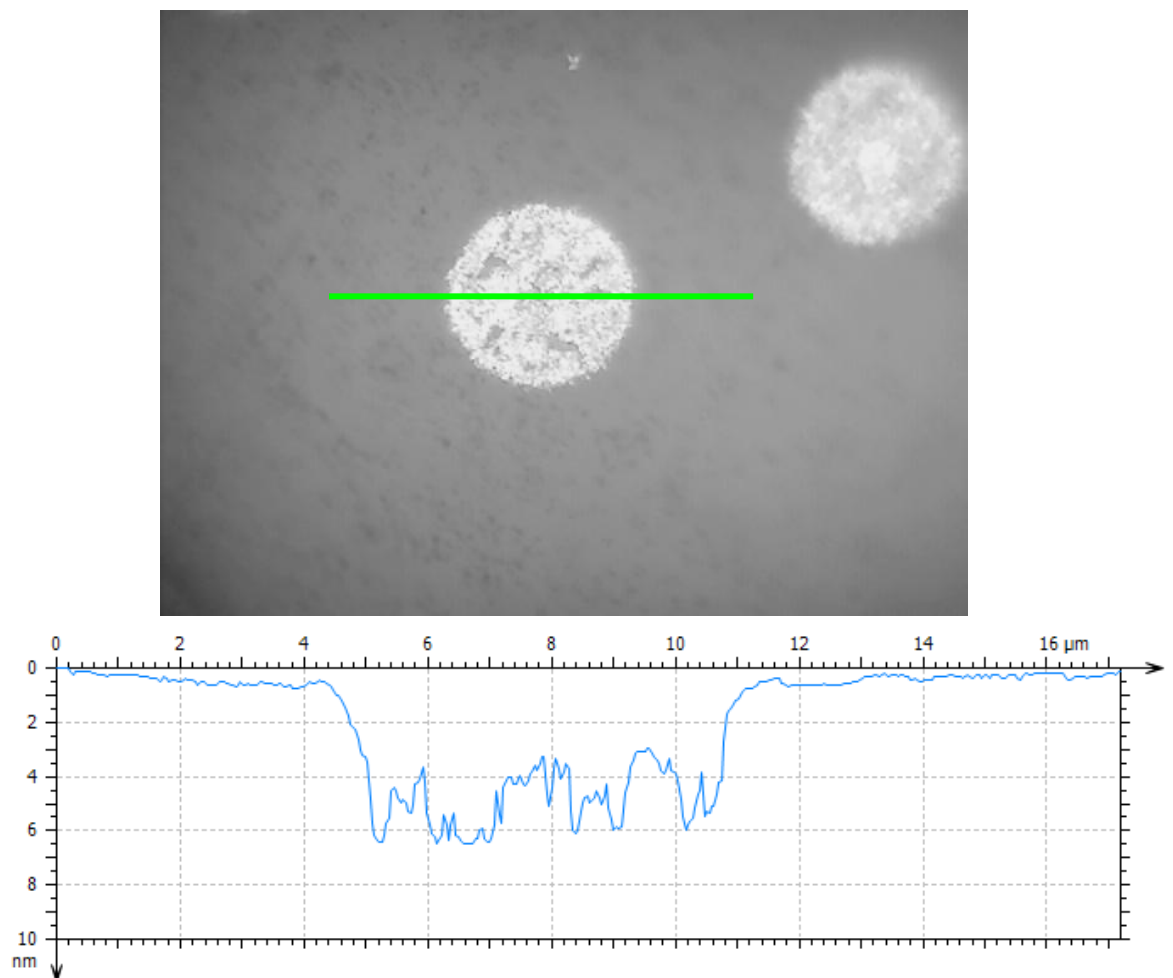
Figure 48 Microscope image of degraded area exactly in contact zone between drop and FDTS layer by 2V applied voltage, surface profile following green line
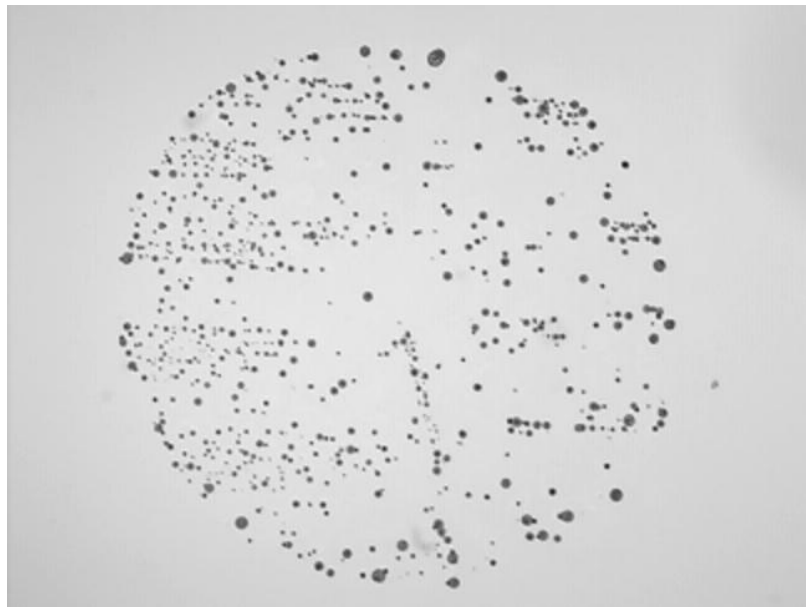
Figure 49 Microscope image of degraded area exactly in contact zone between drop and FDTS layer by 5V applied voltage
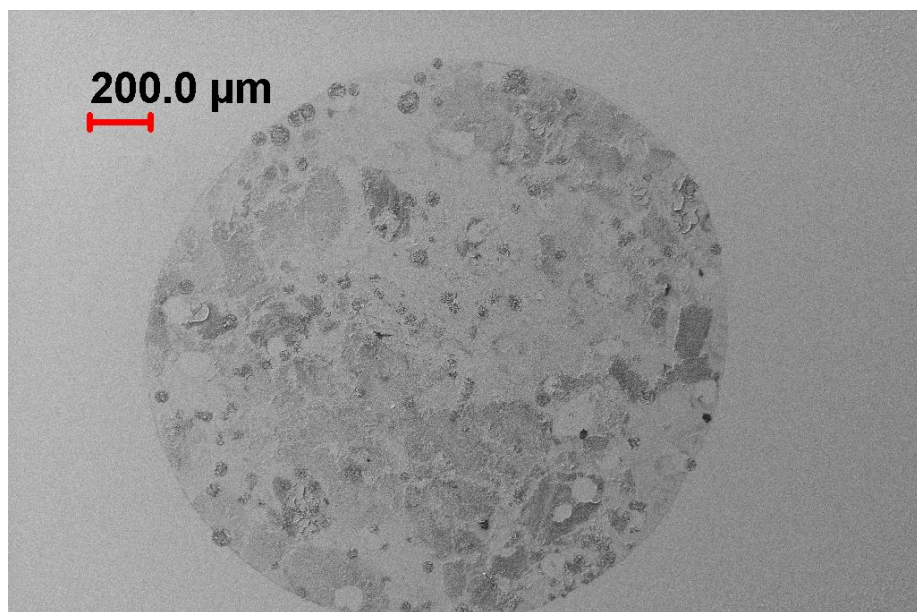
Figure 50 SEM image of degraded area exactly in contact zone between drop and FDTS layer by 10V applied voltage

When the voltage is removed still the surface shows high hydrophobicity, as it is illustrated in Figure 51 ; even by dragging we were not able to role the drop on the surface as it was trapped in the degraded area.
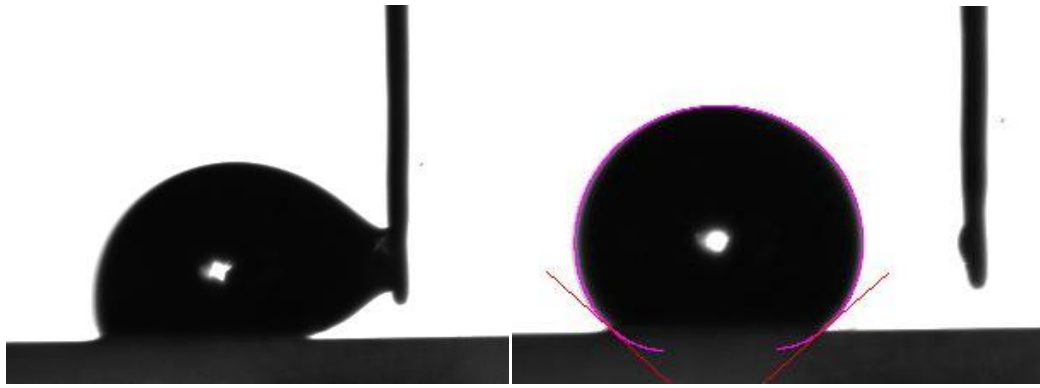
Figure 51 dragging liquid drop on surface with needle

Trichlorosilane coatings are bonded to alumina surface through silicon-oxygen-silicon (Si-O-Si) bonds. The alkyl chains in the silane are, from a chemical point of view, very stable, as in the case of fluorocarbons. The weak point of these coatings, however, is the bonding at the interface between the Si-substrate and the silane molecules. This type of silicon-oxygen bond has been considered susceptible to hydrolysis in humid or aqueous conditions. The stability of the monolayers in air is excellent. However, upon immersion in water, the film rapidly degrades over time and the degradation speed increases by applying voltage to liquid, Hence applying voltage in the contact mode is not suitable to achieve variation of contact angle and obtain ultra-low voltage EWOD liquid lens.

5.1.2.4 FDTS Contactless EWOD

Once the degradation of the surface of FDTS has been assessed in the previous section, the EWOD potential has to be estimated using another means to bring charge to the triple line less harmful to the layer integrity. We investigate the contactless EWOD as it was successfully used already for electrowetting [171,172]. Experiments were done by using a controlled ion-gun[173,174]. Conventional corona ionizers use a needle electrode, an extremely high voltage that causes the ionization of air molecules and, increases the static charge trapped in the triple line. We observed that using the corona ionizer gun for EWOD significant variation of contact angle was achieved. This technique was recently introduced [171] using a corona charge equipment. In this work however we used a commercial ion gun. Other works have also shown the potential to scale-up this technique, building arrays of micro ion guns. Figure 52 shows the experimental arrangement where the ion gun is shown in the vicinity of the triple line.
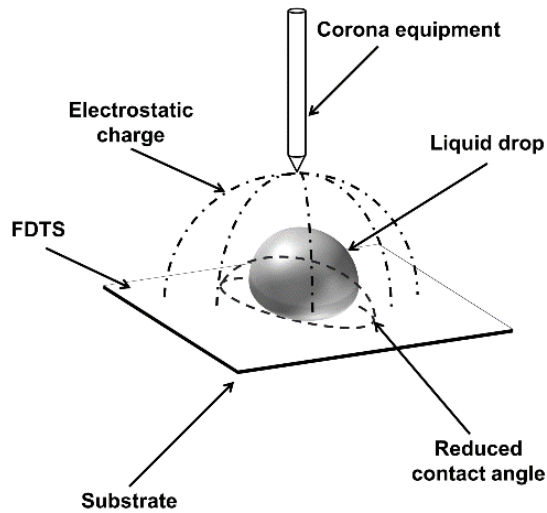
Figure 52 schematic of contactless electrowetting liquid lens

The 10µl water was drop was placed on top of the FDTS covered surface with a vertical syringe as it is illustrated in the front view of liquid Figure 53. The measured initial contact angle was 165.68º. By applying the ion-gunshot the contact angle was reduced by ~36º which shows high contactless EWOD phenomena. With a top view capture of liquid lens, it shows high variation of focal length obtaining a clear image of letter "M" underneath the liquid as shown in Figure 53.
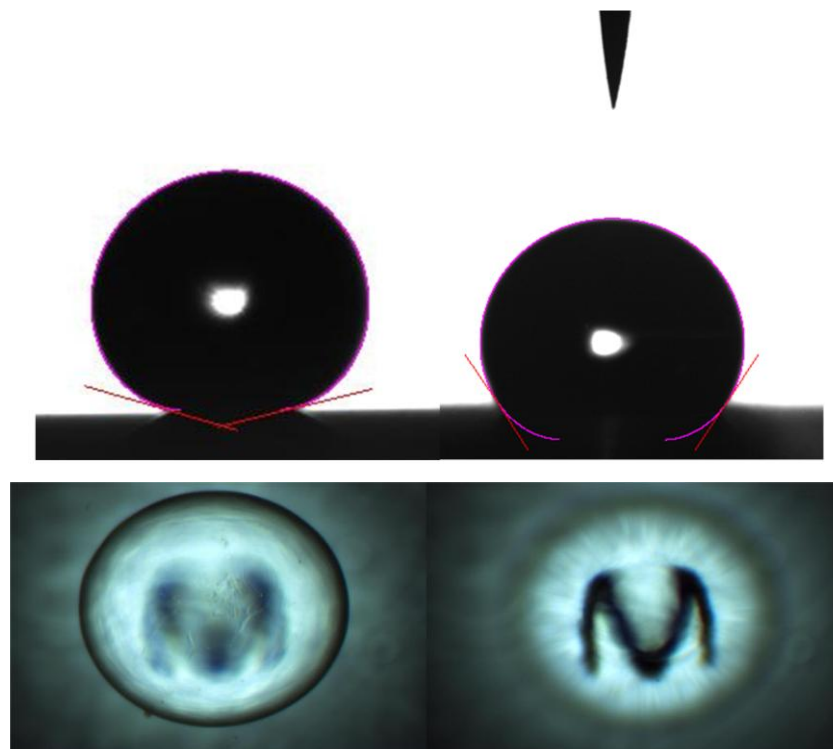
Figure 53 contactless EWOD with water front view , top view

On other hand we used polar liquid mixture of 33.3% as shown in Figure 54. The initial contact angle is a bit lower than that of water 148.26º and after by applying an ion-gun shot we obtained high variation of contact angle of ~38º. As it was expected using PLM-33.3% shows higher variation of contact angle.
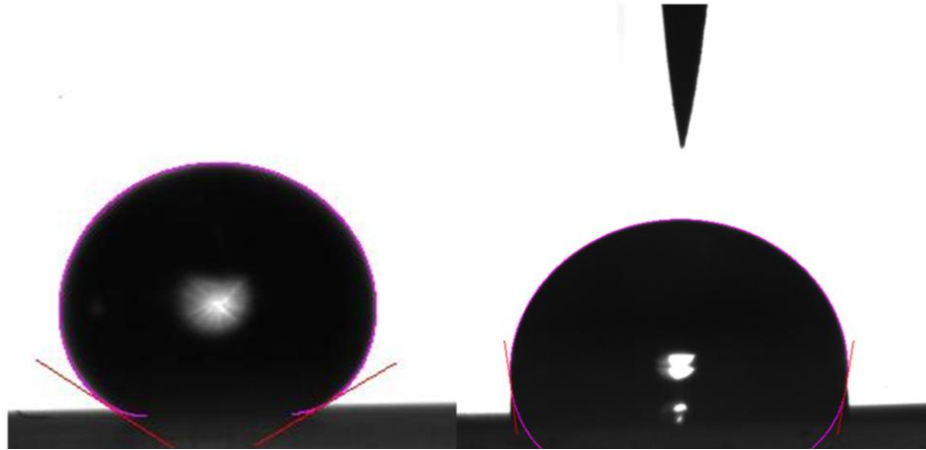
Figure 54 contactless EWOD with PLM33.3% front view

Moreover, we have studied the contact angle recovery after applying ion-gun shot , approximately 60s after of applying corona charge, we have recorded 100% recovery of contact angle. Figure 55 shows a plot of the value of contact angle as function of time. At the beginning of experiment (t=0) the ion-gun shot was directed towards the droplet from above and the transient that developed thereafter was recorded. As can be seen we have recorded 5ms before applying corona charge then a sharp drop of the contact angle value was recorded. In case of water, after the shot, the contact angle changed from ~165.86º to ~129.85º and from ~148.26º to ~110.26º for a polar liquid mixture. The contact angle remained at the low value with some ripple but always around ~130º for water and ~110º for the polar liquid mixture. After approximately 2s the contact angle starts recovering slowly towards the initial value. The recovery time depends on the liquid that has been used, on the amount of trapped charge and on the charge removal procedure. Among the several techniques to remove trapped charge, heating the substrate, blowing nitrogen and applying reverse voltage are the most common. As we are avoiding direct contact to the liquid, no reverse voltage technique was used and simply nitrogen blowing was applied. As can be seen in Figure 55, typically full recovery was reached after 60 seconds approximately.

Inspection of the FDTS layer after contactless electrowetting experiments did not show any degradation or cracking and the experiment could be performed many times sequentially.
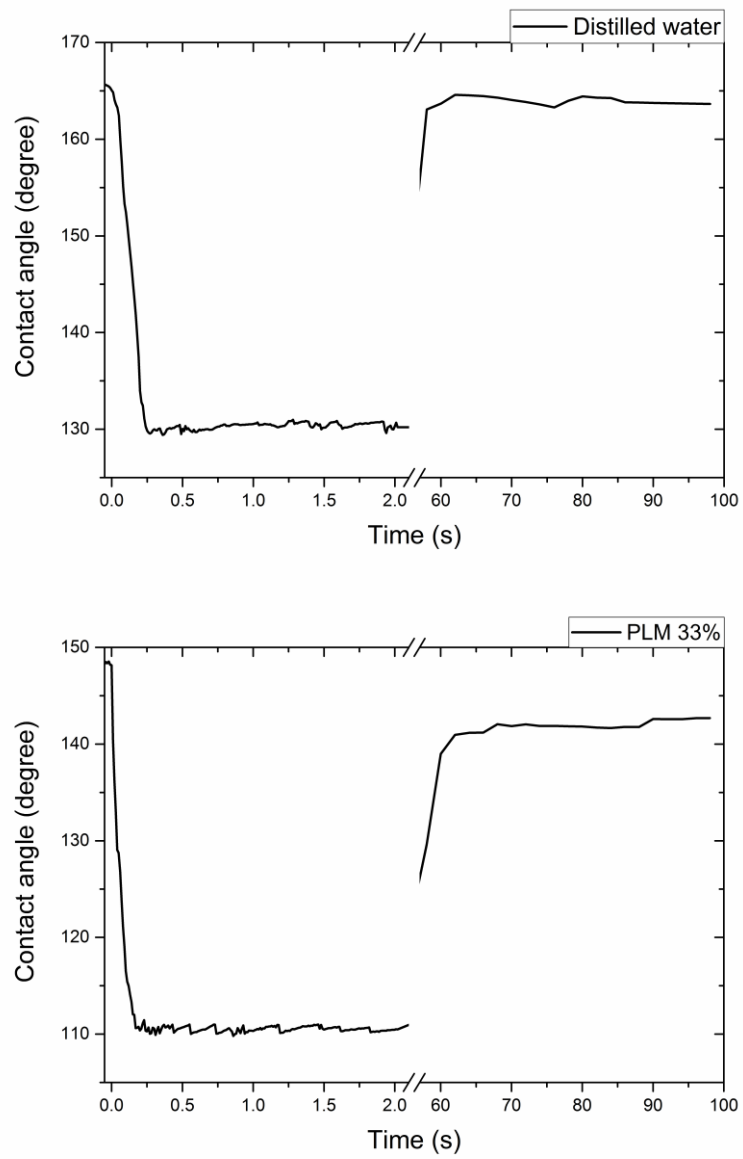
Figure 55 Contact angle variation by applying corona charge and recovery of contact angle for both (a) water (b) PLM33.3%

5.1.3 Conclusions ad discussion

The superhydrohpic FDTS layer have significant potential for EWOD and microfluidic devices. In this chapter we have characterized the surface morphology of superhydrophobic layers deposited with a SAM technique and have demonstrated the effect of roughness on the hydrophobicity. Since the micro fluidic devices operate in continuous contact with liquids and are subject to harsh chemical environments the hydrophobic protective coatings have to survive long-term exposure to various liquids and withstand frequent mechanical abrasion due to wiping. However, the ultra-thin FTDS coatings are very robust in micro fluidic applications. We have experimentally shown that , in contact mode EWOD, superhydrophobic layers of FDTS tend to degrade upon applying voltage to the liquids. However the potential of the FDTS is clear as the contact angle is very high and significant changes can be achieved providing charge to the interface. If the charge is provided by a contact procedure the FDTS losses its integrity whereas if contactless procedures are used the integrity is preserved.

Chapter 6:

Behavioral modelling framework

6.1   Introduction

In this chapter modeling issues are investigated aiming at bridging the gap between the microfluidics and conventional electronic circuit simulator environments. Modeling of microfluidics components generally requires computer fluid modeling and finite element approaches. Most of the time this is very time consuming depending on the accuracy required. However as the microfluidics components are getting used as another component inside a more complex system where electronics plays an important role (see for example the case of liquid lenses or displays) it becomes urgent to find ways to incorporate the response of fluidic components into conventional standard circuit simulators such as PSpice.

This chapter is a first attempt to bridge this gap. It must be stated from the beginning that what it is relevant in this approach is to find models that, rather to fully represent the underlying physics, are capable to model the operation of the device. This is generally called ' Behavioral modeling' and represents a high level of abstraction in most cases. There are a number of examples where this approach has proved to be very useful, such as in photovoltaic cells and systems [175,176] or more generally in digital circuit design [177]. For the purpose of this work we have followed the following approach for modeling and parameter extraction.

1. Experimentally acquire measurements of the dynamic response of droplets when they undergo an step-like electrowetting stimulus

2. Fit the experimental points to an analytical charge coupled electrowetting model previously developed at UPC [171,172] and fluidic model parameter extraction

3. Fit the experimental points to the response of a second order system as it has been already proven that it works well for the response of a droplet in a microchannel [178] and extraction of the second order effective parameter values

4. Compare the values of the parameter extracted using both approaches to find an equivalence between them

5. Feed the values of the effective parameters in a PSpice version of a second order system model

6. Run the PSpice model for several stimulus waveforms, beyond step-like response, and compare with experimental results found for the same device.

6.2 Experimental

6.2.1 Analytical charge coupled electrowetting model

The analytical charge couple model aforementioned that is summarized in the following equations:

$$-\zeta\,\alpha\,\Omega(\theta)\frac{d^2\theta}{dt^2} - \zeta\,\alpha\,\frac{d\Omega(\theta)}{d\theta}\left(\frac{d\theta}{dt}\right)^2 - \gamma_{LV}\,\sin\theta\,\frac{d\theta}{dt} - \frac{q_A}{C_A}\frac{dq_A}{dt} = 0 \qquad [20]$$

$$\frac{dq_A}{dt} = \frac{V_s}{A\,R} - \frac{q_A}{A}\left(\frac{dA}{d\theta}\frac{d\theta}{dt} + \frac{1}{C_A\,R}\right) \qquad [21]$$

That corresponds to the droplet- excitation arrangement shown in Figure 56.
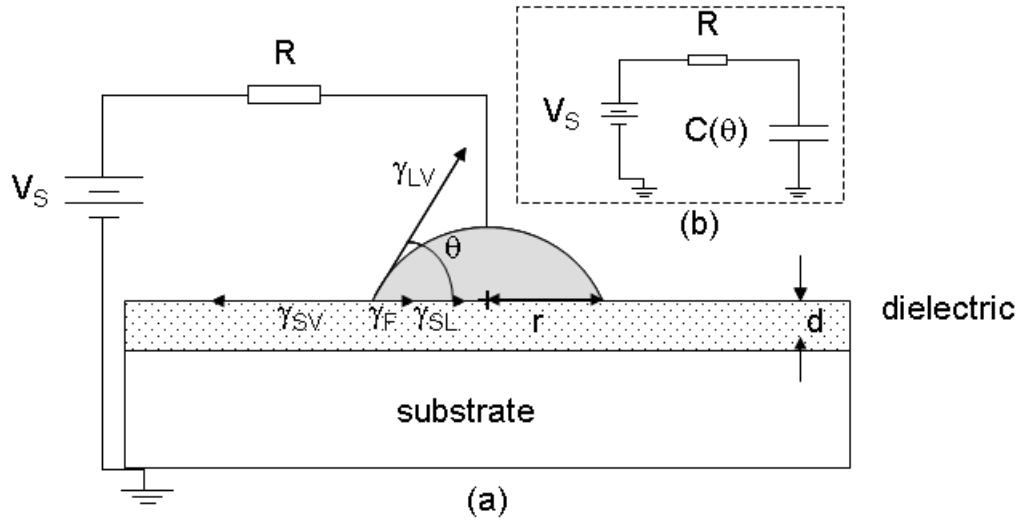
Figure 56 Schematic of microfluidic modelling base on capacitive behaviour of liquid

In the equations above the parameters have the following meaning; θ is the contact angle γ_{LV} is the surface tension water-air, ζ is the friction coefficient

$$\alpha = \left(\frac{3\ vol}{\pi}\right)^{1/3}$$

$$\Omega(\theta) = \frac{(1-\cos\theta)^2}{(2 - 3\cos\theta - \cos^3\theta)^{4/3}}$$

vol is the droplet volume, q_A is the charge per unit area stored in the liquid-dielectric-substrate capacitor, $C_A=\varepsilon/d$ is the effective capacitance per unit area, A is the area of the droplet surface in contact with the substrate and d is the dielectric thickness, V_S is the source voltage and R is the internal resistance of the source.

In the case we are considering here the experimental structure is made of two layers one on top of the other. The first is a 24 nm (t1=24nm) thick alumina layer that has a relative permittivity of ε_1=9.8 while the second is a 4 nm thick FDTS layer (t2=4nm) having a relative permittivity value of ε_2=24. The structure behaves as a two series capacitors and hence the effective capacitance per unit area of the stack of the two layers is:

$$\frac{1}{C_A} = \frac{t_1}{\varepsilon_1} + \frac{t_2}{\varepsilon_2} = \frac{1}{\varepsilon_1}\left(t_1 + t_2\frac{\varepsilon_1}{\varepsilon_2}\right) = \frac{d}{\varepsilon_1} \qquad [22]$$

In Equation 26 it can be seen that the unit area capacitance is equivalent to a capacitor having ε_1=9.8 of dielectric permittivity and a effective thickness of d=26.3 nm.

6.2.2   Spring model

The behavior of a drop actuation by applying voltage can be described as a damped mass-spring system.

$$M\frac{d^2x}{dt^2} = -k_{eq}x - c_{eq}\frac{dx}{dt} - F \qquad [23]$$

Where M (kg) is drop mass, x (m) is radius of drop contact line, the equivalent viscous damping coefficient is c_{eq} (Ns/m), the equivalent spring constant k_{eq} (N/m) and F(N) is actuation force by applied voltage and TLP position.

$$F = \frac{1}{2}.\frac{\varepsilon\varepsilon_0}{d}.V^2.x_0 \qquad [24]$$

Where ε is equivalent dielectric permittivity, ε_0 is vacuum permittivity, d is equivalent thickness, V is applied voltage, and x_0 is initial position of TPL. the variation of TPL position (x) has linear relation to variation of contact angle. Analytical models frequently use a simplification of the shape of a drop on top of a surface by considering a spherical cap shape.

$$x = \left(\frac{3vol}{\pi}\right)^{\frac{1}{3}} \frac{\sin\theta}{(2-3\cos\theta+\cos^3\theta)^{\frac{1}{3}}} \qquad [25]$$

6.2.3 PSpice model:

With the aim to provide models for electrowetting components in the most extended circuit modeling and simulation platform that is PSpice. A first demonstration of the methodology includes a PSpice model of the moving triple line based on the built-in Laplace function. This function is one of the possible definitions of voltage sources accepting as argument a transfer function in the s-transformed domain. The simplest case is that of the spring-mass-damping transfer function (see Equation 26) where the parameters values are the same as extracted from the spring model by fitting to the experimental measurements. One of the good things of this approach is that accurate PSpice models can be written with any kind of rational function of the complex variables as many times. The experimental behavior of the dynamics of the triple line is not well represented by simple first or second order functions but sometimes it is required to use terms such as Cole-Cole [179], including non integer power of S in the polynomials. An example is given by the following equation:

$$Y_1 = \frac{1}{M} . S^{cole} + C_{eq}.S + K_{eq} \qquad [26]$$

Where the parameter 'cole' is typically 0.5 and the input parameters: drop mass M (kg), the equivalent viscous damping coefficient is Ceq (Ns/m), the equivalent spring constant Keq (N/m) and the actuation force, F (N) are obtained from spring model fitting by Matlab. .

An example oif the PSpice code used in this experiment is the following PSpice code:

```
******************* Modelo masa muelle lente líquida ****************
***************Unidades en S.I
.param m=0.000001
.param k=0.1265
.param b=0.0017
.param cole=1
Vappl 1 0 PWL (0,0) (0.1m, 0.00019925891626773)
eresponse 10 0 laplace {v(1)} = {1/(m*s^(cole)+b*s+k)}
.tran 0 500m 0 100u;
.STEP param cole 0.25 2 0.25
.options itl4=500 itl1=500 VNTOL=0.1 reltol=0.01 abstol=0.1p
```

Of course the flexibility of PSpice includes the use of different kinds of excitations, not only step function but also arbitrary Piecewise Linear (PWL) Source Function and then the output is able to show the triple line behavior in presence of staircases for instance in very easy and quick way.

6.2.4   Results and discussion

For our purpose we select one of the experimental results found in Chapter 5 in Figure 55 where the step-like electrowetting response has been recorded for a water droplet on top of a two layer stack of alumina and FDTS. We concentrate in the first step down response. We have adjusted the model parameters to fit the experimental results and the results are shown in Figure 57. As can it be seen, the analytical model fits quite well using physical parameters from the origin of time up to 0.175 s. where the model departs from the experimental points that, as can be seen, undertake a ringing mode around the asymptotic value of the contact angle.
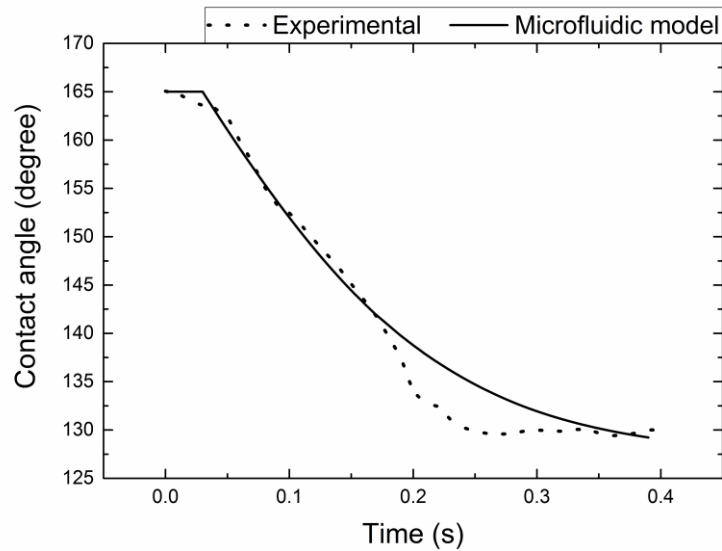
Figure 57 Fitting an analytical charge coupled electrowetting model with contactless EWOD on top of superhydrophobic substrate
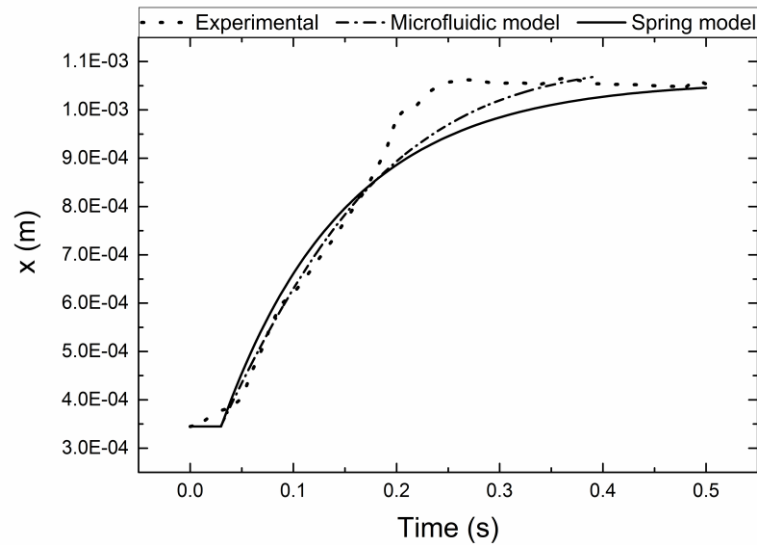
Figure 58 Variation of TPL position contactless EWOD on superhydrophobic surface (Experimental 'o' versus Micro-fluid model '-.-' and Spring model '-')

Figure 59 to Figure 62 shows comparison of the experimental results with the mains fluidic models, the spring-mass-damping matlab model and the PSpice model. It can be seen the agreement and considering that these are "behavioral" models is quite good but the overshoot shown by the experimental points is not reproduced. This makes us think that a simple 2nd order system could be subject to experiment in some cases. Fitting parameters such as damping coefficient and spring constant of dynamic EWOD by applying different voltage 10V to 50V is presented in Table 8.

Table 8 Fitting parameters of spring model for dynamic EWOD

Columna1	10V	15V	25V	50V
Fx	1.99E-04	4.35E-04	0.0012	0.005
Ceq (damping coefficient)	0.0017	0.01	0.0035	0.0077
Keq (Spring constant)	0.1265	0.253	0.717	2.915
m (kg)	1.00E-06	1.00E-06	1.00E-06	1.00E-06

Based on this parameters we have tried to modify the transfer function shown in Equation 30 by including a "cole-cole" term accounting for phenomena no represented by integer powers by of complex variable s, but as s^{cole} with cole<1 and in parts under cole=0.5 the effect can be seen in below figures where a combination of values of α and of the damping coefficient seem to better represent the experimental results.
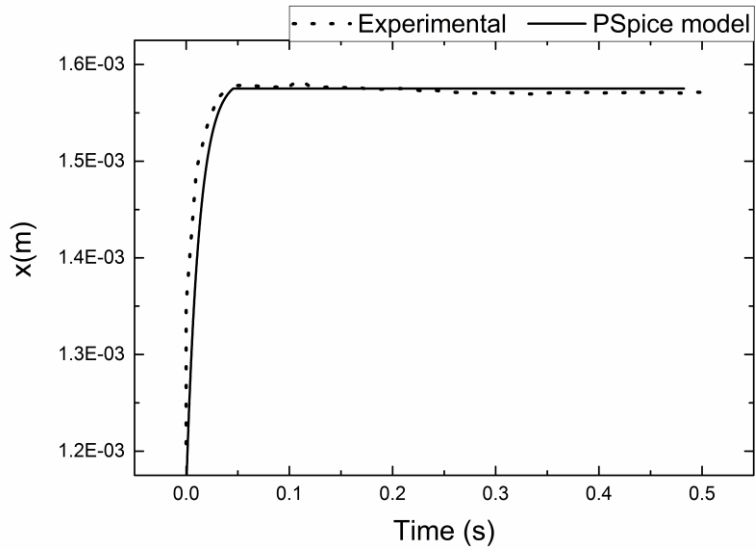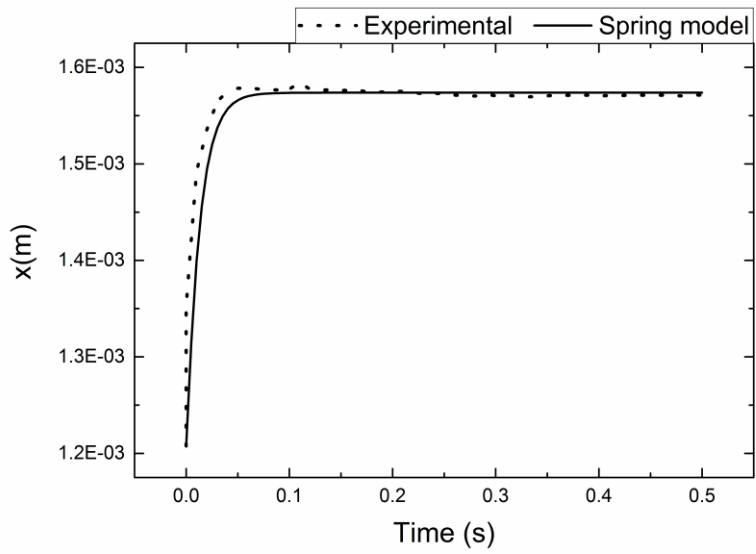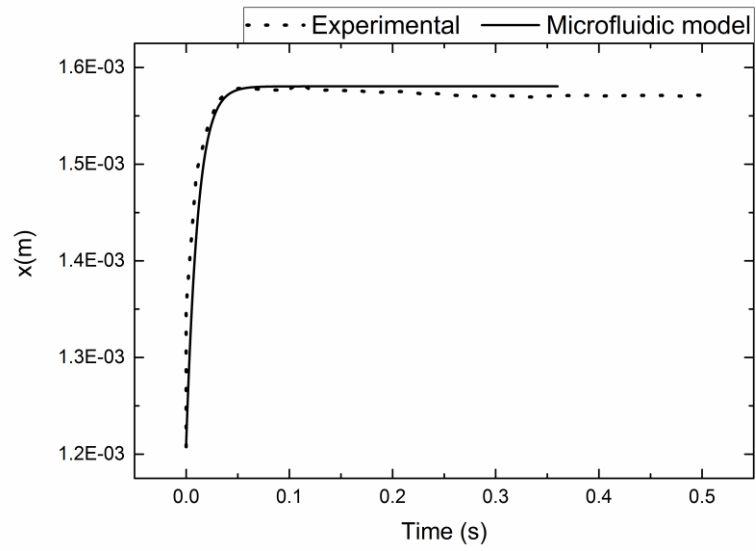
Figure 59 fitting with different models models for electrowetting modelling by 10V applied voltage
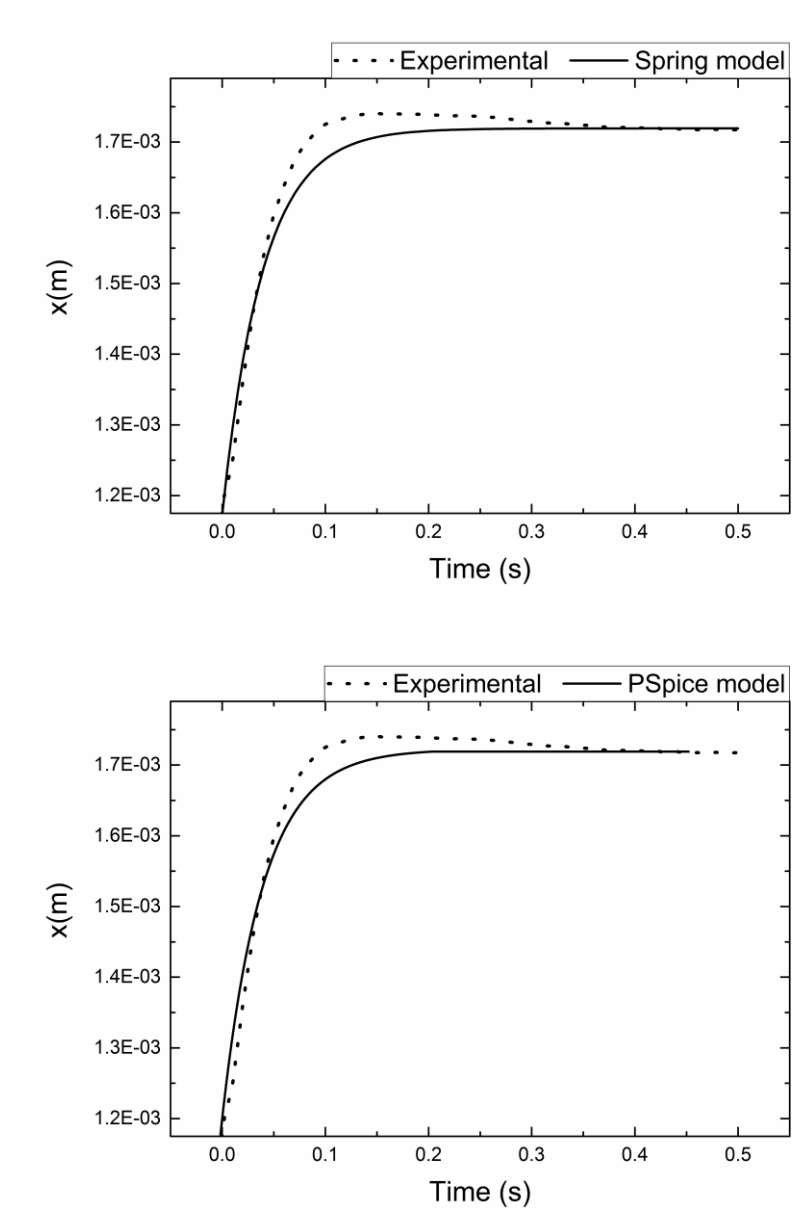
Figure 60 fitting with different models models for electrowetting modelling by 15V applied voltage
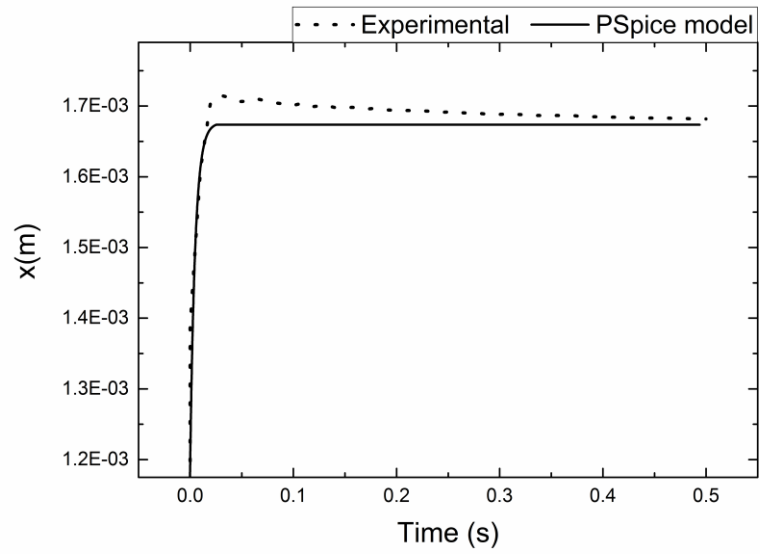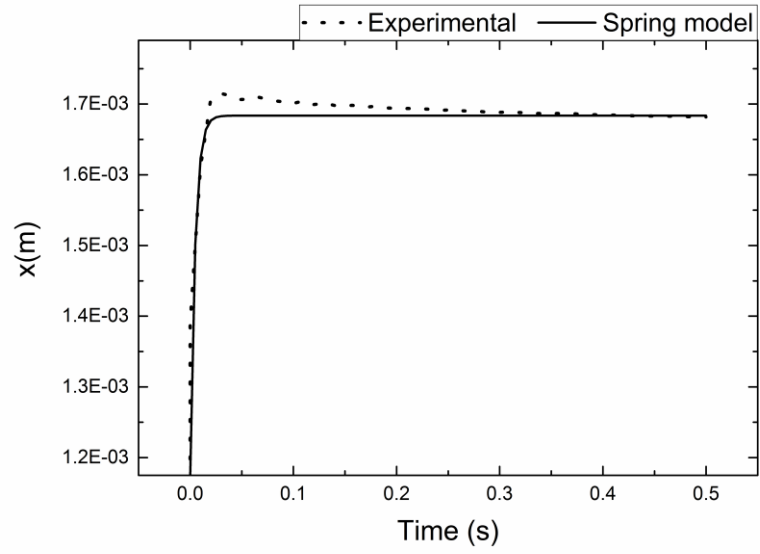
Figure 61 fitting with different models models for electrowetting modelling by 25V applied voltage
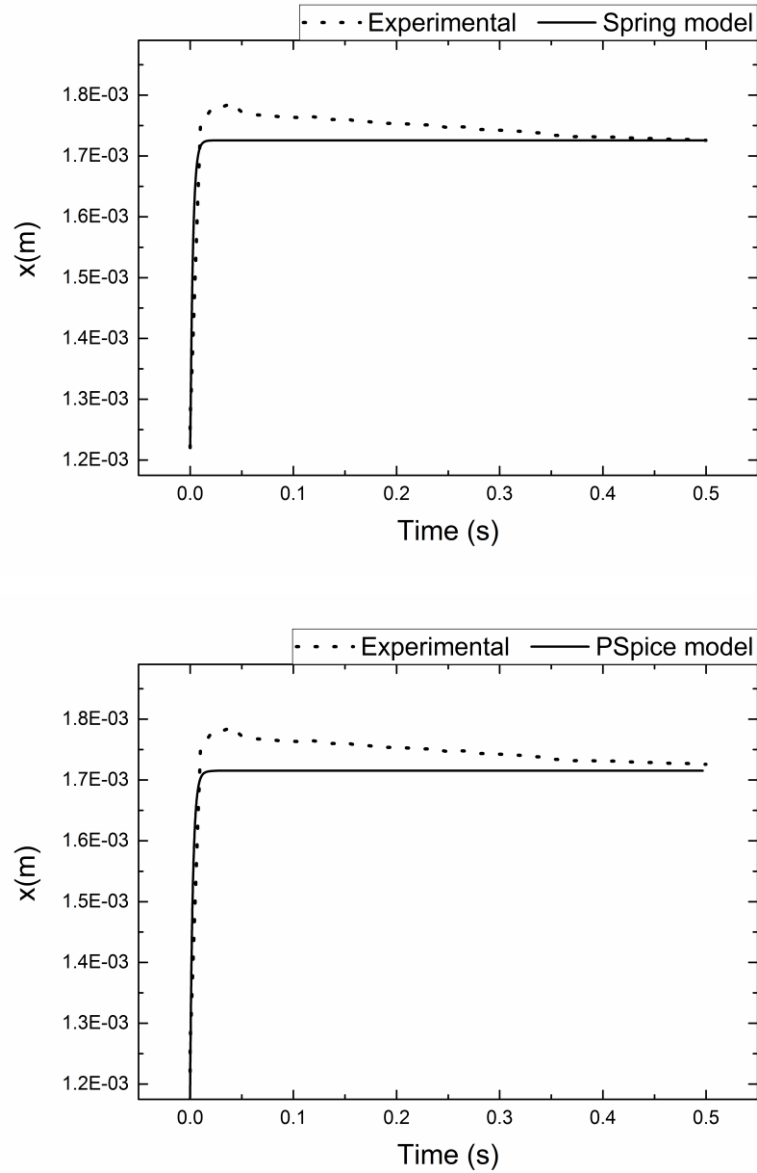
Figure 62 fitting with different models for electrowetting modelling by 50V applied voltage

As an outcome of this "behavioral" approach we show in Figure 63 how the PSpice model could be used to model a staircase-like driving waveform that is the most commonly used driving in voltammetric measurements. As it was explained in chapter 4, practically the EWOD phenomena does not follow the behavior of a perfect capacitor but it is affected by various phenomena such as the leak resistance and the amount of trapped charge in the dielectric itself or in the micro-drops. The experimental response is lagging behind the theoretical simulation as could be represented by a memory effect.
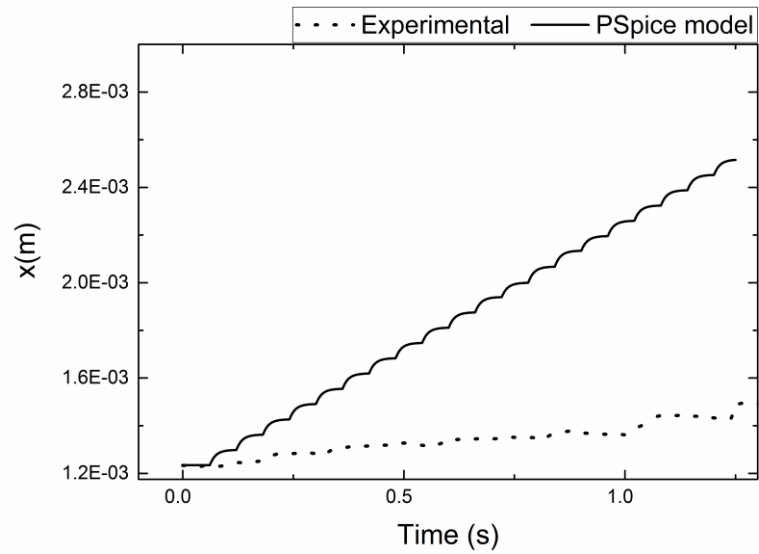
Figure 63 Stair-case simulation results versus experimental results , the difference in final approach is because of memory effect

6.2.1 Conclusion

It is expected that the microfluidc components enter the mass market and they will co-exist in the same system with other electronic devices or circuits such as for example driving sources. The capability to have equivalent PSpice models of those microfuidic components greatly expands the global system simulation along with the access to key operational parameters such as the power consumed, expected electrical currents and voltages, noise etc. Within this framework it is a lot of work still to be done but as this chapter shows, the methodology is simple and gives the opportunity to find behavioral models many times very useful for fast simulations compared to more physical models.

Chapter 7:

Liquid lens, one side electrode contact for 2D movement

7.1 Introduction

Microfluidic movement based on electrowetting, is being used to create the next generation lenses for a wide variety of Micro-Opto-Electro-Mechanical Systems (MOEMS) applications. Many of current devices involve electrode contacts in both the upper and bottom faces [180] or and 1D [9] (or circular symmetry) control of the shape of the droplet surface. Many applications found in the literature exhibit a 1-D control of the liquid. In reference [181] single side contacts were used although only symmetric movement was shown. One of the main goals of this thesis is to achieve a 2-D reversible drive of the droplet based on electrowetting on dielectric (EWOD). In this chapter, the single face electrodes fabrication and characterization of 2D reversible drive of the droplet based on capacitive − coupled electrowetting is described. Both electrodes are placed on the same face of the device and one of the electrodes is split to provide several control electrodes and hence allowing 2D control of the droplet shape.
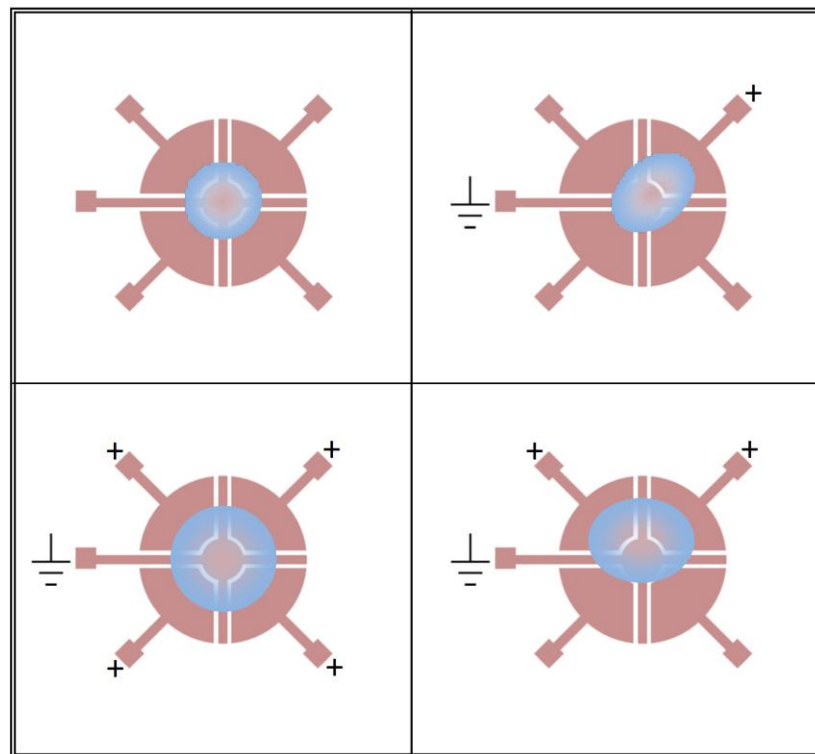
Figure 64 Liquid lens behavior by applying voltage on different sectors, (a) Without applying voltage, (b) Applying voltage on one sector, (c) Applying voltage on 2 sectors, (d) Applying voltage on 4 sectors

As it is obvious from Figure 64, at the zero state (without applying potential), the liquid drop placed the center has a circular. When we apply potential on one sector, the contact angle and the shape of the drop will change and it moves through the current flow. When we apply potential in two sectors, the contact angle changes and the drop shape equally change

through the two sectors. Finally, when we apply a voltage to the 4 sectors, the drop lens will expand uniformly at the center and the contact angle will also change accordingly.

7.2   Experimental results

Theoretically of Electrodynamic of moving of liquid lens [11] by applying a voltage to the electrode, a fringing field is generated between the central ground electrode and positive electrodes. The fringing field is simply illustrated in Figure 65 for different design; the intensity of the electric field is constant due to the constant gap between positive and negative electrodes.
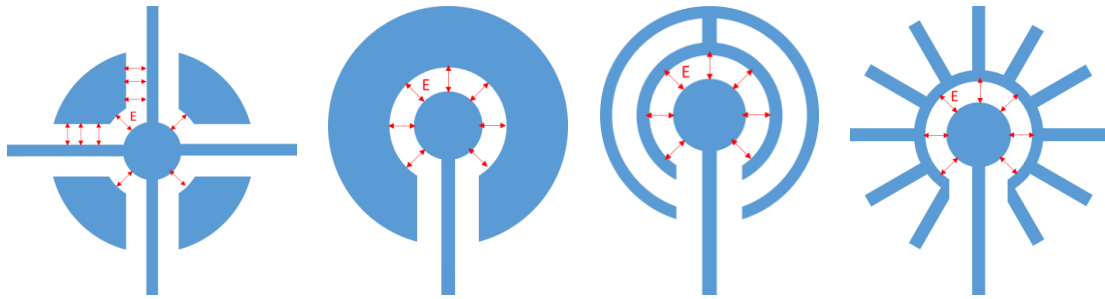
Figure 65 the fringing field between adjacent electrodes for different design

As result the dielectric force exerts on the droplet surface is expressed by [182]:

$$F = \frac{1}{2} \, \varepsilon_0 (\varepsilon_1 - \varepsilon_2) \nabla E^2 \qquad\qquad [27]$$

Would be constant, where ε0, ε1, and ε2 represent the permittivity of free space, the dielectric constant of the droplet, and the dielectric constant of the surrounding medium, respectively, and ∇E denotes the gradient of the electric field. If ε1 < ε2, the force will push the droplet to shift toward the region with the higher electric field. Owing to the circular-symmetrical distribution of the electric field, the dielectric force can move the liquid droplet toward current way. Since the liquid droplet exhibits a lens character, if the applied voltage is symmetric its focal length can be changed or by Asymmetric applied voltage shape of drop can be change from circular to elliptic or ovate shape depending on electrodes design. When the voltage is removed, the dielectric force disappears. The droplet has to recover to its original state due to its interfacial tensions. Thus according Lippmann–Young equation contact angle could be defined as:

$$\gamma_{sl} = \gamma_{\circ sl} - F$$

$$\theta = \cos^{-1}\left(\frac{\gamma_{sv} - \gamma_{\circ sl} - F}{\gamma_{lv}}\right) \qquad\qquad [28]$$

7.2.1 Fabrication of 2D EWOD liquid lens

The fabrication consists of eight steps as shown in

Figure 66. The pattern is formed on the substrate using a mask and photoresist, which defines the areas of the resist surface that will be exposed to radiation and those that will be covered (Lithography). The chemical properties of the photoresist regions struck by radiation change depend on the type of photoresist that has been used. The irradiated regions of positive photoresists will become more soluble in the developer and, so, positive resists form a positive image of the mask on the wafer. Negative photoresists form a negative image of the mask on the wafer because the exposed regions become less soluble in the developer. By depositing transparent conductive metal layer (ITO) on the developed substrate with the sputtering machine then the critical steps Lift-off has to be performed carefully because in this step the sacrificial layer (photoresist) is washed away by acetone including the deposited material on the top of it, thus the patterned electrodes will remain in the regions where it had a direct contact with the substrate. The 24nm Alumina as dielectric coated on top of ITO by ALD , HMDS deposited by spin coating with velocity of 7000rpm, acceleration of 1000rpm/s for 60s then a 10% Teflon AF solution (DuPont) was spin-coated at 3000 rpm for 60s , giving 200nm thick hydrophobic layer film. The Teflon-covered ITO glass slides were then heat-treated for 6 min at 112 °C, 5 min at 165 °C, and 15 min at 328 °C in order to remove residual solvent and improve the adhesion of the Teflon layer to the substrate.
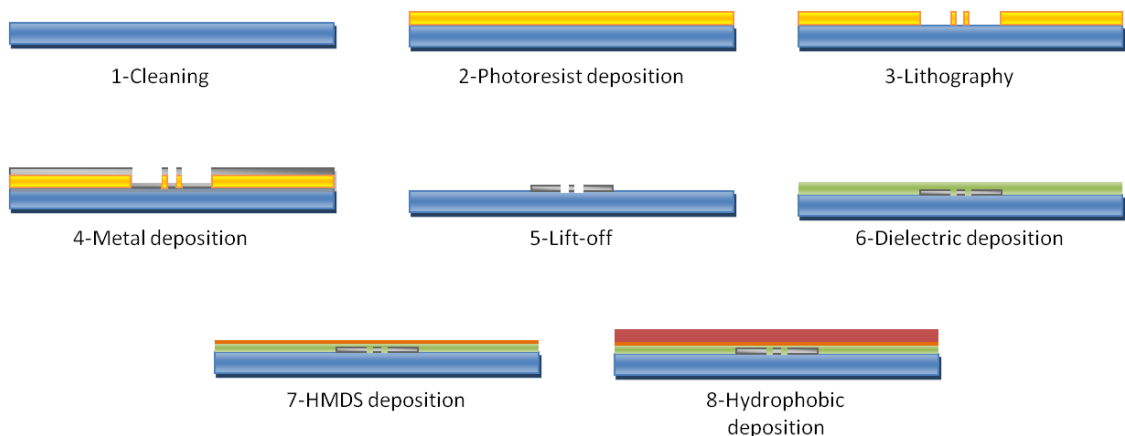
Figure 66 Fabrication process

After fabrication of base for 2D EWOD, the liquid lens holder was placed into a goniometric device (CAM200), 10µL drops of water were formed with a vertical syringe on top of the lens holder. Side-view images of the drops were obtained using a high speed digital camera with velocity of $400F.s^{-1}$. A potential difference was applied across the insulated ITO electrode with a power supply (Agilent 4156C). The high-voltage source was connected to the ITO electrodes with the stainless steel needle (probe-head). For each measurement, a single pulse voltage applied. The variation of contact angle was captured by high speed camera and top view by normal high definition camera.

7.2.2   2D EWOD liquid lens

The Planar electrode is commonly used in microfluidic channels for directing liquid within channel. Here the same concept has been implied for planar liquid lens. The planar liquid lens consists of two electrodes one as anode electrode (ground electrode) and another one as cathode (positive positive), In order to obtain 2D control of EWOD liquid lens several designs have been carried out, as the first design shown by details in Figure 67 the aim is to modify focal length of liquid lens in additionally asymmetric shape control of liquid lens in different direction. The designed mask consists of two different shapes in the patterns, one is with 4 sectors and another is with 8 sectors. The number of electrodes allows capturing behavior of the liquid lens with different resolution as it is exposed in Figure 64. The free space gap between positive and ground electrode is 100µm.
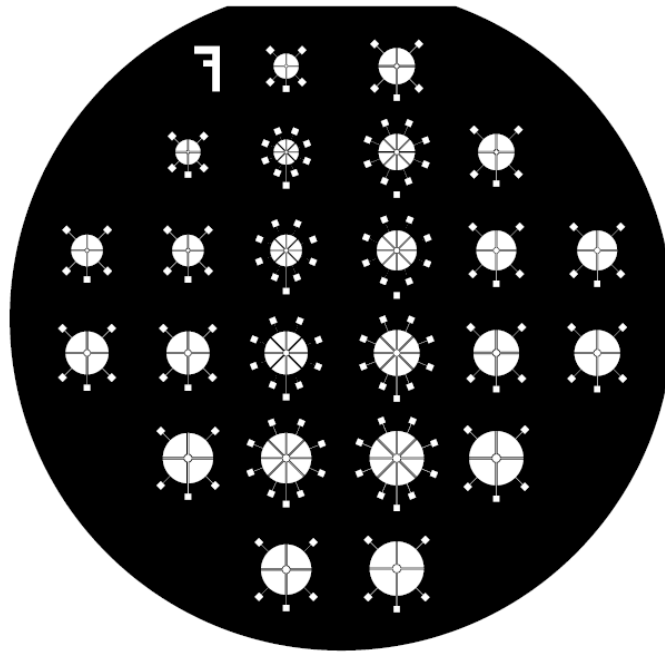
Figure 67 Plastic Mask, Designed by Sandra Bermejo, MNT Group, UPC University

The transparent liquid is a 10μL water droplet, sat on a transparent lens holder. Voltage can be applied to one or several of planar electrodes. When a voltage is applied to one of the active electrodes, the contact angle and the shape of the drop changes according to Lippmann-Young equation, but in this case the total applied voltage is divided by the capacitive voltage divider composed by the capacitances C1 and C2 shown in Figure 68. This way control electrodes can be placed in the same face although the effective voltage applied to the interface between active electrode and the conductive drop is described in the equation.

$$V_{ef} = V . \frac{C_2}{C_1 + C_2}$$
[29]

C1 is equivalent capacitor corresponding area of positive electrode, C2 is equivalent capacitor corresponding ground electrode.
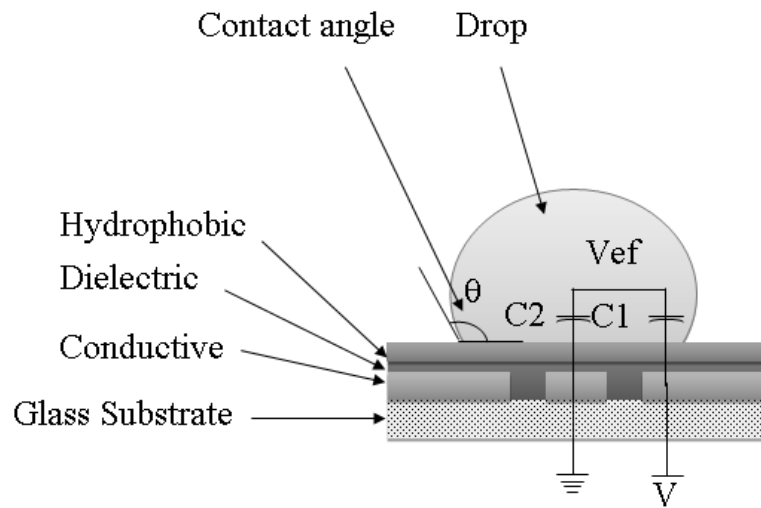
Figure 68 Electrowetting on dielectric circuit schematic.

In the devices reported here where the left side contact angle is smaller than the right side and the droplet has moved leftward. Figure 70 shows a top view of the droplet where voltage is applied to one of the electrodes, identified in the picture by the point contact probe to the right.
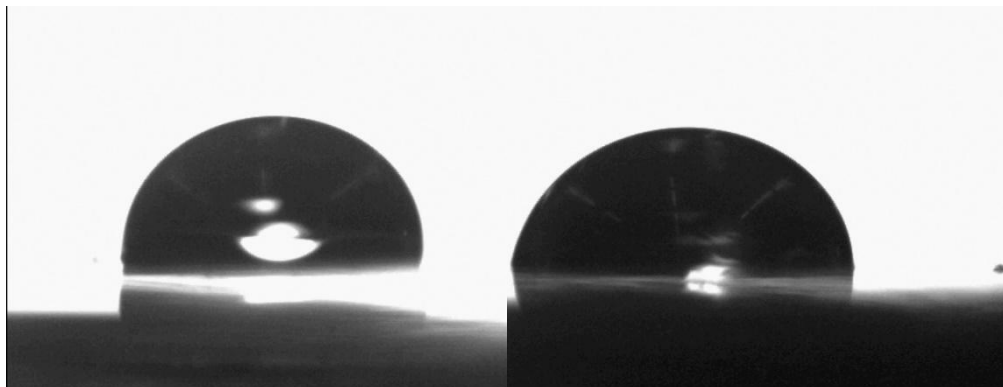
Figure 69 Front view of the contact angle variation by applying 25V
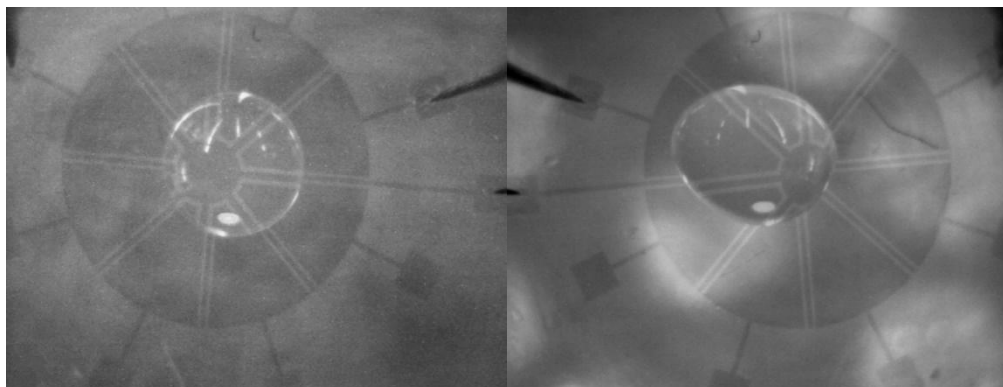
Figure 70 Top view of 2D control of drop shape by applying 25V

The 2D modification liquid lens base of EWOD with planar electrode has been achieved for voltages exceeding 10V as can be seen in Figure 71 where the contact angle at the leading edge of the drop is shown as a function of time for three values of the applied voltage, as can be seen higher voltages tend to induce vibrations or oscillations.
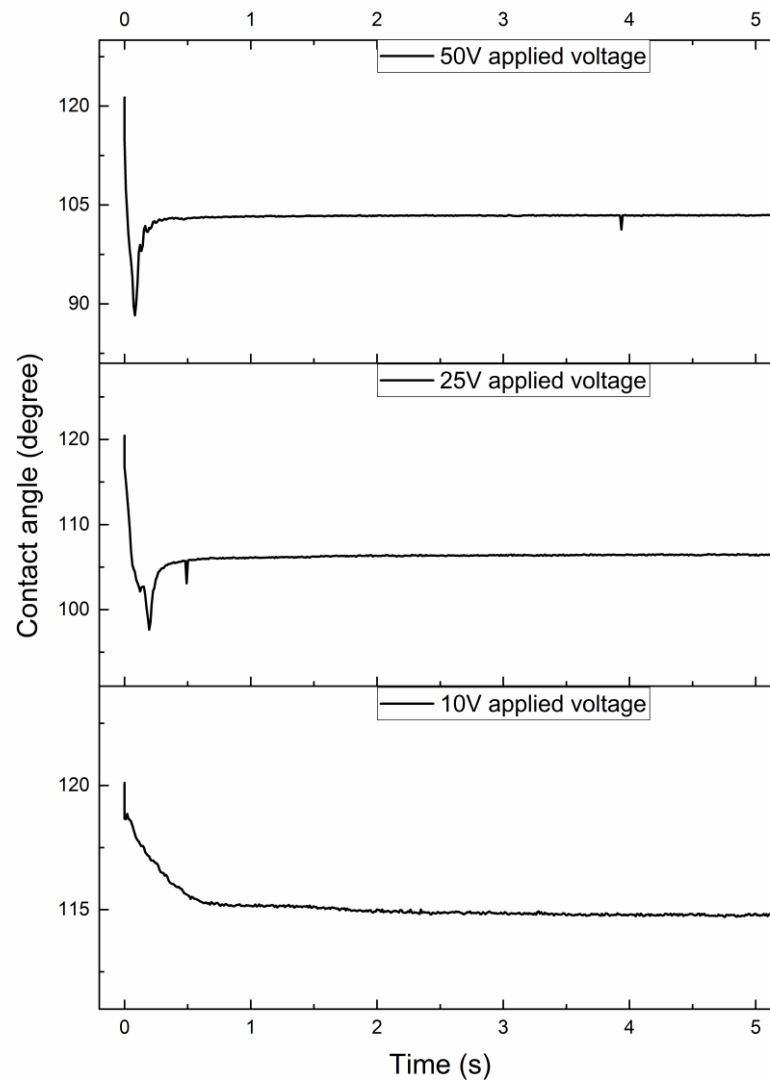
Figure 71 Measured contact angle when 10V, 25V and 50V are applied . The volume of the drop is 20 μl

7.2.3   Geometrical effect on planar EWOD liquid lens

We have generally studied the effect of different planar electrodes. A second mask has been designed with different designs: star shape, ring shape and continues shape electrodes. The common parameter between them is the size of the grounded electrode area and the diameter of the positive electrode. In this mask the ground electrode has 2mm diameter, positive electrodes 7mm diameter and the small separation gap between the electrodes is 0.2mm.
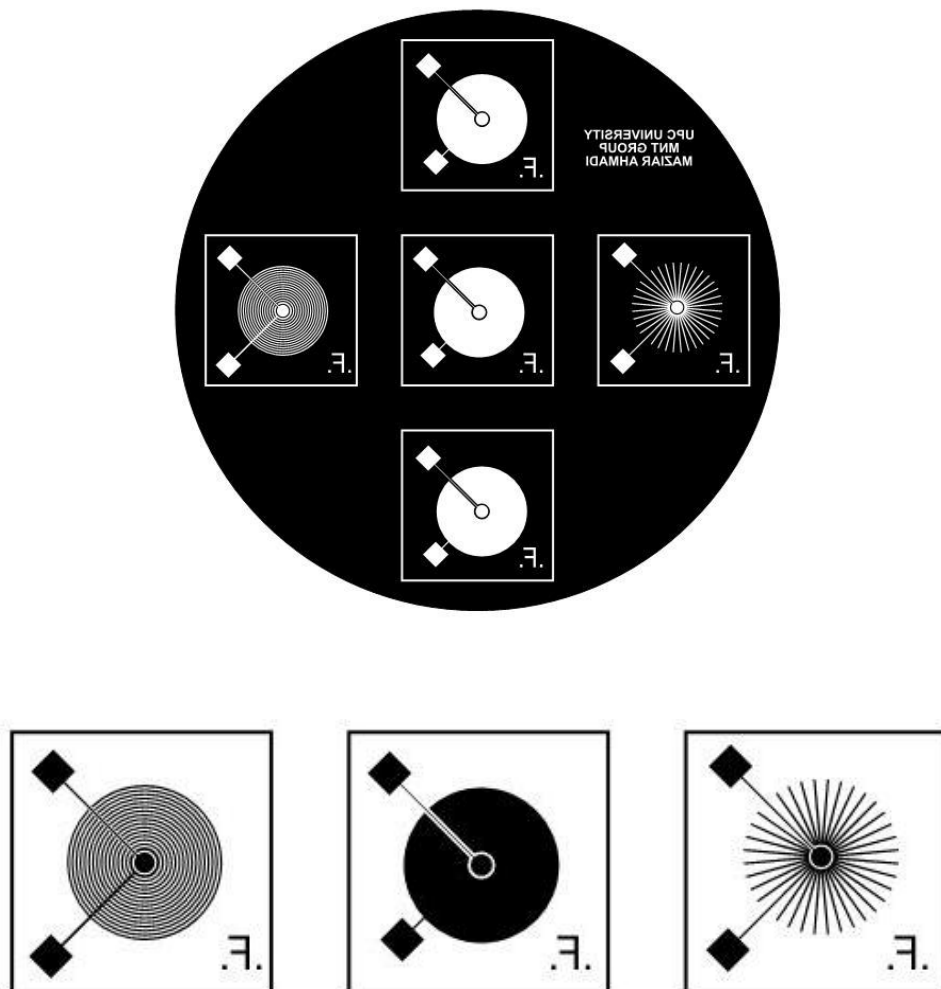
Figure 72 PET Mask, Designed by Maziar Ahmadi, MNT Group, UPC University (a) Alignment Mask, (b) Stripes Circle Shape, (c) Solid circle shape

The change of contact angle induced by the bias voltage depends on the geometrical shape of electrode and was studied experimentally, as it is illustrated in different experimental results obtaining max variation of contact angle depends on the surface area of

the positive electrode. According to the Equation 23 the equivalent capacitor corresponding to discontinue positive electrode is defined as two parallel capacitors:

$$C_1 = C_{11} + C_{12} \rightarrow C_1 = \frac{\varepsilon}{d}(A_1 + A_2) \hspace{2cm} [30]$$
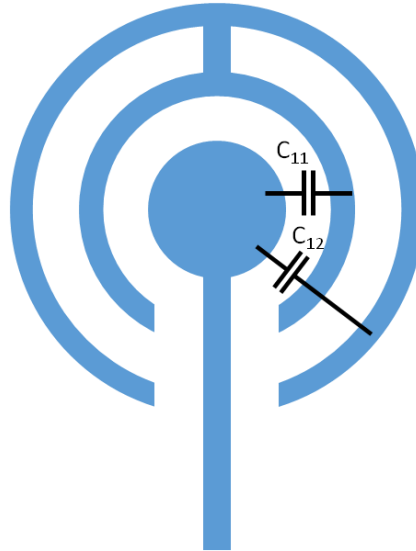
Figure 73 example of equivalent capacitor in discontinues electrode design
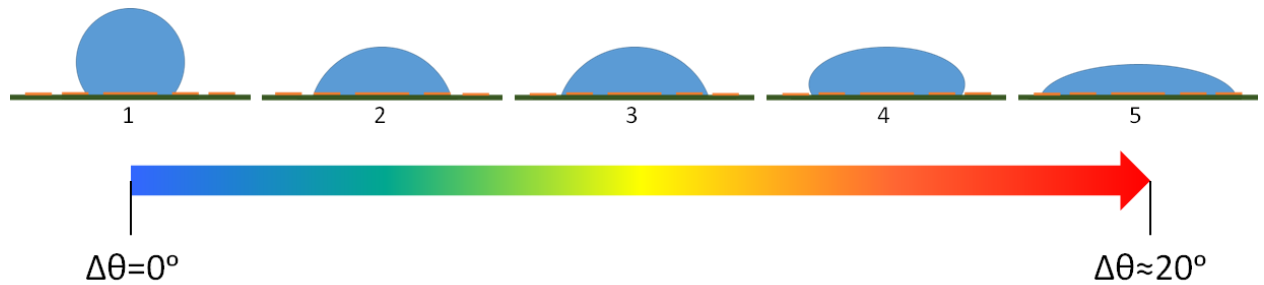
Figure 74 Schematic behavior of liquid lens on top of discontinuous electrode

Especially in the designs with Ring and Star shape electrode as it is exposed schematically in Figure 74 variation of contact angle is happening in different steps in the zero state (no voltage) a water drop has high contact angle , by applying voltage stage 2 according to the Lippmann-Young equation the contact angle reduces depends of equivalent capacity of effective electrode after reaching to maximum reduction (stage 3) the energy surfaces reach to second equilibrium state (stage 4) that the contact angle will increase , by continues applying voltage and increase of effective surface of electrode the total capacity will increase that cause second reduction of contact angle (stage 5).

7.2.3.1 Star shape electrode:

With Start shape electrode the contact angle variation of $\Delta\theta \approx 10^{\circ}$ was obtained by first effective part of electrode the by slowly reaching drop to the second effective electrode area the total capacity increases by:
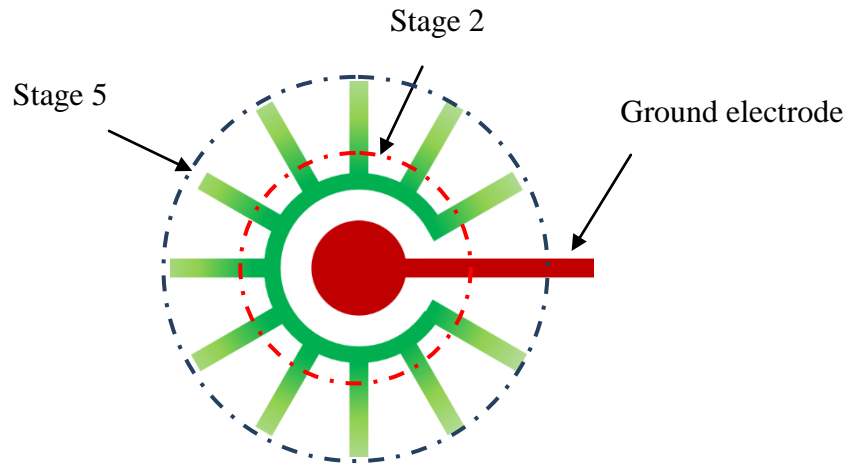
Figure 75 Effective area of star shape electrode

Which the C1 is the equivalent capacity related to first stage and C2 is a parallel capacity related to second stage. As results in variation of contact angle captured by CAM200 two time reduction of contact angle were observed.
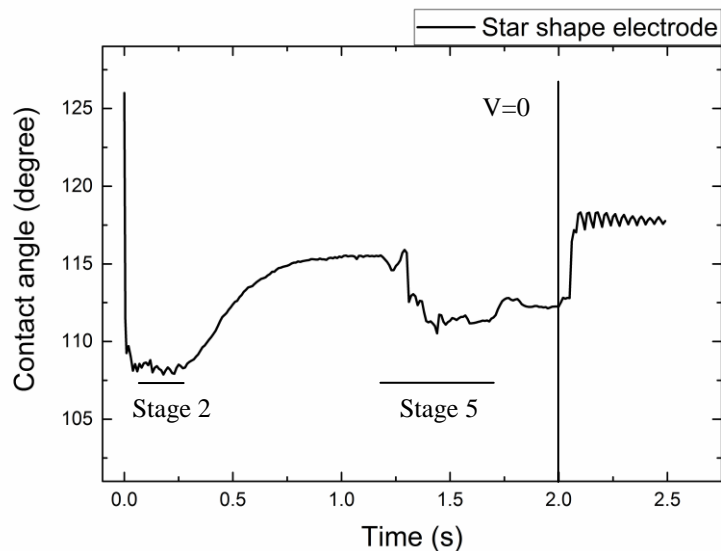
Figure 76 Variation of contact angle on star shape electrode

7.2.3.2 Ring Shape electrode:

The shape electrode has same behaviors as star shape electrode with difference is the second effective area of ring shape is bigger than star shape and it passing first stage, lower contact with electrode , low surface tension of substrate as result increase of contact angle , then by reaching to next ring parallel capacity cause increasing of total capacity thus high reduction of contact angle were observed.
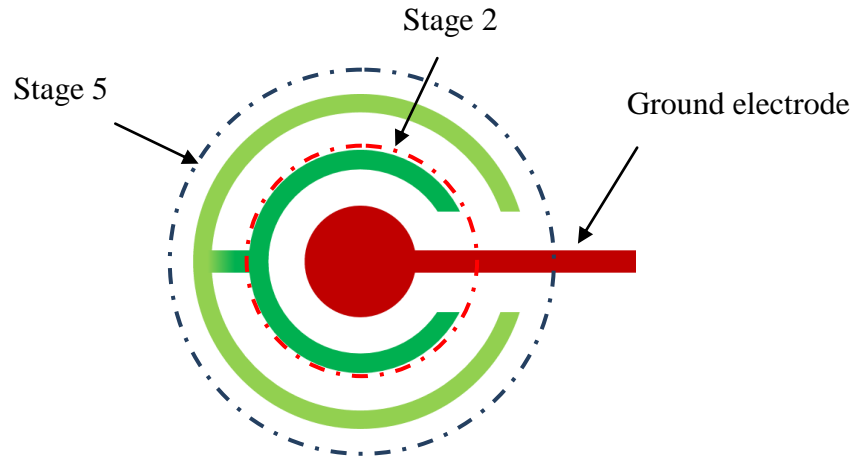
Figure 77 Effective area of ring shape electrode
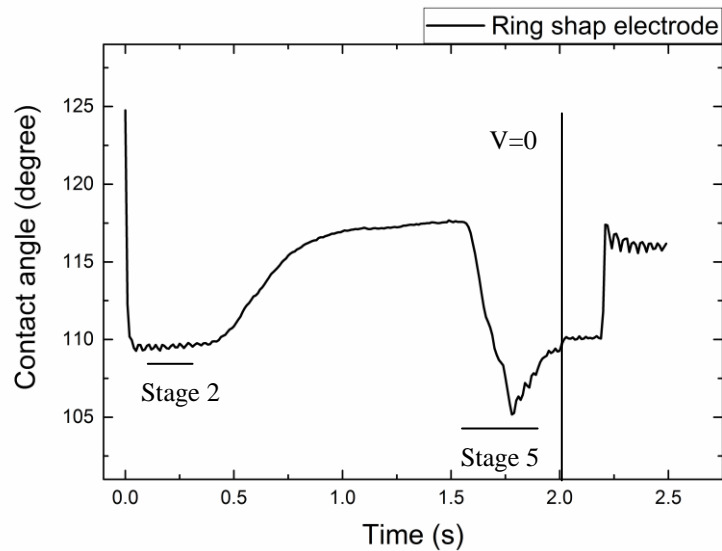
Figure 78 Variation of contact angle on ring shape electrode

7.2.3.3   All Solid shape electrode:

In all solid electrodes equivalent capacitor is related to complete surface area of positive electrode which could be explained as:

Positive electrode with
 max surface area

Ground electrode
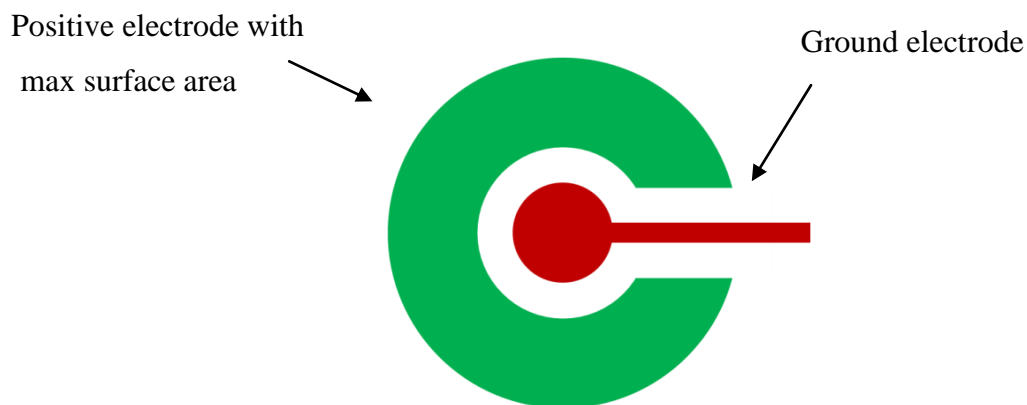
Figure 79 Effective area of all solid shape electrode

Thus a high variation of contact angle $\Delta\theta \approx 30^{\circ}$ with high recovery of 92.13% were obtain due to maximum capacity of positive electrode.
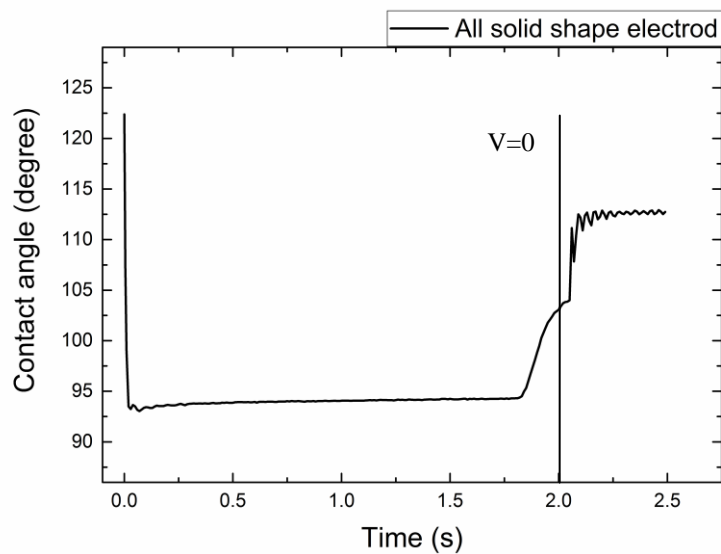
Figure 80 Variation of contact angle on all solid shape electrode

7.3 Conclusion ad discussion

We were able to explain the effect of electrode area on electrowetting on dielectric. Following Lippmann–Young equation there is two important parameters that are effecting variation of contact angle , applied Voltage , and Capacity , as we have explain by designing specific pattern we were able to have constant electrodynamic force but have variable capacity. The capacity is related to effective area of electrode, we have designed three type of electrodes: Solid, Spring and Star shape. When you have solid electrode you have higher effective area which cause higher variation of contact angle, but within Spring and Star design you have less effective surface area but same electrodynamic force, the variation of contact angle is less which is proving effect of electrode surface area on EWOD.

Chapter 8:

Conclusion

8.1 Conclusion
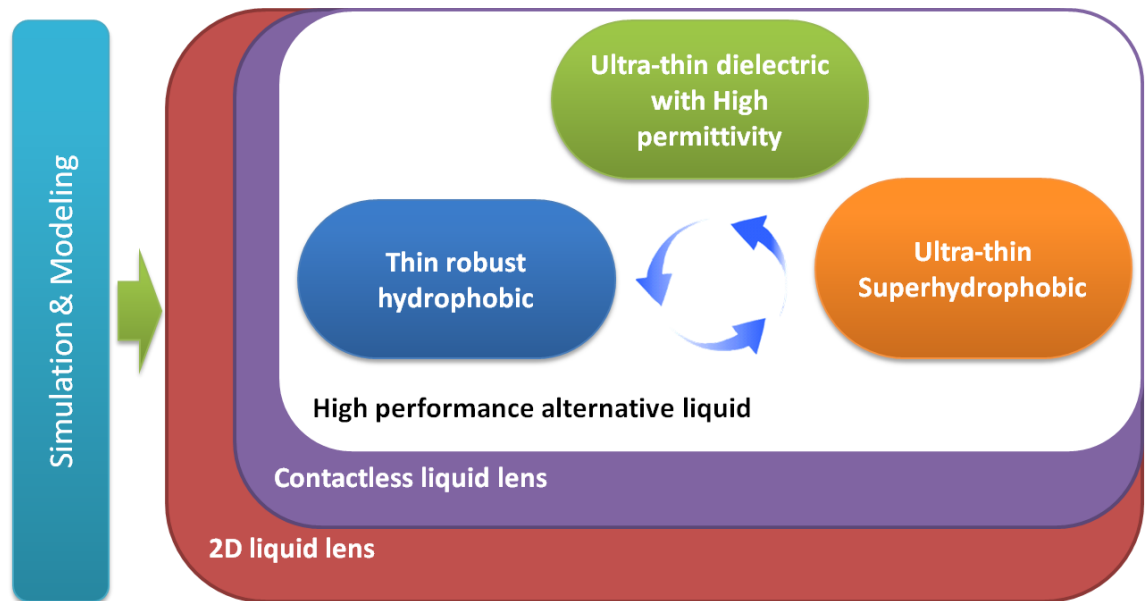
Figure 81 Pert diagram of thesis

As it is illustrated in the Figure 81, the evolution of thesis project can be divided in two stages, the first stage is the optimization of materials and processes, and the second one is the fabrication and evaluation of the device performance with two different EWOD technologies. Modeling was done to validate the behavior of the device methodology.

The thickness and the dielectric permittivity of the dielectric layer are the main parameters to reduce the required applied voltage for EWOD. By selecting ultra-thin dielectric with high permittivity, the required applied voltage was significantly reduced. The fabrication of the hydrophobic layer was optimized by adding HMDS. This has improved the hydrophobicity and the stability of Teflon layer, allowing lower thickness and thus decreasing the necessary applied voltage. Results demonstrated a high variation of contact angle ($\Delta\theta>20^\circ$) applying 10V for a 100nm conductive transparent ITO, 24nm of Alumina layer, HMDS treatment and Teflon 10% of 200nm thickness.

Following the pert chart, the analysis of different liquids for EWOD devices was done.. Polar liquid mixtures as an alternative to water were validated and characterized. The performance of different mixtures of polar liquid mixture (PLM) (Ethylene glycol and Glycerol) was evaluated and compared to water by measuring the static and dynamic contact angle. The PLM of 33% showed a high initial contact angle value of ≈106º which similar to natural initial contact angle of water upon Teflon, and a high variation of contact angle value

of 19.48º by applying 10V, in comparison to water's contact angle variation, $\Delta\theta = 18.63º$, by the same applied voltage. Additionally, the life cycle of PLM33% was compared to water after 1000 cycles of switching a 10 V amplitude voltage. The contact angle behavior showed better stability of PLM33% in comparison to water.

Besides, the superhydrohpic FDTS layer was studied as an alternative layer to Teflon. The surface morphology and physical properties of FDTS layer were studied. Results show that, even though it was to achieve high contact angle variation with a required voltage of <5V, FDTS layers tend to degrade upon applying voltages. As an alternative, these layers were tested under contactless driving EWOD using corona charge equipment. Results showed significant and reversible variation of contact angle by applying charge using corona charge equipment.

Additionally, we have studied the effect of planar electrode geometrical design and effective surface area on variation of contact angle in a EWOD 2D liquid lens. Based on Lippmann–Young equation, two parameters are playing an important role in the contact angle variation; the applied voltage and the existing equivalent capacity. Based on the fact that the capacity is related to the effective electrode surface area, three different designs of electrodes with different shape and effective surface area were compared. The results proved that, the geometrical design and effective surface area influence variations of the contact angle.

Finally, the modeling of a liquid lens based on EWOD was performed. Three different models were compared: the analytical charge coupled electrowetting model, the spring-mass model and electronic PSpice model. The two analytical models were used to provide inputs for PSpice model by fitting the simulation results to experimental results. PSPICE model was chosen to pave the way to add and integrate the liquid lens as an electronic component coupled with other co-exist component in the final systems. The equivalent PSpice models of liquid lens components allowed us to expand the global system simulation along with the access to key operational parameters such as the power consumed, expected electrical currents and voltages, noise, etc.

8.2 Future lines

The work done in this thesis paves the way to the same key subjects:

- Complete the geometrical analysis of EWOD devices, exploring different electrode configurations, topologies and designs.
- Complete the study of different driving modes: contactless EWOD, contact EWOD with current drive, alternatively change the polarity of the applied voltage,, ramp Potential, etc.
- Fabrication of a complete laboratory scale Display pixel based on electrowetting technology.

8.3 Material Published

- ➢ Patent that our research group has recently submitted "**Luminaria con óptica líquida de orientación controlada mediante señal eléctrica**" (Spanish patent number: P201232001).
- ➢ -Maziar Ahmadi Zeidabadi; Bermejo, S .; Castañer, L. "**EWOD using nonaqueous liquids**" Microelectronic Engineering, Volume 139, 1 May 2015, Pages 19–25
- ➢ -Maziar Ahmadi Zeidabadi; Bermejo, S .; Castañer, L. "**Improving the hydrophobicity and reversibility electrowetting layers of Teflon**". A: International Conference on Micro and Nano Engineering. "Book of Abstracts: 39th International Conference on Micro and Nano Engineering, London, 16-19 September 2013". London: 2013, p. 293.
- ➢ Maziar Ahmadi Zeidabadi; Bermejo, S .; Castañer, L. "**Low Voltage 2D capacitive-coupled electrowetting**". A: International Conference on Micro and Nano Engineering. "Book of Abstracts: 39th International Conference on Micro and Nano Engineering, London, 16-19 September 2013". London: 2013

Low Voltage 2D capacitive-coupled electrowetting

M. Ahmadi Zeidabadi *, S. Bermejo, L. Castañer

Grup de recerca en Micro i Nano Tecnologies
Universitat Politècnica de Catalunya, Jordi Girona 1-3, 08034 Barcelona, Spain
* maziar.ahmadi@upc.edu

Abstract

Main applications exhibit a 2-D reversible drive of the droplet based on electrowetting on dielectric (EWOD). Both electrodes are placed on the same face of the device and one of the electrodes is split to provide several control electrodes and hence allowing 2D control of the droplet shape. It is shown that reversible control is feasible for 25V and contact angles changes up to 22.75° with a reversibility of 92.48%.

Motivation

Microfluidic movement based on electrowetting, is being used to create the next generation lenses for a wide variety of Micro-Opto-Electro-Mechanical Systems (MOEMS). The main motivation of this project is to achieve a complete control of **Contact angle , Shape , Position** of the liquid lens based on electrowetting on dielectric (EWOD).
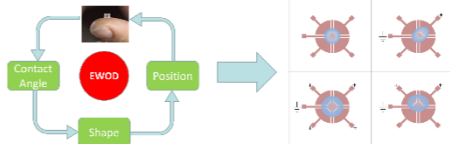
Set-up and Device description

To examine the 2D change of the liquid surface a goniometric device (CAM200) was used to measure the contact angle.

Top view of the metal pattern layout
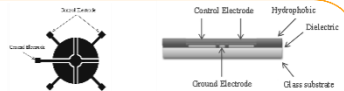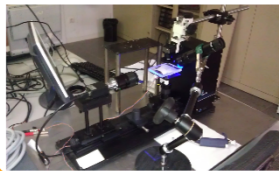
Schematic of cross section of the 2D liquid lens holder.

$$V_{ef} = V \cdot \frac{C_2}{C_1 + C_2}$$

The total applied voltage is divided by the capacitive voltage divider composed by the capacitances C1 and C2.

Results
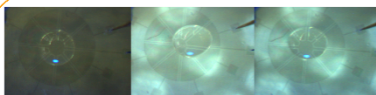
Top view of 2D control of drop shape and position by applying 55V.
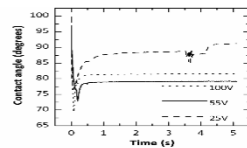
Measured contact angle when 25V, 55V and 100V are applied , the volume of the drop is 20 µl.

Highlights

- Both electrodes are placed on the same face of the device and one of the electrodes is split to provide several control electrodes and hence allowing 2D control of the droplet shape.
- Contact angles changes up to 22.75° with 25 V applied voltage related to the thicknesses of the dielectric and hydrophobic layer used
- High percentage of reversibility of 92.48% contact angle are achievedof after removing the electric potential

---

Improving the hydrophobicity and electrowetting reversibility of Teflon layers

M. Ahmadi Zeidabadi *, S. Bermejo, L. Castañer

Grup de recerca en Micro i Nano Tecnologies
Universitat Politècnica de Catalunya, Jordi Girona 1-3, 08034 Barcelona, Spain
* maziar.ahmadi@upc.edu

Abstract

We describe a novel fabrication process for durable hydrophobic surface layer capable of achieving a high contact angle. This layer is made of a combination of Teflon Af1600 and HDMS (Hexamethyldisilazane) and provides a best result at a 126,172° contact angle, for distilled water. We also analyze anti-freezing and shock resistant liquid as an alternative to distilled water used in MOEMs controlled by capacitive – coupled electrowetting.

Motivation

- Problem: Teflon layer integrity is compromised when applying voltage on a distilled water drop, hence the wettability of surface increases and it will cause the hydrolysis of distilled water that will damage the electrode (Figure 1).

Alternative:
- Combination of Teflon Af1600 and HDMS shows better integrity.
- Ethylene glycol has excellent heat transfer properties: a higher boiling point and a freezing point of -13° C, -36.4ºC when mixed with Glycerol

Figure 1. (a) AFM image of Teflon surface after applying potential (b) Continuous roughness plot (c) Hydrolyzation of distilled water by applying voltage

Fabrication technology and Device Setup
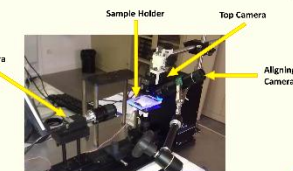
- Different mixtures of Ethylene Glycol and Glycerol (100/X%) in order to compare the results with the characterization of distilled water

Results

- Measured contact angle results for Ethylen glycol-Glycerol 50% on protected hydrophobic and unprotected hydrophobic layer
- Compare initial contact angle of Distilled water and Ethylen glycol-Glycerol 50% on different surfaces
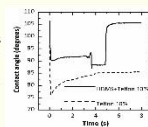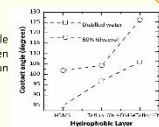
Compared initial contact angle of different mixture of Ethylene glycol-Glycerol with distilled water

Distilled Water 126.172°
Ethylene glycol-Glycerol 50% 105.998°
Ethylene glycol-Glycerol 41% 105.195°
Ethylene glycol-Glycerol 33% 105.181°
Ethylene glycol-Glycerol 25% 103.165°
Ethylene glycol-Glycerol 12.5% 101.795°

Highlights

- Improvement in the deposition process of the Teflon itself in order to avoid damage in the surface.
- Nonaqueous electrowetting fluids used as alternative conductive liquids instead of distilled water.
- High contact angle for 50% mixture (105.998°) on HDMS plus Teflon 10% that is comparable with the contact angle of distilled water (104.221°) on Teflon 10%.
- High percentage of reversibility of 99.32% of contact angle of Ethylene glycol Glycerol 50% mixture after removing the electric potential.

Bibliography

[1]   W.C. Nelson, C.-J. "CJ" Kim, Droplet Actuation by Electrowetting-on-Dielectric (EWOD): A Review, J. Adhes. Sci. Technol. ahead-of-p (2012) 1–25. doi:10.1163/156856111X599562.

[2]   S.K. Cho, H. Moon, C.-J. Kim, Creating, transporting, cutting, and merging liquid droplets by electrowetting-based actuation for digital microfluidic circuits, J. Microelectromechanical Syst. 12 (2003) 70–80. doi:10.1109/JMEMS.2002.807467.

[3]   J. Lee, H. Moon, J. Fowler, T. Schoellhammer, C.-J. Kim, Electrowetting and electrowetting-on-dielectric for microscale liquid handling, Sensors Actuators A Phys. 95 (2002) 259–268. doi:10.1016/S0924-4247(01)00734-8.

[4]   Varioptic - Liquid lens solutions, Auto Focus M12 and C-mount lens modules, (n.d.). http://www.varioptic.com/ (accessed July 24, 2014).

[5]   Home - Liquavista - Electrowetting based low power, always viewable color video displays, (n.d.). http://www.liquavista.com/ (accessed July 24, 2014).

[6]   S. Chen, P.Y. Keng, R.M. Van Dam, C. Kim, Synthesis of 18 f-labeled probes on ewod platform for positron emission tomography (pet) preclinical imaging crump institute for molecular imaging , 4 mechanical and aerospace engineering dept ., (2011) 980–983.

[7]   S. Chen, A. a. Dooraghi, M. Lazari, R.M. van Dam, A.F. Chatziioannou, C.-J.C. Kim, On-chip product purification for complete microfluidic radiotracer synthesis, 2014 IEEE 27th Int. Conf. Micro Electro Mech. Syst. (2014) 284–287. doi:10.1109/MEMSYS.2014.6765631.

[8]   J.-M. Choi, H.-M. Son, Y.-J. Lee, Biomimetic variable-focus lens system controlled by winding-type SMA actuator, Opt. Express. 17 (2009) 8152. doi:10.1364/OE.17.008152.

[9]   S. Kuiper, B.H.W. Hendriks, Variable-focus liquid lens for miniature cameras, Appl. Phys. Lett. 85 (2004) 1128–1130. doi:10.1063/1.1779954.

[10] D.W. Lee, Y.-H. Cho, A 4 bit digital liquid lens for variable focal length, J. Micromechanics Microengineering. 20 (2010) 035029. doi:10.1088/0960-1317/20/3/035029.

[11] M. Xu, X. Wang, H. Ren, Tunable Focus Liquid Lens with Radial-Patterned Electrode, Micromachines. 6 (2015) 1157–1165. doi:10.3390/mi6081157.

[12] D.Y. Zhang, V. Lien, Y. Berdichevsky, J. Choi, Y.H. Lo, Fluidic adaptive lens with high focal length tunability, Appl. Phys. Lett. 82 (2003) 3171–3172. doi:10.1063/1.1573337.

[13] J. Keskinen, E. Sivonen, S. Jussila, M. Bergelin, M. Johansson, A. Vaari, et al., Printed supercapacitors on paperboard substrate, Electrochim. Acta. 85 (2012) 302–306. doi:10.1016/j.electacta.2012.08.076.

[14] B. Berge, E. Normale, S. De Lyon, L. France, Liquid lens technology: principle of electrowetting based lenses and applications to imaging, 18th IEEE Int. Conf. Micro Electro Mech. Syst. 2005. MEMS 2005. (2005) 227–230. doi:10.1109/MEMSYS.2005.1453908.

[15] E. Simon, B. Berge, F. Fillit, H. Gaton, M. Guillet, O. Jacques-Sermet, et al., Optical design rules of a camera module with a liquid lens and principle of command for AF and OIS functions, Proc. SPIE. 7849 (2010) 784903. doi:10.1117/12.871634.

[16] B. Berge, J. Peseux, Variable focal lens controlled by an external voltage: An application of electrowetting, Eur. Phys. J. E. 3 (2000) 159–163. doi:10.1007/s101890070029.

[17] H.H. Shen, S.K. Fan, C.J. Kim, D.J. Yao, EWOD microfluidic systems for biomedical applications, Microfluid. Nanofluidics. 16 (2014) 965–987. doi:10.1007/s10404-014-

1386-y.

[18] P.S. Dittrich, A. Manz, Lab-on-a-chip: microfluidics in drug discovery., Nat. Rev. Drug Discov. 5 (2006) 210–218. doi:10.1038/nrd1985.

[19] G. Lippmann, Relations entre les phénomènes électriques, Ann. Chim. El Phys. 5 (1875) 494–549.

[20] J.H. Song, R. Evans, Y.Y. Lin, B.N. Hsu, R.B. Fair, A scaling model for electrowetting-on-dielectric microfluidic actuators, Microfluid. Nanofluidics. 7 (2009) 75–89. doi:10.1007/s10404-008-0360-y.

[21] F. Mugele, J.-C. Baret, Electrowetting: from basics to applications, J. Phys. Condens. Matter. 17 (2005) R705–R774. doi:10.1088/0953-8984/17/28/R01.

[22] J. Restolho, J.L. Mata, B. Saramago, Electrowetting of Ionic Liquids: Contact Angle Saturation and Irreversibility, J. Phys. Chem. C. 113 (2009) 9321–9327. doi:10.1021/jp902393r.

[23] S. Chevalliot, J. Heikenfeld, S. Member, L. Clapp, A. Milarcik, Analysis of Nonaqueous Electrowetting Fluids for Displays, 7 (2011) 649–656.

[24] M. Makihara, N. Sato, F. Shimokawa, Y. Nishida, Micromechanical optical switches based on thermocapillary integrated in waveguide substrate, J. Light. Technol. 17 (1999) 14–18. doi:10.1109/50.737415.

[25] T. Kaneko, T. Ohmi, N. Ohya, N. Kawahara, T. Hattori, A new, compact and quick-response dynamic focusing lens, in: Proc. Int. Solid State Sensors Actuators Conf. (Transducers '97), IEEE, n.d.: pp. 63–66. doi:10.1109/SENSOR.1997.613582.

[26] W. Wang, J. Fang, Variable Focusing Microlens Chip for Potential Sensing Applications, IEEE Sens. J. 7 (2007) 11–17. doi:10.1109/JSEN.2006.886991.

[27] H. Jiang, X. Zeng, Microlenses: Properties, Fabrication and Liquid Lenses, CRC Press, 2013. https://books.google.com/books?id=ySPOBQAAQBAJ&pgis=1 (accessed February 7, 2016).

[28] P.J. Smith, E.M. McCabe, C.M. Taylor, D.R. Selviah, S.E. Day, L.G. Commander, Variable-focus microlenses as a potential technology for endoscopy, in: J.-A. Conchello, C.J. Cogswell, A.G. Tescher, T. Wilson (Eds.), BiOS 2000 Int. Symp. Biomed. Opt., International Society for Optics and Photonics, 2000: pp. 187–192. doi:10.1117/12.384195.

[29] S. Sato, Applications of Liquid Crystals to Variable-Focusing Lenses, Opt. Rev. 6 (1999) 471–485. doi:10.1007/s10043-999-0471-z.

[30] N. Chronis, G. Liu, K.-H. Jeong, L. Lee, Tunable liquid-filled microlens array integrated with microfluidic network, Opt. Express. 11 (2003) 2370. doi:10.1364/OE.11.002370.

[31] J. Chen, W. Wang, J. Fang, K. Varahramyan, Variable-focusing microlens with microfluidic chip, J. Micromechanics Microengineering. 14 (2004) 675–680. doi:10.1088/0960-1317/14/5/003.

[32] K. Mishra, C. Murade, B. Carreel, I. Roghair, J.M. Oh, G. Manukyan, et al., Optofluidic lens with tunable focal length and asphericity., Sci. Rep. 4 (2014) 6378. doi:10.1038/srep06378.

[33] R.D. Niederriter, A.M. Watson, R.N. Zahreddine, C.J. Cogswell, R.H. Cormack, V.M. Bright, et al., Electrowetting lenses for compensating phase and curvature distortion in arrayed laser systems., Appl. Opt. 52 (2013) 3172–7. doi:10.1364/AO.52.003172.

[34] X. Zeng, H. Jiang, Liquid Tunable Microlenses based on MEMS techniques., J. Phys. D. Appl. Phys. 46 (2013) 323001. doi:10.1088/0022-3727/46/32/323001.

[35] D.-Y. Zhang, N. Justis, Y.-H. Lo, Fluidic adaptive zoom lens with high zoom ratio and widely tunable field of view, Opt. Commun. 249 (2005) 175–182. doi:10.1016/j.optcom.2005.01.010.

[36] C.-C. Cheng, C.A. Chang, C.-H. Liu, J.A. Yeh, A tunable liquid-crystal microlens with hybrid alignment, J. Opt. A Pure Appl. Opt. 8 (2006) S365–S369. doi:10.1088/1464-4258/8/7/S12.

[37] K. Wei, N.W. Domicone, Y. Zhao, Electroactive liquid lens driven by an annular membrane., Opt. Lett. 39 (2014) 1318–21. doi:10.1364/OL.39.001318.

[38] S. Shian, R.M. Diebold, D.R. Clarke, Tunable lenses using transparent dielectric elastomer actuators., Opt. Express. 21 (2013) 8669–76. doi:10.1364/OE.21.008669.

[39] L. Ren, R.H. Lee, H.R. Park, H. Ren, C. Nah, I.-S. Yoo, A Liquid Lens Driven by Bubble Actuator, J. Microelectromechanical Syst. 22 (2013) 1222–1228. doi:10.1109/JMEMS.2013.2262586.

[40] D.-Y. Zhang, V. Lien, Y. Berdichevsky, J. Choi, Y.-H. Lo, Fluidic adaptive lens with high focal length tunability, Appl. Phys. Lett. 82 (2003) 3171. doi:10.1063/1.1573337.

[41] H. Ren, D. Fox, P.A. Anderson, B. Wu, S.-T. Wu, Tunable-focus liquid lens controlled using a servo motor, Opt. Express. 14 (2006) 8031. doi:10.1364/OE.14.008031.

[42] H. Oku, M. Ishikawa, High-speed liquid lens with 2 ms response and 80.3 nm root-mean-square wavefront error, Appl. Phys. Lett. 94 (2009) 221108. doi:10.1063/1.3143624.

[43] D. Koyama, R. Isago, K. Nakamura, Compact, high-speed variable-focus liquid lens using acoustic radiation force., Opt. Express. 18 (2010) 25158–69. doi:10.1364/OE.18.025158.

[44] B.A. Malouin, M.J. Vogel, J.D. Olles, L. Cheng, A.H. Hirsa, Electromagnetic liquid pistons for capillarity-based pumping., Lab Chip. 11 (2011) 393–7. doi:10.1039/c0lc00397b.

[45] B. a. Malouin, M.J. Vogel, A.H. Hirsa, Electromagnetic control of coupled droplets, Appl. Phys. Lett. 96 (2010) 214104. doi:10.1063/1.3428787.

[46] W. Xiao, S. Hardt, An adaptive liquid microlens driven by a ferrofluidic transducer, J. Micromechanics Microengineering. 20 (2010) 055032. doi:10.1088/0960-1317/20/5/055032.

[47] H.-C. Cheng, S. Xu, Y. Liu, S. Levi, S.-T. Wu, Adaptive mechanical-wetting lens actuated by ferrofluids, Opt. Commun. 284 (2011) 2118–2121. doi:10.1016/j.optcom.2010.12.073.

[48] C.-C. Yang, C.-W.G. Tsai, J.A. Yeh, Dynamic Behavior of Liquid Microlenses Actuated Using Dielectric Force, J. Microelectromechanical Syst. 20 (2011) 1143–1149. doi:10.1109/JMEMS.2011.2162493.

[49] S. Xu, H. Ren, Y. Liu, S.-T. Wu, Dielectric Liquid Microlens With Switchable Negative and Positive Optical Power, J. Microelectromechanical Syst. 20 (2011) 297–301. doi:10.1109/JMEMS.2010.2100032.

[50] C.-C. Cheng, J.A. Yeh, Dielectrically actuated liquid lens, Opt. Express. 15 (2007) 7140. doi:10.1364/OE.15.007140.

[51] H. Ren, H. Xianyu, S. Xu, S.-T. Wu, Adaptive dielectric liquid lens, Opt. Express. 16 (2008) 14954. doi:10.1364/OE.16.014954.

[52] G. McHale, C. V Brown, M.I. Newton, G.G. Wells, N. Sampara, Dielectrowetting driven spreading of droplets., Phys. Rev. Lett. 107 (2011) 186101. doi:10.1103/PhysRevLett.107.186101.

[53] S. Grilli, L. Miccio, V. Vespini, A. Finizio, S. De Nicola, P. Ferraro, Liquid micro-lens array activated by selective electrowetting on lithium niobate substrates., Opt. Express. 16 (2008) 8084–93. http://www.ncbi.nlm.nih.gov/pubmed/18545521 (accessed February 7, 2016).

[54] S. Kuiper, B.H.W. Hendriks, Variable-focus liquid lens for miniature cameras, Appl. Phys. Lett. 85 (2004) 1128. doi:10.1063/1.1779954.

[55] T. Krupenkin, S. Yang, P. Mach, Tunable liquid microlens, Appl. Phys. Lett. 82 (2003) 316. doi:10.1063/1.1536033.

[56] A.W. Adamson, A.P. Gast, Physical Chemistry of Surfaces Sixth Edition, (n.d.).

[57] R. Fürstner, W. Barthlott, C. Neinhuis, P. Walzel, Wetting and self-cleaning properties of artificial superhydrophobic surfaces., Langmuir. 21 (2005) 956–61. doi:10.1021/la0401011.

[58] B. Bhushan, Y.C. Jung, K. Koch, Self-cleaning efficiency of artificial superhydrophobic surfaces., Langmuir. 25 (2009) 3240–8. doi:10.1021/la803860d.

[59] A. Nakajima, K. Hashimoto, T. Watanabe, K. Takai, G. Yamauchi, A. Fujishima, Transparent Superhydrophobic Thin Films with Self-Cleaning Properties, Langmuir. 16 (2000) 7044–7047. doi:10.1021/la000155k.

[60] R. Blossey, Self-cleaning surfaces--virtual realities., Nat. Mater. 2 (2003) 301–6. doi:10.1038/nmat856.

[61] H.J. Ensikat, P. Ditsche-Kuru, C. Neinhuis, W. Barthlott, Superhydrophobicity in perfection: the outstanding properties of the lotus leaf, Beilstein J. Nanotechnol. 2 (2011) 152–161. doi:10.3762/bjnano.2.19.

[62] W. Chen, A.Y. Fadeev, M.C. Hsieh, D. Öner, J. Youngblood, T.J. McCarthy, Ultrahydrophobic and Ultralyophobic Surfaces: Some Comments and Examples, Langmuir. 15 (1999) 3395–3399. doi:10.1021/la990074s.

[63] B. Cortese, S. D'Amone, M. Manca, I. Viola, R. Cingolani, G. Gigli, Superhydrophobicity due to the hierarchical scale roughness of PDMS surfaces., Langmuir. 24 (2008) 2712–8. doi:10.1021/la702764x.

[64] P.N. Manoudis, I. Karapanagiotis, A. Tsakalof, I. Zuburtikudis, C. Panayiotou, Superhydrophobic composite films produced on various substrates., Langmuir. 24 (2008) 11225–32. doi:10.1021/la801817e.

[65] L. Gao, T.J. McCarthy, The "lotus effect" explained: two reasons why two length scales of topography are important., Langmuir. 22 (2006) 2966–7. doi:10.1021/la0532149.

[66] N.J. Shirtcliffe, G. McHale, M.I. Newton, G. Chabrol, C.C. Perry, Dual-Scale Roughness Produces Unusually Water-Repellent Surfaces, Adv. Mater. 16 (2004) 1929–1932. doi:10.1002/adma.200400315.

[67] H.-M. Bok, T.-Y. Shin, S. Park, Designer Binary Nanostructures toward Water Slipping Superhydrophobic Surfaces, Chem. Mater. 20 (2008) 2247–2251. doi:10.1021/cm703038j.

[68] T. Nakanishi, T. Michinobu, K. Yoshida, N. Shirahata, K. Ariga, H. Möhwald, et al., Nanocarbon Superhydrophobic Surfaces created from Fullerene-Based Hierarchical Supramolecular Assemblies, Adv. Mater. 20 (2008) 443–446. doi:10.1002/adma.200701537.

[69] R.N. Wenzel, RESISTANCE OF SOLID SURFACES TO WETTING BY WATER, Ind. Eng. Chem. 28 (1936) 988–994. doi:10.1021/ie50320a024.

[70] R.N. Wenzel, Surface Roughness and Contact Angle., J. Phys. Colloid Chem. 53 (1949) 1466–1467. doi:10.1021/j150474a015.

[71] A.B.D. Cassie, Contact angles, Discuss. Faraday Soc. 3 (1948) 11. doi:10.1039/df9480300011.

[72] P. van der Wal, U. Steiner, Super-hydrophobic surfaces made from Teflon, Soft Matter. 3 (2007) 426–429. doi:10.1039/B613947G.

[73] B.S. Gallardo, Electrochemical Principles for Active Control of Liquids on Submillimeter Scales, Science (80-.). 283 (1999) 57–60. doi:10.1126/science.283.5398.57.

[74] C. Rosslee, N.L. Abbott, Active control of interfacial properties, Curr. Opin. Colloid Interface Sci. 5 (2000) 81–87. doi:10.1016/S1359-0294(00)00035-2.

[75] K. Tajima, T. Huxur, Y. Imai, I. Motoyama, A. Nakamura, M. Koshinuma, Surface activities of ferrocene surfactants, 94 (1995) 243–251.

[76] B.S. Gallardo, K.L. Metcalfe, N.L. Abbott, Ferrocenyl Surfactants at the Surface of Water: Principles for Active Control of Interfacial Properties, Langmuir. 12 (1996) 4116–4124. doi:10.1021/la960199m.

[77] C. Rosslee, N. Abbott, Active control of interfacial properties, Curr. Opin. Colloid Interface Sci. 5 (2000) 81–87. doi:10.1016/S1359-0294(00)00035-2.

[78] L. Gao, T.J. McCarthy, Contact angle hysteresis explained., Langmuir. 22 (2006)

6234–7. doi:10.1021/la060254j.

[79] J.F. Joanny, P.G. de Gennes, A model for contact angle hysteresis, J. Chem. Phys. 81 (1984) 552. doi:10.1063/1.447337.

[80] R.H. Dettre, R.E. Johnson, Contact Angle Hysteresis. IV. Contact Angle Measurements on Heterogeneous Surfaces 1, J. Phys. Chem. 69 (1965) 1507–1515. doi:10.1021/j100889a012.

[81] R.E. Johnson, R.H. Dettre, Contact Angle Hysteresis. III. Study of an Idealized Heterogeneous Surface, J. Phys. Chem. 68 (1964) 1744–1750. doi:10.1021/j100789a012.

[82] M. Luo, R. Gupta, J. Frechette, Modulating contact angle hysteresis to direct fluid droplets along a homogenous surface, ACS Appl. Mater. Interfaces. 4 (2012) 890–896. doi:10.1021/am201557k.

[83] E.B. Dussan V., R.T.-P. Chow, On the ability of drops or bubbles to stick to non-horizontal surfaces of solids, J. Fluid Mech. 137 (2006) 1. doi:10.1017/S002211208300227X.

[84] C.G.. Furmidge, Studies at phase interfaces. I. The sliding of liquid drops on solid surfaces and a theory for spray retention, J. Colloid Sci. 17 (1962) 309–324. doi:10.1016/0095-8522(62)90011-9.

[85] L. Castañer, V. Di Virgilio, S. Bermejo, Charge-coupled transient model for electrowetting., Langmuir. 26 (2010) 16178–85. doi:10.1021/la102777m.

[86] S. Chevalliot, S. Kuiper, J. Heikenfeld, Experimental Validation of the Invariance of Electrowetting Contact Angle Saturation, J. Adhes. Sci. Technol. (2012). http://www.tandfonline.com/doi/abs/10.1163/156856111X599580 (accessed February 11, 2016).

[87] A.I. Drygiannakis, A.G. Papathanasiou, A.G. Boudouvis, On the connection between dielectric breakdown strength, trapping of charge, and contact angle saturation in electrowetting., Langmuir. 25 (2009) 147–52. doi:10.1021/la802551j.

[88] H.J.J. Verheijen, M.W.J. Prins, Reversible Electrowetting and Trapping of Charge: Model and Experiments, Langmuir. 15 (1999) 6616–6620. doi:10.1021/la990548n.

[89] M.A. Fontelos, U. Kindelán, The Shape of Charged Drops over a Solid Surface and Symmetry-Breaking Instabilities, SIAM J. Appl. Math. 69 (2008) 126–148. doi:10.1137/080713707.

[90] M. Vallet, M. Vallade, B. Berge, Limiting phenomena for the spreading of water on polymer films by electrowetting, Eur. Phys. J. B. 11 (1999) 583–591. doi:10.1007/s100510051186.

[91] F. Mugele, S. Herminghaus, Electrostatic stabilization of fluid microstructures, Appl. Phys. Lett. 81 (2002) 2303. doi:10.1063/1.1508808.

[92] W.C. Nelson, C.-J. "Cj" Kim, Droplet Actuation by Electrowetting-on-Dielectric (EWOD): A Review, J. Adhes. Sci. Technol. ahead-of-p (2012) 1–25. doi:10.1163/156856111X599562.

[93] L. Chen, E. Bonaccurso, Electrowetting - From statics to dynamics, Adv. Colloid Interface Sci. 210 (2014) 2–12. doi:10.1016/j.cis.2013.09.007.

[94] H. Liu, S. Dharmatilleke, D.K. Maurya, A.A.O. Tay, Dielectric materials for electrowetting-on-dielectric actuation, Microsyst. Technol. 16 (2010) 449–460. doi:10.1007/s00542-009-0933-z.

[95] M. Maillard, J. Legrand, B. Berge, Two liquids wetting and low hysteresis electrowetting on dielectric applications, Langmuir. 25 (2009) 6162–6167. doi:10.1021/la804118y.

[96] H. Moon, S.K. Cho, R.L. Garrell, C.J. Kim, Low voltage electrowetting-on-dielectric, J. Appl. Phys. 92 (2002) 4080–4087. doi:10.1063/1.1504171.

[97] C. Peng, Z. Zhang, C.-J.C.J. Kim, Y.S. Ju, EWOD (electrowetting on dielectric) digital microfluidics powered by finger actuation., Lab Chip. 14 (2014) 1117–22. doi:10.1039/c3lc51223a.

[98] C.-C. Cheng, C.A. Chang, J.A. Yeh, Variable focus dielectric liquid droplet lens, Opt. Express. 14 (2006) 4101. doi:10.1364/OE.14.004101.

[99] M. Khodayari, N.B. Crane, A.A. Volinsky, Electrochemical explanation for asymmetric electrowetting response, Thin Solid Films. 548 (2013) 632–635. doi:10.1016/j.tsf.2013.10.011.

[100] B.K. and C.-J. Kim, Evaluation of repeated electrowetting on three different fluoropolymer top coatings, J. Micromechanics Microengineering. 23 (2013) 67002. doi:10.1088/0960-1317/23/6/067002.

[101] U.C. Yi, C.J. Kim, Soft printing of droplets pre-metered by electrowetting, Sensors Actuators, A Phys. 114 (2004) 347–354. doi:10.1016/j.sna.2003.12.003.

[102] H.J.J. Verheijen, M.W.J. Prins, Reversible electrowetting and trapping of charge: Model and experiments, Langmuir. 15 (1999) 6616–6620. doi:10.1021/la990548n.

[103] Y.L. Pan, D.Y. Li, X.Z. Zhao, Role of Electric Field on Electroviscosity, Adv. Mater. Res. 803 (2013) 438–441. doi:10.4028/www.scientific.net/AMR.803.438.

[104] J. Chang, D. Choi, X. You, Low Voltage Electrowetting on Atomic-Layer- Deposited Aluminum Oxide, Proc. 2010 5th IEEE Int. Conf. Nano/Micro Eng. Mol. Syst. January 20-23, 2010, Xiamen, China. (2010) 605–608. doi:10.1109/NEMS.2010.5592477.

[105] H. Moon, S.K. Cho, R.L. Garrell, C.-J. "Cj" Kim, Low voltage electrowetting-on-dielectric, J. Appl. Phys. 92 (2002) 4080. doi:10.1063/1.1504171.

[106] S. Berry, J. Kedzierski, B. Abedian, Low voltage electrowetting using thin fluoroploymer films., J. Colloid Interface Sci. 303 (2006) 517–24. doi:10.1016/j.jcis.2006.08.004.

[107] Y.-Y. Lin, R.D. Evans, E. Welch, B.-N. Hsu, A.C. Madison, R.B. Fair, Low voltage electrowetting-on-dielectric platform using multi-layer insulators, Sensors Actuators B Chem. 150 (2010) 465–470. doi:10.1016/j.snb.2010.06.059.

[108] X. Zhang, Y. Cai, Ultralow voltage electrowetting on a solidlike ionic-liquid dielectric layer, Angew. Chemie - Int. Ed. 52 (2013) 2289–2292. doi:10.1002/anie.201207857.

[109] A.A. Kornyshev, A.R. Kucernak, M. Marinescu, C.W. Monroe, A.E.S. Sleightholme, M. Urbakh, Ultra-Low-Voltage Electrowetting, J. Phys. Chem. C. 114 (2010) 14885–14890. doi:10.1021/jp101051e.

[110] J.L. Bates, C.W. Griffin, D.D. Marchant, J.E. Garnier, Electrical conductivity, Seebeck Coefficient, and structure of In_2O_3-SnO_2, Am. Ceram. Soc. Bull. 65 (1986) 673–678. http://inis.iaea.org/Search/search.aspx?orig_q=RN:17072086 (accessed February 15, 2016).

[111] K.L. Chopra, S. Major, D.K. Pandya, Transparent conductors—A status review, Thin Solid Films. 102 (1983) 1–46. doi:10.1016/0040-6090(83)90256-0.

[112] U. Betz, M. Kharrazi Olsson, J. Marthy, M.F. Escolá, F. Atamny, Thin films engineering of indium tin oxide: Large area flat panel displays application, Surf. Coatings Technol. 200 (2006) 5751–5759. doi:10.1016/j.surfcoat.2005.08.144.

[113] A. Hassanfiroozi, T.-H. Jen, Y.-P. Huang, H.-P.D. Shieh, Liquid crystal lens array for a 3D endoscope, SPIE Newsroom. (2014) 2–6. doi:10.1117/2.1201405.005419.

[114] S.K. Park, J.I. Han, W.K. Kim, M.G. Kwak, Deposition of indium–tin-oxide films on polymer substrates for application in plastic-based flat panel displays, Thin Solid Films. 397 (2001) 49–55. doi:10.1016/S0040-6090(01)01489-4.

[115] N. Balasubramanian, A. Subrahmanyam, Effect of substrate temperature on the electrical and optical properties of reactively evaporated indium tin oxide films, Mater. Sci. Eng. B. 1 (1988) 279–281. doi:10.1016/0921-5107(88)90008-6.

[116] N. Balasubramanian, A. Subrahmanyam, Electrical and optical properties of reactively evaporated indium tin oxide (ITO) films-dependence on substrate temperature and tin concentration, J. Phys. D. Appl. Phys. 22 (1989) 206–209. doi:10.1088/0022-3727/22/1/030.

[117] M. Higuchi, S. Uekusa, R. Nakano, K. Yokogawa, Postdeposition Annealing Influence

on Sputtered Indium Tin Oxide Film Characteristics, Jpn. J. Appl. Phys. 33 (1994) 302–306. doi:10.1143/JJAP.33.302.

[118] Heungsoo Kim, J. S. Horwitz, W.H. Kim, Z. H. Kafafi, D. B. Chrisey, High Quality Sn-Doped In$_2$O$_3$ Films Grown by Pulsed Laser Deposition for Organic Light-Emitting Diodes, MRS Proc. 780 (2003) Y1.6. doi:10.1557/PROC-780-Y1.6.

[119] K. Sreenivas, T. Sudersena Rao, A. Mansingh, S. Chandra, Preparation and characterization of rf sputtered indium tin oxide films, J. Appl. Phys. 57 (1985) 384. doi:10.1063/1.335481.

[120] S. Laux, N. Kaiser, A. Zöller, R. Götzelmann, H. Lauth, H. Bernitzki, Room-temperature deposition of indium tin oxide thin films with plasma ion-assisted evaporation, Thin Solid Films. 335 (1998) 1–5. doi:10.1016/S0040-6090(98)00861-X.

[121] Y. Sawada, C. Kobayashi, S. Seki, H. Funakubo, Highly-conducting indium☐tin-oxide transparent films fabricated by spray CVD using ethanol solution of indium (III) chloride and tin (II) chloride, Thin Solid Films. 409 (2002) 46–50. doi:10.1016/S0040-6090(02)00102-5.

[122] H. Mbarek, M. Saadoun, B. Bessaïs, Screen-printed Tin-doped indium oxide (ITO) films for NH3 gas sensing, Mater. Sci. Eng. C. 26 (2006) 500–504. doi:10.1016/j.msec.2005.10.037.

[123] J. Puetz, M.A. Aegerter, Direct gravure printing of indium tin oxide nanoparticle patterns on polymer foils, Thin Solid Films. 516 (2008) 4495–4501. doi:10.1016/j.tsf.2007.05.086.

[124] Z.B. Zhou, R.Q. Cui, Q.J. Pang, Y.D. Wang, F.Y. Meng, T.T. Sun, et al., Preparation of indium tin oxide films and doped tin oxide films by an ultrasonic spray CVD process, Appl. Surf. Sci. 172 (2001) 245–252. doi:10.1016/S0169-4332(00)00862-X.

[125] R. Pommier, C. Gril, J. Marucchi, Sprayed films of indium tin oxide and fluorine-doped tin oxide of large surface area, Thin Solid Films. 77 (1981) 91–98. doi:10.1016/0040-6090(81)90363-1.

[126] G. Qin, L. Fan, A. Watanabe, Formation of indium tin oxide film by wet process using laser sintering, J. Mater. Process. Technol. 227 (2016) 16–23. doi:10.1016/j.jmatprotec.2015.07.011.

[127] R. Tueta, M. Braguier, Fabrication and characterization of indium tin oxide thin films for electroluminescent applications, Thin Solid Films. 80 (1981) 143–148. doi:10.1016/0040-6090(81)90216-9.

[128] B.H. Lee, S.-H. Lee, Effect of process parameters on the characteristics of indium tin oxide thin film for flat panel display application, Thin Solid Films. 302 (1997) 25–30. doi:10.1016/S0040-6090(96)09581-8.

[129] L. Hu, G. Gruner, J. Gong, C.J. Kim, B. Hornbostel, Electrowetting devices with transparent single-walled carbon nanotube electrodes, Appl. Phys. Lett. 90 (2007) 093124. doi:10.1063/1.2561032.

[130] S. Sohail, D. Das, S. Das, K. Biswas, Study of PDMS as Dielectric Layer in Electrowetting Devices Shiraz, (2014) 7–10. doi:10.1007/978-3-319-03002-9.

[131] W. Dai, Y.-P. Zhao, The Nonlinear Phenomena of Thin Polydimethylsiloxane (PDMS) Films in Electrowetting, Int. J. Nonlinear Sci. Numer. Simul. 8 (2007) 519–526. doi:10.1515/IJNSNS.2007.8.4.519.

[132] V. Kumar, N.N. Sharma, SU-8 as hydrophobic and dielectric thin film in electrowetting-on- dielectric based microfluidics device, J. Nanotechnol. 6 (2012) 239. doi:10.1155/2012/312784.

[133] H.-J. Ding, K. Liu, L.-B. Zhao, Q. Zeng, Z.-X. Guo, F. Guo, et al., A Smart Electrowetting Device Based on PDMS and Glass for Manipulating Cells in Droplet, 2007 1st Int. Conf. Bioinforma. Biomed. Eng. (2007) 1317–1320. doi:10.1109/ICBBE.2007.340.

[134] J.H. Koschwanez, R.H. Carlson, D.R. Meldrum, Thin PDMS films using long spin times or tert-butyl alcohol as a solvent., PLoS One. 4 (2009) e4572.

doi:10.1371/journal.pone.0004572.

[135] A. Tröls, S. Clara, B. Jakoby, Fluid Dynamics of an Electrowetting-on-dielectrics Tube Oscillator, Procedia Eng. 120 (2015) 189–193. doi:10.1016/j.proeng.2015.08.607.

[136] V. Bahadur, S. V. Garimella, Electrowetting-based control of static droplet states on rough surfaces, Langmuir. 23 (2007) 4918–4924. doi:10.1021/la0631365.

[137] Y.Y. Lin, E.R.F. Welch, R.B. Fair, Low voltage picoliter droplet manipulation utilizing electrowetting-on- dielectric platforms, Sensors Actuators, B Chem. 173 (2012) 338–345. doi:10.1016/j.snb.2012.07.022.

[138] S.-K. Fan, H. Yang, T.-T. Wang, W. Hsu, Asymmetric electrowetting—moving droplets by a square wave, Lab Chip. 7 (2007) 1330. doi:10.1039/b704084a.

[139] D. Chatterjee, H. Shepherd, R.L. Garrell, Electromechanical model for actuating liquids in a two-plate droplet microfluidic device., Lab Chip. 9 (2009) 1219–29. doi:10.1039/b901375j.

[140] A. WIXFORTH, Acoustically Driven Programmable Microfluidics for Biological and Chemical Applications, J. Assoc. Lab. Autom. 11 (2006) 399–405. doi:10.1016/j.jala.2006.08.001.

[141] U.-C. Yi, C.-J. "CJ" Kim, Soft printing of droplets pre-metered by electrowetting, Sensors Actuators A Phys. 114 (2004) 347–354. doi:10.1016/j.sna.2003.12.003.

[142] M.G. Pollack, R.B. Fair, A.D. Shenderov, Electrowetting-based actuation of liquid droplets for microfluidic applications, Appl. Phys. Lett. 77 (2000) 1725. doi:10.1063/1.1308534.

[143] M.J. Schertzer, R. Ben-Mrad, P.E. Sullivan, Using capacitance measurements in EWOD devices to identify fluid composition and control droplet mixing, Sensors Actuators B Chem. 145 (2010) 340–347. doi:10.1016/j.snb.2009.12.019.

[144] S. Cho, H. Moon, J. Fowler, S. Fan, C. Kim, Splitting a liquid droplet for electrowetting-based microfluidics, Proc. 2001 ASME Inter Mech …. (2001). https://scholar.google.es/scholar?q=%E2%80%9CSplitting+a+liquid+droplet+for+elec trowetting-based+microfluidics&btnG=&hl=en&as_sdt=0%2C5#0 (accessed March 6, 2016).

[145] J. Wu, R. Yue, X. Zeng, L. Liu, Droplets actuating chip based on electrowetting-on-dielectric, Front. Electr. Electron. Eng. China. 2 (2007) 345–349. doi:10.1007/s11460-007-0065-0.

[146] A. Wheeler, E. Miller, Digital microfluidics for screening assays, … Miniaturized Syst. …. (2008). http://www.rsc.org/binaries/LOC/2008/PDFs/Papers/257_0310.pdf (accessed March 6, 2016).

[147] N. Howell, W. Li, Modeling and simulation of droplet translocation and fission by electrowetting-on-dielectrics (EWOD), Front. Mech. Eng. China. 5 (2010) 376–388. doi:10.1007/s11465-010-0104-z.

[148] J. Chang, D. Choi, X. You, Low voltage electrowetting on atomic-layer-deposited aluminum oxide, Nano/Micro Eng. …. (2010). http://ieeexplore.ieee.org/xpls/abs_all.jsp?arnumber=5592477 (accessed March 6, 2016).

[149] J. Chang, D. Choi, S. Han, J. Pak, Driving characteristics of the electrowetting-on-dielectric device using atomic-layer-deposited aluminum oxide as the dielectric, Microfluid. Nanofluidics. (2010). http://link.springer.com/article/10.1007/s10404-009-0511-9 (accessed March 6, 2016).

[150] Y.-Y. Lin, R.D. Evans, E. Welch, B.-N. Hsu, A.C. Madison, R.B. Fair, Low Voltage Electrowetting-on-Dielectric Platform using Multi-Layer Insulators., Sens. Actuators. B. Chem. 150 (2010) 465–470. doi:10.1016/j.snb.2010.06.059.

[151] J. Restolho, J.L. Mata, B. Saramago, On the interfacial behavior of ionic liquids: surface tensions and contact angles., J. Colloid Interface Sci. 340 (2009) 82–6. doi:10.1016/j.jcis.2009.08.013.

[152] S. Millefiorini, A.H. Tkaczyk, R. Sedev, J. Efthimiadis, J. Ralston, Electrowetting of ionic liquids., J. Am. Chem. Soc. 128 (2006) 3098–101. doi:10.1021/ja057606d.

[153] J. Ou, B. Perot, J.P. Rothstein, Laminar drag reduction in microchannels using ultrahydrophobic surfaces, Phys. Fluids. 16 (2004) 4635. doi:10.1063/1.1812011.

[154] G.M. Whitesides, A.D. Stroock, Flexible methods for microfluidics, Phys. Today. 54 (2001) 42–48. doi:10.1063/1.1387591.

[155] J. Eijkel, Liquid slip in micro- and nanofluidics: recent research and its possible implications., Lab Chip. 7 (2007) 299–301. doi:10.1039/b700364c.

[156] T. Braun, E. Jung, J. Bauer, Contactless component handling on PCB using EWOD principles, EPTC IEEE. (2008) 186–192.

[157] J. Lu, Y. Nakano, H. Takagi, R. Maeda, High-Efficient Chip to Wafer Self-Alignment and Bonding Applicable to MEMS-IC Flexible Integration, 13 (2013) 651–656.

[158] K.D. Esmeryan, G. McHale, C.L. Trabi, N.R. Geraldi, M.I. Newton, Manipulated wettability of a superhydrophobic quartz crystal microbalance through electrowetting, J. Phys. D. Appl. Phys. 46 (2013) 345307. doi:10.1088/0022-3727/46/34/345307.

[159] M. Nosonovsky, B. Bhushan, Superhydrophobic surfaces and emerging applications : Non-adhesion , energy , green engineering, Curr. Opin. Colloid Interface Sci. 14 (2009) 270–280. doi:10.1016/j.cocis.2009.05.004.

[160] J. Genzer, K. Efimenko, Recent developments in superhydrophobic surfaces and their relevance to marine fouling: a review., Biofouling. 22 (2006) 339–60. doi:10.1080/08927010600980223.

[161] M. Lee, C. Yim, S. Jeon, M. Lee, C. Yim, S. Jeon, Anti-icing characteristics of superhydrophobic surfaces investigated by quartz crystal microresonators, J. Chem. Phys. 142 (2015) 1–3. doi:10.1063/1.4906510.

[162] S. Farhadi, M. Farzaneh, S.A. Kulinich, Anti-icing performance of superhydrophobic surfaces, Appl. Surf. Sci. 257 (2011) 6264–6269. doi:10.1016/j.apsusc.2011.02.057.

[163] G. Mchale, M.I. Newton, N.J. Shirtcliffe, M. Curie, Immersed superhydrophobic surfaces : Gas exchange , slip and drag reduction properties, (2010). doi:10.1039/b917861a.

[164] J. Lu, H. Takagi, R. Maeda, Chip to Wafer Temporary Bonding with Self-alignment by Patterned FDTS Layer for Size-free MEMS Integration, (2011) 3–6.

[165] B. Kobrin, T. Zhang, M.T. Grimes, K. Chong, M. Wanebo, J. Chinn, et al., An Improved Chemical Resistance and Mechanical Durability of Hydrophobic FDTS Coatings, J. Phys. Conf. Ser. 34 (2006) 454–457. doi:10.1088/1742-6596/34/1/074.

[166] A. Marmur, Solid-Surface Characterization by Wetting, Annu. Rev. Mater. Res. 39 (2009) 473–489. doi:10.1146/annurev.matsci.38.060407.132425.

[167] J. Lee, B. He, N. a Patankar, A roughness-based wettability switching membrane device for hydrophobic surfaces, J. Micromechanics Microengineering. 15 (2005) 591–600. doi:10.1088/0960-1317/15/3/022.

[168] T.N. Krupenkin, J.A. Taylor, T.M. Schneider, S. Yang, From rolling ball to complete wetting: The dynamic tuning of liquids on nanostructured surfaces, Langmuir. 20 (2004) 3824–3827. doi:10.1021/la036093q.

[169] N. a. Patankar, Mimicking the lotus effect: Influence of double roughness structures and slender pillars, Langmuir. 20 (2004) 8209–8213. doi:10.1021/la048629t.

[170] M. Per, Resistance of surfaces to wetting by water, Ind. Eng. Chem. 28 (1936) 988–994.

[171] L. Castañer, V. Di Virgilio, S. Bermejo, Charge-coupled transient model for electrowetting, Langmuir. 26 (2010) 16178–16185. doi:10.1021/la102777m.

[172] V. Di Virgilio, S. Bermejo, L. Castañer, Wettability Increase by " Corona " Ionization, Langmuir. 27 (2011) 9614–9620.

[173] B. Chua, A.S. Wexler, N.C. Tien, D. a. Niemeier, B. a. Holmén, Micro corona based particle steering air filter, Sensors Actuators, A Phys. 196 (2013) 8–15. doi:10.1016/j.sna.2013.03.029.

[174] B. Chua, A.S. Wexler, N.C. Tien, D.A. Niemeier, B.A. Holm, Collection of Liquid Phase Particles by Microfabricated Electrostatic Precipitator, 22 (2013) 1010–1019.

[175] Castañer L., S. Silvestre, Modelling photovoltaic systems using PSpice, 2002.

[176] A. Moreno, J. Julve, SPICE macromodeling of photovoltaic systems, Prog. …. (2000).

[177] M. Lin, Digital system designs and practices: using Verilog HDL and FPGAs, 2008. http://dl.acm.org/citation.cfm?id=1502316 (accessed March 15, 2016).

[178] H. Oprins, B. Vandevelde, M. Baelmans, Modeling and control of electrowetting induced droplet motion, Micromachines. 3 (2012) 150–167. doi:10.3390/mi3010150.

[179] S. Bishay, Numerical methods for the calculation of the cole-cole parameters, Egypt. Mater. Res. Soc. Jan. (2000).

[180] M.G. Pollack, R.B. Fair, A.D. Shenderov, Electrowetting-based actuation of liquid droplets for microfluidic applications, Appl. Phys. Lett. 77 (2000) 1725. doi:10.1063/1.1308534.

[181] F.O.F. Ouyang, J.W.J. Wu, M.K.M. Kang, R.Y.R. Yue, L.L.L. Liu, Planar Variable-Focus Liquid Lens Based on Electrowetting on Dielectric, 2007 2nd IEEE Int. Conf. Nano/Micro Eng. Mol. Syst. (2007) 834–837. doi:10.1109/NEMS.2007.352147.

[182] H. Haus, P.P. Jr, VII. ELECTRODYNAMICS OF MOVING MEDIA, (1967). http://citeseerx.ist.psu.edu/viewdoc/download?doi=10.1.1.468.1032&rep=rep1&type=pdf (accessed March 6, 2016).